Doctoral Dissertation

Cryopreservation by intracellular permeation of polyampholytes and correlation between polymer structure and cryoprotective effect

Ryota Yamasaki

Supervisor: Kazuaki Matsumura

Graduate School of Advanced Science and Technology

Japan Advanced Institute of Science and Technology

Materials Science

March 2024

Abstract

During cryopreservation, cryoprotectants are used to protect cells from cryoinjury. Currently, 10% dimethyl sulfoxide (DMSO) is commonly used as a cryoprotectant. However, since DMSO is highly cytotoxic and membrane-permeable, it must be removed promptly after freezing and thawing. Polyampholytes have high cryoprotective effects, but the cryoprotective mechanism is poorly understood. In this thesis, I focused on elucidating the cryoprotective mechanism of polyampholytes and their application to cryopreservation using intracellular permeation.

In Chapter 2, in addition to the previously reported poly(2-(dimethyl amino)ethyl methacrylate/methacrylic acid) (pD), I synthesized poly(vinyl acetate/acrylic acid (AA)/2-(dimethyl amino)ethyl acrylate (DMAEA)) (pV) and poly(methyl vinyl ether/AA/DMAEA) (pM) with alternating cations and anions, and poly(2-acrylamido-2-methyl propanesulfonic acid/(3-acrylamidopropyl)trimethyl ammonium chloride) (pA) with a higher degree of dissociation, and correlated their cryoprotective effects and polymer structures. The cell recovery rate of the alternating array pV was the highest and comparable to that of carboxylated ε-poly-L-lysine (PLL). Cryoprotective effect of pA was the lowest, and measurements of residual water volume by temperature variable solid state magic angle spinning NMR showed that freezing of bulk water was significantly higher. In addition, the tendency of vitrification and trapping of Na ions was observed in the higher temperature range of pV and PLL, which showed high cryoprotective effect, suggesting that the ability to adjust salt concentration and vitrification during freezing by trapping salt or water is important for the cryoprotective effect of amphoteric electrolyte polymers.

In Chapter 3, we attempted to enhance the cryoprotective effect by utilizing the permeation of the zwitterionic polymer poly(sulfobtaine) into cells. Furthermore, we synthesized a copolymer of DMSO, a cell-permeable cryoprotectant, and 2-(methyl sulfinyl)ethyl methacrylate (MSEMA), which has the same methyl sulfinyl group, and confirmed its cryoprotective effect. Intracellular permeation was confirmed by the fluorescently modified polymer, and the polymer was found to easily counter diffuse by incubating at 37 ° C for about 30 minutes after permeation. Poly(SPB) and poly(SPB/MSEMA10) improved the cell recovery rate by about 20 or 30% through intracellular permeation. Cell recovery rate after counter diffusion of the polymer at 37 ° C was comparable to that before polymer permeation, and the cell pellets alone can be cryopreserved after polymer permeation, indicating that poly(SPB) can improve cryoprotection by intracellular permeation.

This study revealed that vitrification and salt/water trapping are important for cryoprotection of polyampholytes. This understanding of the cryoprotection mechanism will provide important guidelines for the molecular design of cryoprotectants in the future. Furthermore, the ability of zwitterionic polymers to reversibly permeate into cells and enhance their cryoprotective effects offers the potential for cryopreservation of more complex three-dimensional cellular structures such as spheroids, and the ability of artificial polymers to It is expected that this will open up new avenues for development.

[keyword] Cryopreservation, Polyampholytes, solid-state MAS NMR, Intracellular permeation

Table of Contents

List of tables and Figures

Chapter 1

General introduction

1.1 Cryopreservation

The function and structure of organelles in living cells and tissues may change over time. Cryopreservation is a technology that enables the preservation of cells, tissues, and organs by slowing their metabolism at -80 or -196 ° C. Therefore, it is a very important technology for long term preservation of various biological samples and for clinical applications[1~3]. In 1949, Polge et al. reported the cryopreservation of bird semen using glycerol, the first report on cryopreservation[4]. Since then, research has been conducted on the cryopreservation of various cells and tissues such as sperm of other animals and plants[5-8]. In addition, cryopreservation using dimethyl sulfoxide (DMSO) was reported by Lovelock in 1959[9]. DMSO is currently the commonly used cryoprotectant (CPA) and is typically used at concentrations of around 10%. DMSO has strong hydrogen bonds with water that lower the freezing point and exhibits excellent cryoprotective effects[10,11]. These small molecules CPAs have membrane permeability and permeate into cells during freezing, so an operation to remove CPAs from inside cells is required after thawing[12,13]. Furthermore, DMSO has many problems such as cytotoxicity and induction of stem cell differentiation, however, it is still used today because there are no CPAs to replace[14-16].

Therefore, the development of CPAs to replace DMSO is actively underway. There are two types of cryopreservation methods: slow freezing and vitrification[17]. In the vitrification preservation method, cells are directly cryopreserved in liquid nitrogen, which turns intracellular water into an amorphous state and avoids intracellular ice crystal formation[18]. On the other hand, in the slow freezing method, cells are slowly frozen to -80 ° C, which causes ice crystals to form inside the cells, causing mechanical stress and osmotic shock[19, 20]. However, the slow freezing method is simpler because it can be carried out if there is a deep freezer. Therefore, in this study, cells were cryopreserved using the slow freezing method.

1.2 Cryoinjury

During cell freeze-thaw cycles, cells are subjected to various chemical and physical damages, including osmotic shock, exposure to toxic CPAs such as DMSO, and the formation of intracellular ice crystals[15,19-21]. In the cooling process, the extracellular solution first begins to freeze. At this time, since the ice crystals do not contain solutes, the osmotic pressure increases due to the concentration of the extracellular solution, causing cell dehydration. If the cooling rate is made faster, the outflow of cell water gradually decreases, causing intracellular ice to form. According to Mazur's two-factor hypothesis, during cryopreservation, cell states are classified into three types depending

on the freezing rate[21] (Figure 1.1). When the cooling rate is appropriate, intracellular dehydration increases the solute concentration and inhibits intracellular freezing. However, if the cooling rate is too fast, the dehydration necessary to achieve osmotic equilibrium does not occur, causing intracellular freezing. If the cooling rate is too slow, irreversible damage will occur due to solute concentration by excessive dehydration and cell membrane adhesions. Furthermore, in the thawing process after cryopreservation, water may flow into dehydrated cells beyond the cell membrane, causing swelling and lysis of the cells. Additionally, ice recrystallization is induced during thawing, which can cause mechanical damage to cell membranes by growing small ice crystals into larger ice crystals[22, 23].

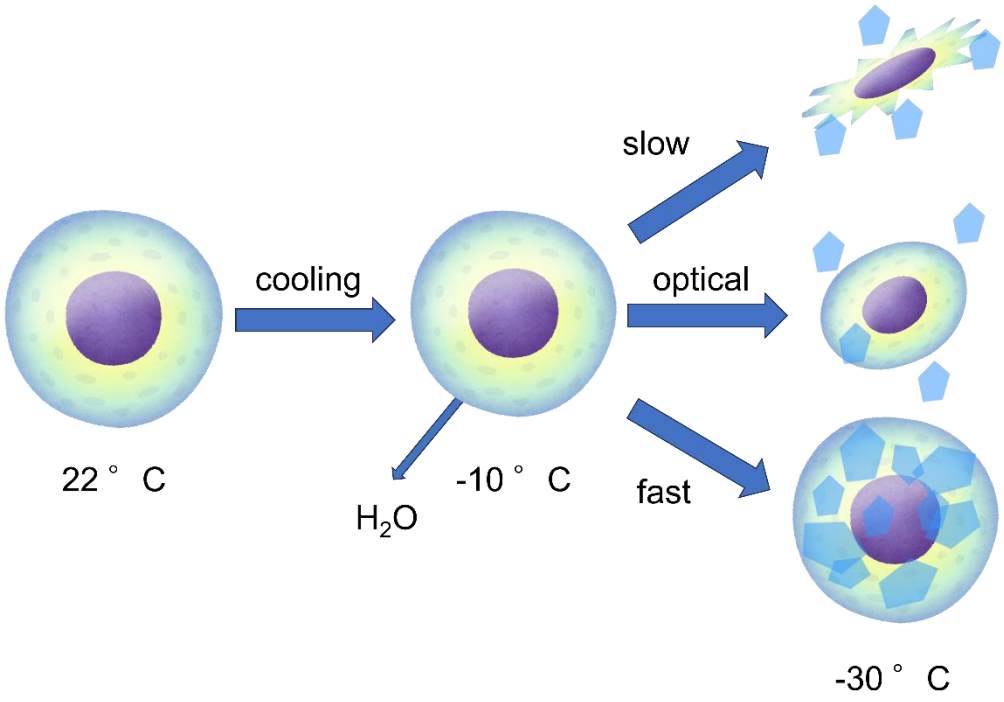

Figure 1.1 Freezing damage due to freezing speed.

1.3 Cryoprotectants

1.3.1 Small molecule CPAs

Small molecule CPAs can be divided into two types, membrane permeable and non-membrane permeable, depending on whether they permeate into cells or not (Figure 1.2).

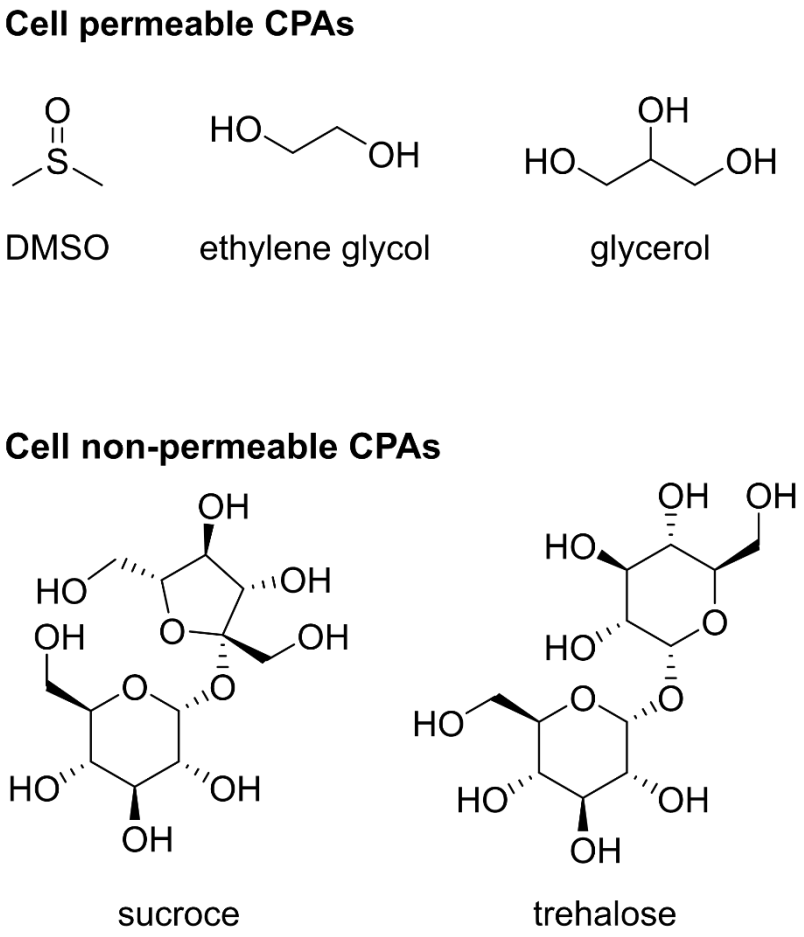

Figure 1.2 structure of small molecular weight CPAs.

DMSO, the most common CPA, is a membrane permeable CPA. DMSO exhibits freezing point depression at certain concentrations[9]. In addition, molecular dynamics simulations

researched between DMSO and water revealed that the proportion of unfrozen water during freezing increases due to hydrogen bonding between DMSO and water[10]. Additionally, because of investigating the hydrogen bonding ability of DMSO and acetone with water using Raman spectroscopy, it was revealed that the hydrogen bond between DMSO and water is stronger than that of acetone and is very similar to the hydrogen bond between water and water. As a result, DMSO is not removed from the hydrogen bond network during freezing and freezes in an amorphous state[11]. However, as mentioned above, DMSO is cytotoxic and may induce differentiation and induction[14-16]. For example, it has been reported that differentiation occurs in embryonic stem cells even at very low concentrations of DMSO of 0.125%. In addition to differentiation, patients transplanted with cells cryopreserved with DMSO have been reported to have significantly increased DMSO-induced side effects. Other side effects such as nausea, hypotension, and arrhythmia have been reported in patients receiving infusions of hematopoietic stem cells cryopreserved in DMSO[24-26]. DMSO is also used to cryopreserve human induced pluripotent stem cells (hiPS), which are attracting attention in the field of cell therapy and regenerative medicine because they differentiate into all cell types. However, the use of DMSO should still be avoided in the cryopreservation of reprogrammed cells, as it increases mRNA levels of the de novo DNA methyltransferase DNMT3A in mouse

embryoid bodies and is accompanied by hyper- or hypomethylation of many gene loci[27]. Furthermore, in order to avoid the side effects of DMSO as raised so far, DMSO needs to be removed when actually used in clinical applications, etc. However, this process of removing DMSO results in fewer cells being recovered. Therefore, DMSO-free cryopreservation methods and alternative CPAs are being actively investigated.

Glycerol is non mutagenic and less toxic than DMSO. It also acts through salt buffering, binding with metal ions, and dehydration of cells, and suppresses intracellular freezing, thereby alleviating cell freezing stress[28-30]. However, glycerol also needs to be removed from the cells after thawing, and some cells may be lost in the process[31].

Sugars are mainly used as non-membrane permeable CPAs. Among them, trehalose is naturally found in high concentrations in the bodies of some yeasts, nematodes, tardigrades, etc., and these microorganisms are known to be resistant to extremely low temperatures and dryness[32-34]. Two hypotheses have been proposed regarding the cryoprotective mechanism of trehalose[35]. First, trehalose forms hydrogen bonds with biopolymers or promotes hydration of biopolymers, allowing cells to retain their functional structure. Second, it halts metabolic activity by forming a glass like matrix with low molecular mobility. However, trehalose has a very weak function as an extracellular CPA, and only when trehalose is present inside and outside cells can it exert a high

cryoprotective effect[36]. Common methods for introducing trehalose into cells include electroporation and expressing trehalose transporter 1 (TRET1) in cells[37, 38]. However, these methods have problems such as membrane damage due to electric shock and the need for genetic modification.

1.3.2 Antifreeze (glyco) Protein (AF(G)P)

Because the Antarctic and Arctic regions have extremely low temperatures and are covered with ice, organisms that live there have developed several survival strategies such as antifreeze peptides and extracellular polysaccharides[39]. AF(G)P is one of these, and has been discovered in various organisms such as diatoms, insects, and fish[40-42] (Figure 1.3).

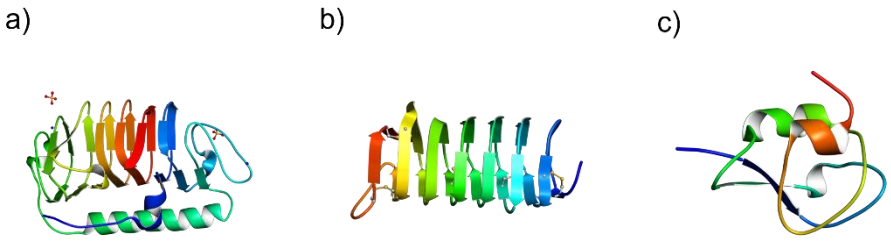

Figure 1.3 Structures of AFP. a) Snow mold fungus AFP[36] (PDB: 5B5H), b) *Choristoneura fumiferana* AFP[37] (PDB: 1Z2F), c) Fish Type III AFP[38] (PDB: 1UCS).

AF(G)P is thought to exert cryoprotective effects by lowering the freezing point through thermal hysteresis (TH) and inhibiting ice crystal formation through ice recrystallization inhibition (IRI). TH is caused by the interaction between AF(G)P and the ice crystal surface due to the difference between the freezing and melting points of the solution[43, 44]. Although the structure, TH, and IRI of AF(G)P differ among insects, fish, and plants, the mechanism of inhibition of ice crystal growth is common. First, the ice-binding surface (IBS) of AF(G)P recognizes ice crystals, and then AF(G)P and ice crystals bind[45]. Ice crystal growth is then inhibited by non-IBS[46]. Because non-IBS is a hydrophobic and charged structure, it effectively increases the curvature of the interface and lowers the local freezing point according to the Kelvin effect, suppressing the crystallization of the incoming water (Figure 1.4).

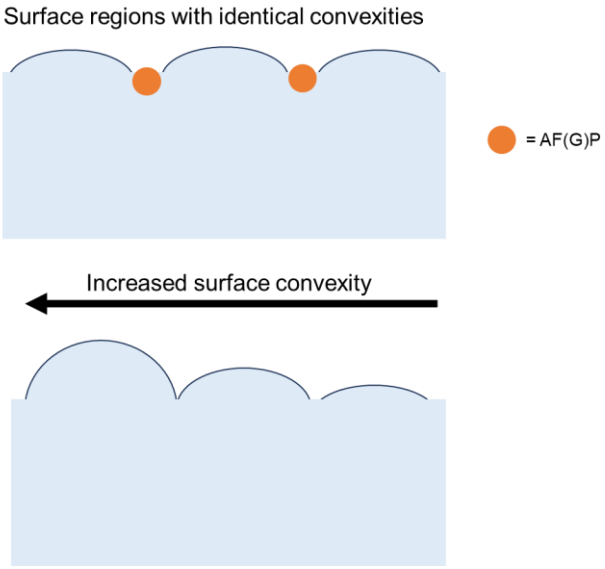

Figure 1.4 Inhibition of ice crystal growth by AF(G)P. When AF(G)P is bound to ice crystals, ice crystal growth is suppressed by the Kelvin effect.

Although AF(G)P is a naturally occurring CPA, it is not always suitable for cryopreservation due to drawbacks such as high cost, potential immunogenic and toxic effects, and needle-shaped ice crystals[47-49].

1.3.3 IRI active polymer

Many of the polymers used as CPAs focus on the IRI of AF(G)P (Figure 1.5). A typical CPA with IRI activity is polyvinyl alcohol (PVA)[50].

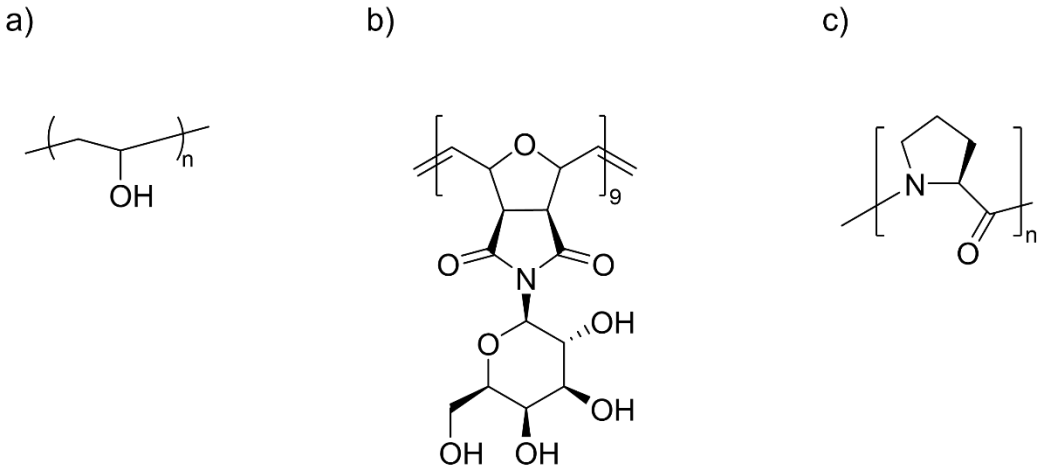

Figure 1.5 Structures of IRI active polymer; a) PVA, b) Facilly amphipathic glycopolymer[52], c) polyproline[53].

Because the atomic distance between hydroxy groups on the molecule (2.92 Å) is close to the prismatic plane of ice crystals (2.74 Å), PVA has higher IRI activity than commercial polymers such as poly(ethylene glycol) (PEG) and hydroxy ethyl starch (HES) used for CPAs[51]. However, when used alone, PVA does not have a very high cryoprotective effect, and other CPAs must be added. Other CPAs that mimic the three-

dimensional structure of AFGP are also being developed. In natural AF(G)P, isolated hydrophobic and hydrophilic groups are also known to be important factors in inhibiting ice crystal growth, and Graham et al. designed a glycopolymer to increase the solubility and IRI activity of the polymer[52]. In addition, since polyproline does not have an amide NH and cannot form intramolecular hydrogen bonds, it has amphipathic properties like type 1 AFP, which contains 70% alanine. Graham et al. have shown that polyproline has high IRI activity and improves the recovery of cell monolayers after cryopreservation compared to DMSO[53]. Furthermore, Qin et al. achieved cryopreservation of oocytes using polyproline[54]. However, these CPAs with IRI activity still have the problem of requiring the addition of DMSO as CPA.

1.3.4 Nanomaterials

Some use nanomaterials as ice crystal growth inhibitors (Figure 1.6). For example, graphene oxide (GO) exhibits a structure similar to natural AFP[55]. Due to the honeycomb-like structure of GO, the ice lattice matches the hydrogen bonds formed between the hydroxyl groups on the top surface of GO and the water and ice molecules, which greatly suppresses the growth of ice crystals[56]. Other carbon-based nanomaterials being studied include oxide quasi-carbon nitride quantum dots[57]. This is also thought to have a high affinity with ice because the interatomic distance on the surface is close to the

hexagonal ice prism surface, increasing IRI activity. In addition, the IRI activity of Zr-based metal-organic frameworks (MOFs) can be adjusted by adjusting the amount of hydrogen-donating groups on the (1,1,1) face of the MOF[58]. However, the cryoprotective effect of these nanomaterials is not very high.

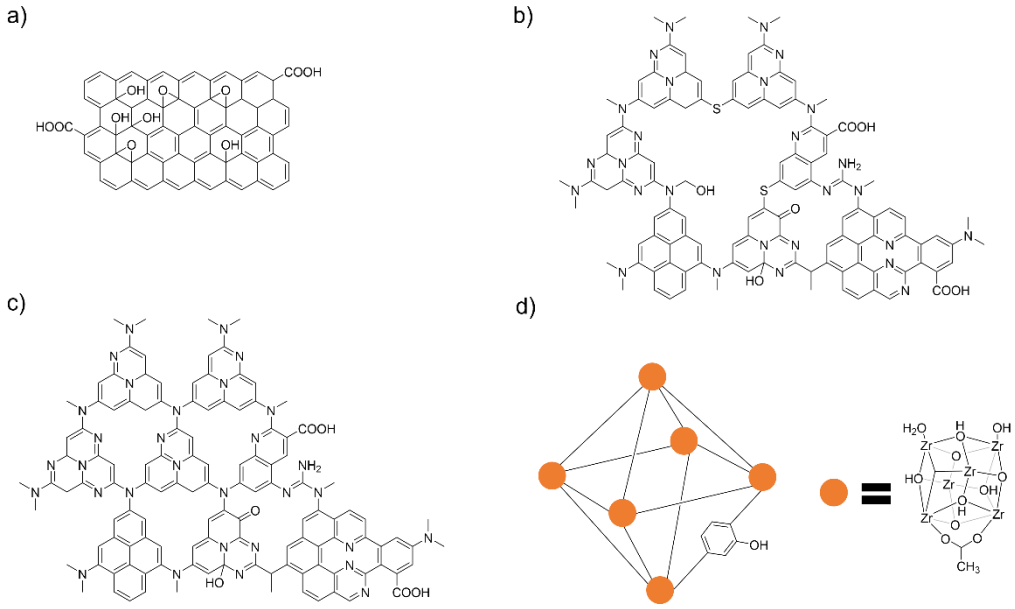

Figure 1.6 Structures of nanomaterial type CPAs. a) GO, b) sulphur-doped oxidized quasi-carbon nitride quantum dots[57], c) oxidized quasi-carbon nitride quantum dots[57], Zr based MOF (UiO-66-OH)[58].

1.4 Polyampholytes

1.4.1 About polyampholytes

Zwitterionic polymers are polymers that were first reported by Alfrey et al. in 1950. The entire polymer is composed of a mixture of charged regions, and due to the mixed charge

state of cations and anions, it has been associated with proteins[59, 60]. Commonly used functional groups include protonated amino, quaternary ammonium, and pyridine as cationic groups, and carboxylates, sulfonates, and phosphates as anionic groups[61-65] (Figure 1.7 a)). Zwitterionic polymers can be divided into two types: betaine types and polyampholyte types (Figure 1.7 b)).

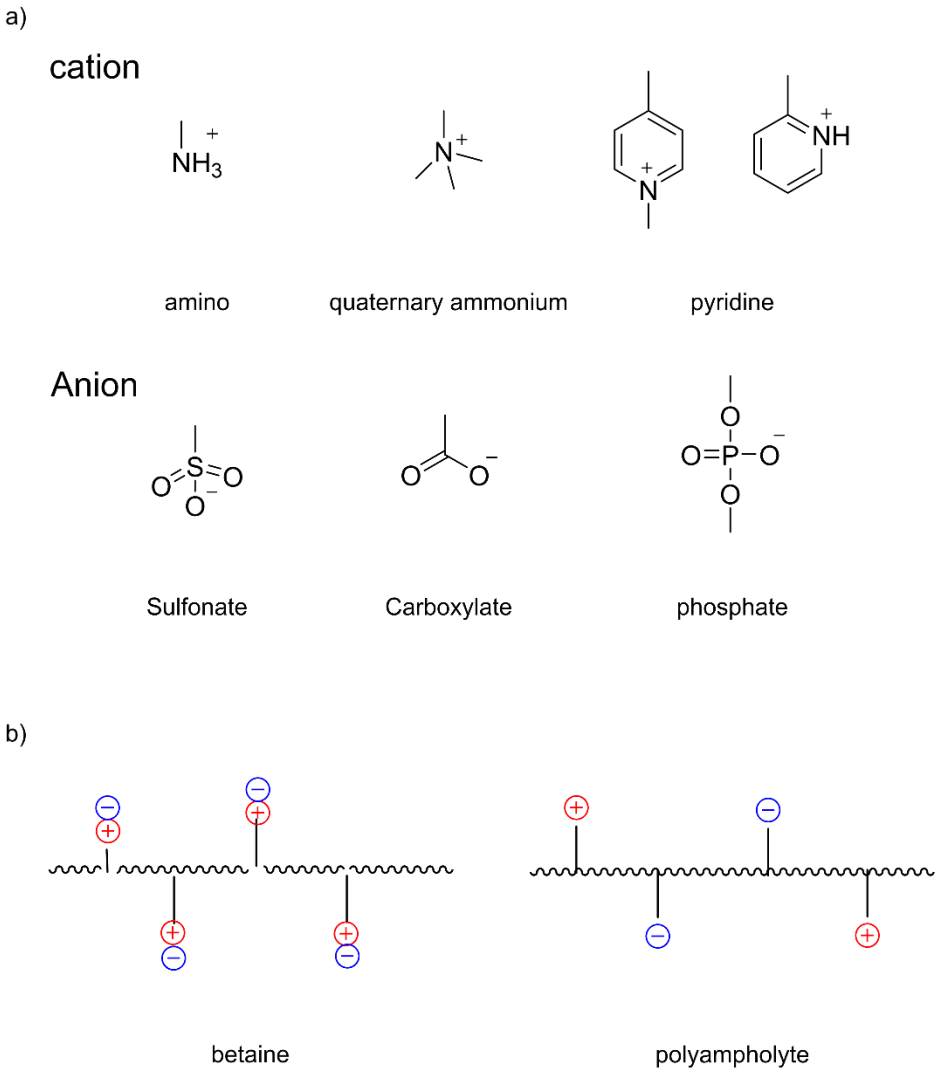

Figure 1.7 Structures of zwitterionic polymer. a) Commonly used cationic and anionic, b) Types of zwitterionic polymer.

Betaine type of polymers refers to a polymer that has both cation and anion regions in one side chain. There are equal numbers of positive and negative charges on the polymer, so the net charge is zero, and the electrostatic charge within the molecule upon interaction, it assumes a spherical folded conformation[61, 66, 67]. In addition, betaine polymer chains are salt responsive and swell due to external inorganic salts, which affects the mechanical properties of hydrogels, etc.[68]. In the polyampholyte type, the polymer is composed of a mixture of several charged monomers. Unlike betaine type of polymers, the charge can be easily adjusted by changing the ratio of monomers, so it has the advantage of allowing one charge to be dominant. Additionally, polymers with environmentally responsive properties can be designed based on the composition and structure of the polymer. These zwitterionic polymers have excellent hydrophilicity because they have abundant anions and cations in the polymer chain. Furthermore, the zwitterionic polymer selectively binds to oppositely charged species through electrostatic interactions, so it has pH responsiveness. Therefore, there is growing interest in applying polymer brushes to biomedical applications such as antifouling coatings and drug delivery systems (DDS)[61, 69].

1.4.2 Polyampholytes for cryopreservation

In addition to antifouling coatings and DDS, zwitterionic polymers are also being studied as CPAs (Figure 1.8). However, intracellular freezing and membrane adhesion due to dehydration rates and other factors are more important in actual cryoinjury. In fact, the cryoprotective effect of polymers with high IRI activity alone is low. It has also been reported that AFPs with similar IRI activity have different cryoprotective effects.

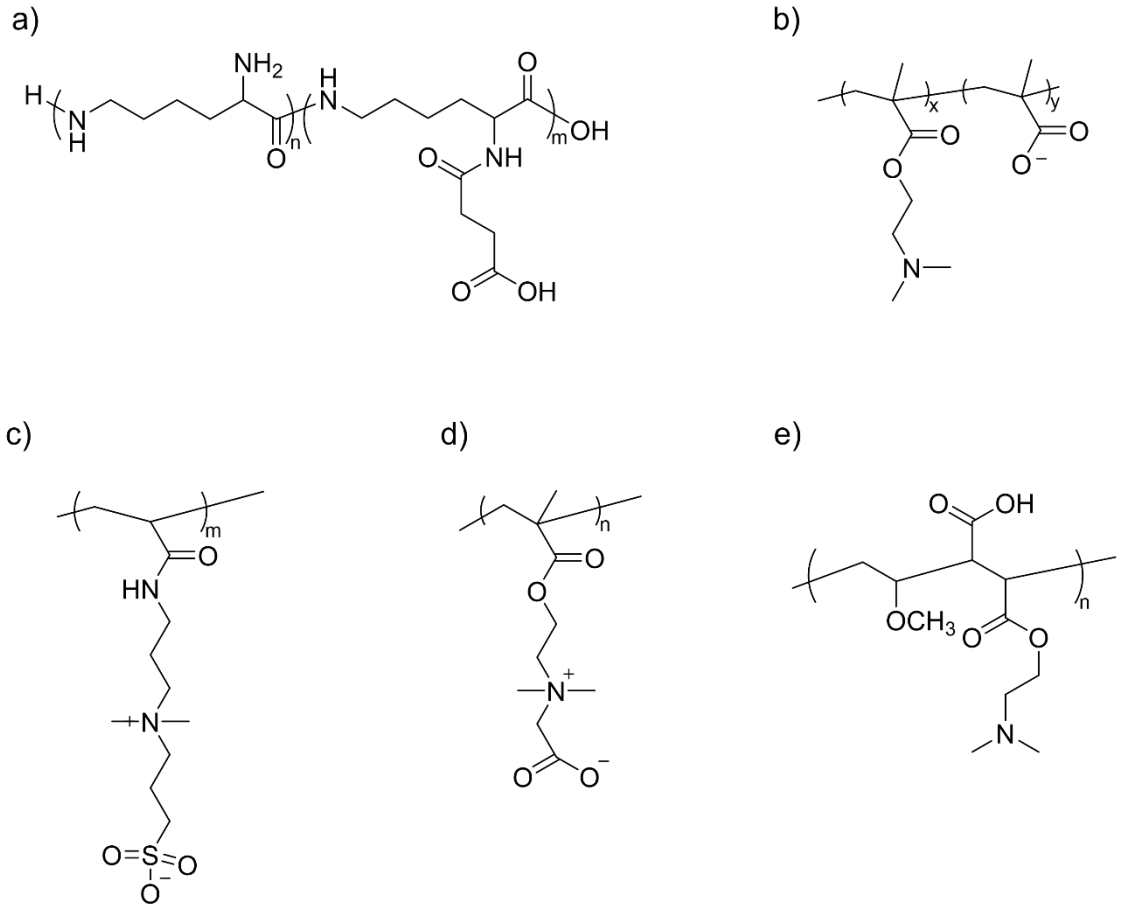

Figure 1.8 Structures of zwitterionic polymers for cryoprotectant. a) PLL-SA[66], b) poly(DMAEMA/MAA)[71], c) poly(SPB)[72], b) poly(CMB)[72], poly(DMAEMA/MAA) in alternating periodic arry[73].

Matsumura et al. synthesized carboxylated poly-L-lysine (PLL-SA), an polyampholyte, using ε-poly-L-lysine (PLL) and succinic anhydride (SA), and demonstrated its cryoprotective effect[70]. PLL-SA shows a high cryoprotective effect when the carboxyl group substitution rate is 50-76%. Rajan et al. also synthesized poly(DMAEMA/MAA) from methacrylic acid (MAA) and 2-(dimethylamino)ethyl methacrylate (DMAEMA) and showed a high survival rate in a 1:1 copolymer[71]. This polymer, like PLL-SA, was also found to have lower cytotoxicity compared to DMSO. Rajan et al. also reported cryoprotective effects for poly(SPB) with sulfobetain (SPB) and poly(CMB) with calboxybetain (CMB)[72]. These polyampholyte types CPAs are promising as new CPAs because the polymers can be cryopreserved on only polymer solution and are less cytotoxic than DMSO. There are many other studies on poly(DMAEMA/MAA) as CPAs, such as Zhao et al. reported on cell survival when the net charge of the polyampholyte is biased negatively, and Bailey et al. alternating periodic polymer[73, 74]. In PLL-SA, it is known that it is important to trap polymer water and salt and form a polymer matrix by using temperature-variable solid-state NMR[75] (Figure 1.9). However, for other polymers, although interaction with cell membranes is known to be important, the clear mechanism of cryoprotection is not known[72]. As a result, the advantages of methacrylate polymers such as poly(DMAEMA/MAA), such as free molecular design, are not exploited.

Therefore, in this study, by synthesizing polyampholytes with different side chain structures and similarly using temperature-variable solid-state NMR, I will correlate the polymer structure and cryoprotective effect and use this as a steppingstone to optimal molecular design of CPAs. In addition, as the present series of studies focused only on the cryoprotective function of the polymer, mouse fibroblasts were used as a model for the actual cryopreservation.

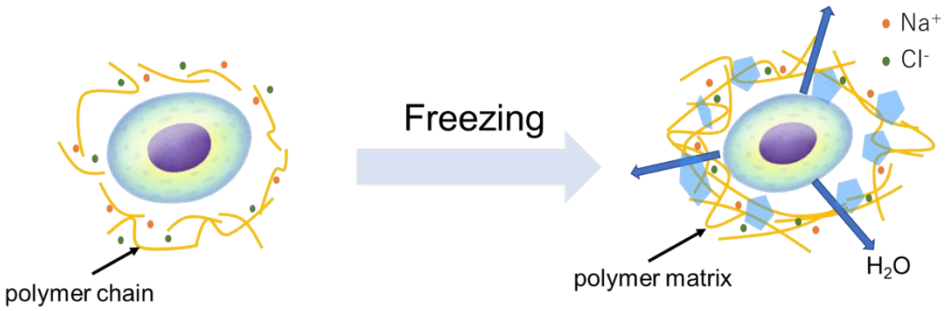

Figure 1.9 Cryoprotection mechanism of PLL-SA by temperature variable solid-state NMR[75].

1.5 Intracellular delivery of cryoprotectants

As already mentioned, trehalose, a membrane-impermeable CPAs, acts as water by forming hydrogen bonds with biomacromolecules and promoting hydration of biomacromolecules so that cellular components can maintain their functional conformation. It is also thought to obtain a cryoprotective effect by temporarily suspending metabolic activity by forming a glass like matrix with extremely low molecular

mobility. However, if trehalose exists only outside the membrane, the cryoprotective effect is not high, and it is thought that trehalose needs to be present inside and outside the cell. Therefore, research is underway to transport trehalose into cells to enhance the cryoprotective effect (Figure 1.10). However, although there are various options for transporting trehalose, they reduce membrane stability and require genetic modification of cells, which limits their use in clinical applications and reduces their cryoprotective effects.

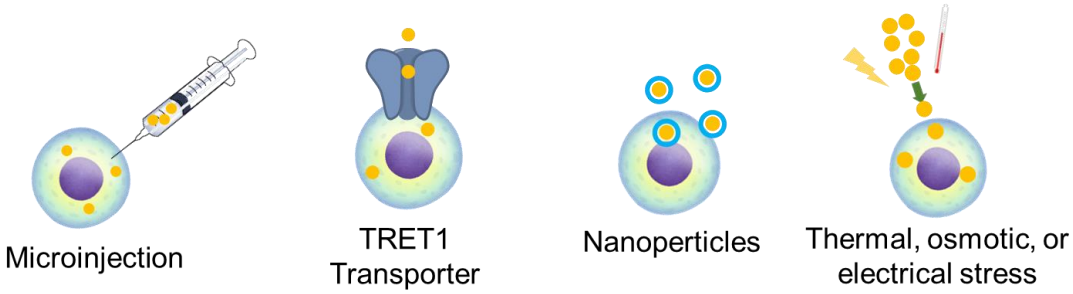

Figure 1.10 Methods of Intracellular delivery trehalose.

It has been reported that the cryoprotective effect of polymeric CPAs can be enhanced by transporting PEG with a low degree of polymerization into cells[76]. In other reports using polymers with the same DMSO structure for cryopreservation, poly(methyl glycidyl sulfoxide) with a PEG structure in the main chain was as effective as DMSO in cryoprotection, whereas when methacrylate polymers were used, the cryoprotective effect methacrylate polymers showed lower cryoprotection[77 78]. The difference between these two polymers is that the polymer with a PEG main chain permeates into cells, whereas

the methacrylate polymer does not permeate into cells. However, these polymers have problems such as long incubation times and endocytosis. It has also been proposed that cytoplasmic macromolecular condensation reduces cytoplasmic free water, providing cells with a rapid thermodynamically driven defense against rapid fluctuations in osmotic strength, temperature, and pressure[79]. Therefore, it is thought that the efficiency of cryoprotection can be increased by transporting the polymer into cells. Here, I will summarize intracellular transport of trehalose and polymers.

1.5.1 Phospholipid-phase transition

The first method to introduce trehalose into cells was to utilize the phase transition of phospholipids. By inducing the phase transition of phospholipids by heat, osmotic pressure, and electrical stress, the permeability of the cell membrane is increased and the transport of trehalose is made possible. In the heat based method, trehalose is transported into the cytoplasm by incubating the cell suspension for about 10 minutes and then placing the suspension at 0 and 39 ° C for up to 2 hours every 10 minutes.[80]. In the osmotic method, trehalose can be transported by incubating it for up to 7 hours in extracellular trehalose at an isotonic pressure or higher[81]. This method may cause cell morphological changes due to prolonged exposure to hypertonic solutions. The electrical method is called electroporation, and it can temporarily and reversibly increase the cell

membrane by applying a short external electric field pulse[37]. However, as with other methods, reduced membrane stability can make it vulnerable to osmotic shock during freezing and thawing.

1.5.2 TRET1

Some organisms that utilize trehalose to enable survival in cold environments have a trehalose transporter known as TRET1 that allows trehalose to accumulate within cells under environmental stress. By expressing TRET1 in cells to be cryopreserved, trehalose can be taken into the cells, and desiccation tolerance and cryoprotection effects are enhanced compared to cells that do not express TRET1[38]. However, because genetic modification of the cells is required, frozen and thawed cells may not be able to be used for actual clinical applications.

1.5.3 Microinjection

Microinjection is the most direct method of introducing trehalose into cells. Eroglu et al. successfully delivered trehalose to discarded human oocytes and frozen them in the presence of extracellular trehalose, and subsequent studies of trehalose-containing oocytes showed good survival rates after cryopreservation[82]. However, this method is not suitable for other cells that are smaller and need to be cryopreserved in large quantities.

1.5.4 Nanoparticles

Nanoparticles are also used in the DDS field, and in the cryopreservation field, they are mainly used to transport trehalose into cells. For example, Rao et al. used pH responsive genipin-cross-linked Pluronic F127-chitosan nanoparticles as nanoparticles to transport and cryopreserve trehalose into primary human adipose-derived stem cells[83]. It has been reported that when trehalose is transported using these nanoparticles, the cell survival rate after thawing is comparable to that of DMSO. In addition, Zhang et al. used low temperature responsive poly(N-isopropylacrylamide-co-butyl acrylate) as nanoparticles for cryopreservation[84]. Unlike Rao et al. nanoparticles, which required 24-hour incubation before cryopreservation, these nanoparticles can transport trehalose into cells in about four hours. It was also shown that even when these nanoparticles were used, the cell survival rate was comparable to that of DMSO. However, methods using such nanoparticles utilize cellular endocytosis, which poses problems such as escape from lysosomes.

1.5.5 Intracellular delivery of polymers

Methods for introducing polymers into cells include methods in which polymer micelles are taken into cells via endocytosis, and methods such as cationic polymers and transmembrane peptides (CPP) that enter cells by making minute holes in the cell membrane[84, 86]. However, when a cationic polymer or CPP is used, it creates minute pores

in the cell membrane, which may cause excessive dehydration during freezing and affect cell growth after thawing. When it is taken up via endocytosis, it is taken up into lysosomes and does not spread throughout the cell. Poly(SPB), which is a betaine polymer, and poly(MPC/BuMA), which is a copolymer of 2-methacryloyloxyethyl phosphorylcholine (MPC) and butyl methacrylate (BuMA), penetrate the entire cytoplasm without going through endocytosis[87-89]. Poly(SPB) has also been reported to have a cryoprotective effect, so it can be said to be very useful for intracellular transport of CPAs[72].

1.6 Spheroid

Most studies in cell biology are performed using cells of interest cultured in 2D monolayers. However, since the actual cellular environment is three-dimensional, a 2D monolayer cannot simulate the complexity and dynamic interactions of the microenvironment[90]. Therefore, three-dimensional cell structures such as spheroids, which can better reproduce the in vivo environment, are attracting attention[91-93]. Since serial cell culture consumes many resources, long term preservation of three-dimensional cell structures is important for industrial use. However, while cryopreservation of suspended cells has been achieved by various CPAs, cryopreservation of three-dimensional cellular constructs is more difficult due to their complexity. There have been some reports on cryopreservation of spheroids, but these require the use of ice nucleating

agents or small molecules CPAs[94, 95].

1.7 Research objects

As mentioned above, the details of the cryoprotective mechanism of polyampholytes such as poly(DMAEMA/MAA), which have a high cryoprotective effect, are unknown. A more detailed understanding of the relationship between the cryoprotection mechanism and polymer structure will provide important guidance for the molecular design of CPAs. Therefore, in Chapter 2, the cryoprotective effects of poly(DMAEMA/MAA) and polymers with different side chain structures are correlated with their structures using variable temperature solid-state NMR, with the aim of elucidating the cryoprotection mechanism. In Chapters 3 and 4, I took advantage of the property of zwitterionic polymers to permeate into cells and developed a new approach to use sulfobetaine polymers as intracellular permeating CPAs. Furthermore, I attempted cryopreservation of spheroids to achieve cryoprotection of three-dimensional cellular constructs. Understanding the cryoprotective mechanisms of these polyampholytes and the use of zwitterionic polymers as intracellularly permeable CPAs will be of great importance for the strategic synthesis of CPAs and for the cryopreservation of more complex tissues.

1.8 Reference

1) N. Blow, *Nat. Methods*, 2009, **6(2)**, 173-177.

2) M. D. Vos, J. Smitz, and T. K. Woodrudff, *Lancet*, 2014, **384**, 1302-1310.

3) T. Takahashi, A. Hirsh, E. Erbe and, R. J. Williams, *Biophys J.*, 1988, **54**,(3) 509-518.

4) C. Polge, A. U. Smith and A. S. Parkes, *Nature*, 1949, **15**, 666.

5) M. Ollero, R. P. -Pe, T. M. -Blanco and J. A. C. -Perez, *Cryobiology*, 1998, **37**, 1-12.

6) M. Legender and R. Billard, *Reprod. Nutr. Develop.*, 1980, **20**, 6, 1859-1868.

7) T. Sugawara and A. Sakai, *Plant Physiol.*, 1974, **54**, 722-724.

8) A. U. Smith, *Lancet*, 1950, **2**, 910-911.

9) J. E. Lovelock and M. W. H. Bishop, *Nature*, 1959, **183**, 1394-1395.

10) N. Zhang, W. Li, C. Chen and J. Zuo, *Comput. Theor. Chem.*, 2013, **1017**, 126-135.

11) N. Gosh, S. Roy, M. Ahmed and J. A. Mondal, *J. Mol. Liq.*, 2018, **266**(15) 118-121.

12) U. Farooq, Z. Haider, Z. M. Liang, K. Memon, S. M. C. Hassain, Y. Zhang, H. Xu, A. Qadir, F. Panhwar, G. Zhao and J. Luo, *Small*, 2019, **15**, 1805361

13) D. Niu, G. Zhan, Xiaoli. Liu and Y. Cao, *Tissue Eng. Part C: Methods*, 2016, **22**(3), 270-279.

14) J. O. M. Karlsson and M. Toner, *Biomaterials*, 1996, **17**, 243-256.

15) G. M. Fahy, *Cryobiology*, 1986, **123**, 1-13.

16) J. -E. Oh, K. K. Raja, J. -H. Shin, A. Pollak, M. Hengstschläger and G. Lubec, *Amino Acids*, 2006, **31**, 289-298.

17) C. J. Hunt, *Methods Mol. Biol.* 2017, **1590**, 41-77.

18) L. L. Kuleshova, S.S Gouk and D. W. Hutmacher, *Biomaterials*, 2007, **28**(9), 1585-1596.

19) P. Mazur and J Gen, *Physiol.*, 1963, **47**, 2, 347-69.

20) A. Bissoyi, B. Nayak, K. Pramanik and S. K. Sarangi, *Biopreserv. Biobank.*, 2014, **12**(1), 23-34.

21) P. Mazur, *Cryobiology*, 1977, **14**, 251-272.

22) A. Fowler and M. Toner, *Ann. N. Y. Acad*, 2006, **1066**, 1, 119-135.

23) B. Jin, K. Kusanagi, M. Ueda, S. Seki, D. M. Valdez Jr., K. Edashige and M. Kasai, *Cryobiology*, 2008, **56**(3), 233-240.

24) A. Donmez, M. Tombuloglu, A. Gunger, N. Soyer, G. Saydam, S. Cagirga, *Transfus. Apher. Sci.*, 2007, **36**(1), 95-101.

25) R. Cordoba, R. Arrieta, A. Kerguelen and F. H.-Navarro, *Bone Marrow Transplantation*, 2007, **40**, 1063-1067.

26) I. Mitrus, A. Smagur, W Fidyk, M. Czech, M. Prokop, A. Chwieduk, M. G.-Kosinska, T. Czerw, M. S.-Kruszelnicka, W. Mendrek, K. Michalak, M. S.-Wojciechowska, J.

Najda, J. Holowiecki, S. Giebel, *Bone Marrow Transplantation*, 2018, **53**, 274-280.

27) M. Iwatani, K. Ikegami, Y. Kremenska, N. Hattori, S. Tanaka, S. Yagi, K. Shiota, D.V.M, *Stem Cells*, 2006, **24**(11), 2549-2556.

28) J. E. Lovelock, *Biochem Biophys Acta,* 1953, **11**, 28-36.

29) W. Lohamann, C. F. Flower, A. J. Moss and W. H. Perkis, *Experientia*, 1964, **20**, 290-293.

30) P. J. Bredderman and R. H. Foote, *J Dairy Sci*, 1969, **28**, 496-501

31) P. Cregan, E. Donegan MD and G. Gotelli, *Transfusion*, 1991, **31**(2), 172-175.

32) J. H. Crowe and L. M. Crowe, *Nat. Biotechnol.*, 2000, **18**, 145-146.

33) M. Potts, *Microbiol. Rev.*, 1994, **58**(4), 755-805.

34) M. Watanabe, T. Kikawada, N. Minagawa and T. Okuda, *J. Exp. Biol.*, 2002, **205**(18), 2799-2802.

35) J. H. Crowe, J. F. Carpenter and L. M. Crowe, *Annu. Rev. Physiol.*, 1998, **60**, 73-103.

36) J. H. Crowe, L. M. Crowe, W. F. Wolkers, A. E. Oliver, X. Ma, J-H. Auh, M. Tang, S. Zhu, J. Norris and F. Tablin, *Integr. Comp. Biol.*, 2005, **45**, 810-820.

37) R. Shirakashi, C. M. Köstner, K. J. Müller, M. Kürschner, U. Zimmermann and V. L. Sukhorukov, *J. Membrane Biol.*, 2002, **189**, 45-54.

38) T. Uchida, M. Furukawa, T. Kikawada, K. Yamazaki and K. Gohara, *Cryobiology*, 2017,

77, 50-57.

39) P. D. Maayer, D. Anderson, C. Cary and D. A. Cowan, *EMBO Rep.*, 2014, **15**, 508-517.

40) J. Cheng, Y. Hanada, A. Miura, S. Tsuda and H. Kondo, *Biochem. J.*, 2016, **473**(21), 4011-4026.

41) C. Li, X. Guo, Z. Jia, B. Xia and C. Jin, *J. Biomol. NMR*, 2005, **32**, 251-256.

42) T. -P. Kon, H. Robinson, Y. -G. Gao, C. -H. C. Cheng, A. L. DeVries and A. H. -J. Wang, *Biophys. J.*, 2003, **84**, 1228-1237.

43) A. Flores, J. C. Quon, A. F. Perez and Y. Ba, *Eur. Biophys. J.*, 2018, **47**, 611-630.

44) L. L. C. Olijve, K. Meister, A. L. DeVries, J. G. Duman, S. Guo, H. J. Bakker and I. K. Voets, *Proc. Natl. Acad. Sci. U. S. A.*, 2016, **113**(14), 3740-3745.

45) A. Hudait, N. Odendahi, Y. Qiu, F. Paesani and V. Molinero, *J. Am. Chem. Soc.*, 2018, **140**(14), 4905-4912.

46) S. Chakraborty and B. Jana, *Langmuir*, 2017, **33**(28), 7202-7214.

47) C. Koshimoto and P. Mazur, *Cryobiology*, 2002, **45**(1), 49-59.

48) H. Chao, P. L. Davies and J. F. Carpenter, *J. Exp. Biol.*, 1996, **199**(9), 2071-2076.

49) K. Nishijima, M. Tanaka, Y. Saki, C. Koshimoto, M. Morimoto, T. Watanabe, J. Fan and S. Kitajima, *Cryobiology*, 2014, **69**(1), 22-25.

50) R. C. Deller, M. Vatish, D. A. Mitchell and M. I. Gibson, *Nat. Commun.*, 2014, **5**, 3244.

51) C. Stubbs, L. E. Wilkins, A. E. E. Fayter, M. Walker and M. I. Gibson, *Langmuir*, 2019, **35**(23), 7347-7353.

52) B. Graham, A. E. R. Fayter, J. E. Houston, R. C. Evans and M. I. Gibson, *J. Am. Chem. Soc.*, 2018, **140**(17), 5682-5685.

53) B. Graham, T. L. Bailey, J. R. J. Healey, M. Marcellini, S. Deville and M. I. Gibson, *Angew. Chem. Int. Ed.*, 2017, **56**, 15941-15944.

54) Q. Qin, L. Zhao, Z. Liu, T. Liu, J. Ou, X. Zhang, R. Li, L. Yan, J. Yan, S. jin, J. Wang and J. Qian, *ACS Appl. Mater. Interface*, 2020, **12**(16), 18352-18362.

55) G. Bai, D. Gao, Z. Liu, X. Zhou and J. Wang, *Nature*, 2019, **576**, 437-441.

56) H. Geng, X. Liu, G. Shi, G. Bai, J. Ma, J. Chen, Z. Wu, Y. Song, H. Fang and J. Wang, *Angew. Cheme. Int. Ed.*, 2017, **56**, 997-1001.

57) G. Bai, Z. Song, H. Geng, D. Gao, K. Liu, S. Wu, W. Rao, L. Guo and J. Wang, *Adv. Mater.*, 2017, **29**, 1606843.

58) W. Zhu, J. Guo, J. O. Agola, J. G. Croissant, Z. Wang, J. Shang, E. Coker, B. Motevalli, A. Zimpel. S. Wuttke and C. J. Brinker, *J. Am. Chem. Soc.*, 2019, **141**(19), 7789-7796.

59) T. Alfrey. Jr. et al., *J. Am. Chem. Soc.*, 1950, **72**(4), 1864.

60) S. E. Kudaibergenov, *Adv Polym Sci.*, 1999, **144**, 155-197.

61) C. Ziemba, M. Khavkin, D. Priftis, H. Acar, J. Mao, M. Benami, M. Gottleb, M. Tirrell, Y. Kaufman and Moshe Herzberg, *Langmuir*, 2019, **35**(5), 1699-1713.

62) A. B. Ihsan, T. L. Sun, T. Kurokawa, S. N. Karobi, T. Nakajima, T. Nonoyama, C. K. Roy, F. Luo and J. P. Gong, *Macromolecules*, 2016, **49**(11), 4245-4252.

63) E. Su and O. Okay, *Eur. Polym. J.*, 2017, **88**, 191-204.

64) A. Laschewsky and A. Rosenhahn, *Langmuir*, 2019, **35**(5), 1056-1071.

65) M. Debayle, E. Balloul, F. Dembele, X. Xu, M. Hanafi, F. Ribot, C. Monzel, M. Coppey, A. Fragola, M. Dahan, T. Pons and N. Lequeux, *Biomaterials*, 2019, **219**, 119357.

66) M. Kikuchi, Y. Terayama, T. Ishikawa, T. Hoshino, M. Kobayashi, N. Ohta, H. Jinnai and A. Takahashi, *Macromolecules*, 2015, **48**(19), 7194-7204.

67) F. Wang, J. Yang and J. Zhao, *Polym. Int.* 2015, **64**, 999-1005.

68) B. Yang and W. Yuan, *ACS Appl. Matter. Interface*, 2019, **11**(43), 40620-40628.

69) D. Zhao, R. Rajan and K. Matsumura, *ACS Appl. Matter. Interface*, 2019, **11**, 43, 39459-39469.

70) K. Matsumura and S. -H. Hyon, *Biomaterials,* 2009, **30**, 4842-4849.

71) R. Rajan, M. Jain and K. Matsumura, *J. Biomater. Sci., Polym. Ed.*, 2013, **24**(15), 1767-1780.

72) R. Rajan, F. Hayashi, T. Nagashima and K. Matsumura, *Biomacromolecules*, 2016, **17**(5), 1882-1893.

73) J. Zhao, M. A. Johnson, R. Fisher, N. A. D. Burke, and H. D. H. Stöver, *Langmuir*, 2019, **35**(5), 1807-1817.

74) T. L. Bailey, C. Stubbs, K. Murray, R. M. F. Tomás, L. Otten and M. I. Gibson, *Biomacromolecules*, 2019, **20**, 3104-3114.

75) K. Matsumura, F. Hayashi, T. Nagashima, R. Rajan and S. -H. Hyon, *Commun. Mater.*, 2021, **2**, 15.

76) M. Patel, J. K. Park and B. Jeong, *Biomater. Res.*, 2023, **27**, 17.

77) A. A. Burkey, A. Hillsley, D. T. Harris, J. R. Baltzegar, D. Y. Zhang, W. W. Sprague, A. M. Rosales and N. A. Lynd, *Biomacromolecules*, 2020, **21**(8), 3047-3055.

78) T. Ishibe, N. -G. Martinez, P. G. Georgiou, K. A. Murray and M. I. Gibson, *ACS Polym. Au*, 2022, **2**(6), 449-457.

79) J. L. Watoson, E. Seinkmane, C. T. Styles, A. Mihut, L. K. Krüger, K. E. McNally, V. J. P. _Herrero, M. Dudek, P. M. McCall, S. Barbiero, M. V. Oever, S. Y. P. -Chew, B. T. Poresbski, A. Zheng, N. M. Rzechorzek, D. C. S. Wong, A. D. Beale, A. Stangherlin, M. Riggi, J. Iwasa, J. Morf, C. Mikiotis, A. Guna, A. J. Inglis, J. Brugués, R. M. Voorhees, J. E. Cambers, Q. -J. Meng, J. S. O'Neill, R. S. Edgar and, E. Derivery,

Nature, 2023, https://doi.org/10.1038/s41586-023-06626-z.

80) X. He, A. A. Amin, A. Flowler and M. Toner, *Cell Preserv. Technol.*, 2006, **4**, 178-187.

81) G. R. Satpathy, Z. Török, R. Bali, D. M. Dwyre, E. Little, N. J. Walker, F. Tablin, J. H. Crowe and N. M. Tsvetkava, *Cryobiology*, 2004, **49**(2), 123-136,

82) A. Eroglu, M. Toner and T. L. Toth, *Fertil. Steril*, 2002, **77**(1), 152-158.

83) W. Rao, H. Huang, H. Wang, S. Zhao, J. Dumbleton, G. Zhao and X. He, *ACS Appl. Mater. Interfaces,* 2015, **7**(8), 5917-5028.

84) Y. Zhang, H. Wang, S. Stewart, B. Jiang, W. Ou, G. Zhao and X. He, *Nono Lett.*, 2019, **19**(12), 9051-9061.

85) H. Hillaireau and P. Couvreur, *Cell. Mol. Life Sci.*, 2009, **66**, 2873-2896.

86) E. Koren and V. P. Torchilin, *Trends Mol. Med.*, 2012, **18**(7), 385-393.

87) T. Goda, Y, Imaizumi, H. Hatano, A. Matsumoto, K. Ishihara and Yuji Miyahara, *Langmuir*, 2019, **35**(24), 8167-8173.

88) N. Morimoto, M. Wakamura, K. Muramatsu, S. Toita, M. Nakayama, W. Shoji, M. Suzuki and F. M. Winnik, *Biomacromolecules*, 2016, **17**(4), 1523-1535.

89) T. Goda, H. Hatano, M. Yamamoto, Y. Miyahara and N. Morimoto, *Langmuir*, 2020, **36**(33), 9977-9984.

90) J. Rodrigues, M. A. Heinrich, L. M. Teixeira and J. Prakash, *Trends Cancer*, 2021,

7(3), 249-264.

91) B. Desoize and J. -C. Jardililier, *Crit. Rev. Oncol. Hematol.*, 2000, **36**(2-3), 193-207.

92) K. Kwapiszewska, A. Michalczuk, M. Rybka, R. Kwapiszewski and Z. Brzózka, *Lab Chip*, 2014, **14**, 2096-2104.

93) J. Zhao, X. Liang, H. Cao and T. Tan, *Bioresour. Bioprocess.*, 2020, **7**, 1.

94) Y. Gao, A. Bissoyi, N. L. H. Kinney, T. F. Whale, Q. Guo and M. I. Gibson, *Chem. Commun.*, 2023, **59**, 9086.

95) K. Matsumura, S. Hatakeyama, T. Naka, H. Ueda, R. Rajan, D. Tanaka and, S. -H. Hyon, *Biomacromolecules*, 2020, **21**(8), 3017-3025.

Chapter 2

Relationship between side chain structure of polyampholytes and cryoprotective effect

2.1 Introduction

Understanding the cryoprotection mechanism of polyampholytes and correlating their structure and function will provide important knowledge for developing new cryoprotectants. Furthermore, the possibility of application of polyampholyte type cryoprotectants to regenerative medicine, etc. increases. Fluorescence staining with fluorescein isothiocyanate has shown that carboxylated polylysine (PLL), a polyampholyte, is a non-membrane permeable substance and that its cryoprotective effect is expressed outside the membrane[1]. In addition, temperature-variable solid-state NMR has shown that PLL traps water and salt during freezing, forming a polymer matrix that prevents a rapid increase in osmotic pressure and intracellular ice formation due to contact with extracellular ice crystals[2]. Another polyampholyte that has been reported to have a high cryoprotective effect is poly(2-(dimethyl amino)ethyl methacrylate (DMAEMA)/methacrylic acid (MAA)) (pD)[3-5]. Although the interaction between the polymer and cell membrane is thought to be important for this polyampholyte, its cryoprotective mechanism is not clear, which hinders the optimal molecular design of

cryoprotectants[4].

Therefore, in Chapter 2, I first synthesized four types of polyampholytes with different side chain structures. The first is the previously reported pD. The second is poly(2-acrylamido-2-methyl propanesulfonic acid (AMPS)/(3-acrylamidopropyl)trimethyl ammonium chloride (APTAC)) (pA), which has a higher degree of dissociation than pD because the anion is sulfonic acid and the cation is quaternary ammonium. In addition, poly(vinyl acetate (VA)/acrylic acid (AA)/2-(dimethyl amino)ethyl acrylate (DMAEA)) (pV) and poly(methyl vinyl ether (MVE)/AA/ DMAEA) (pM), which have the same dissociation degree as pD but different molecular weight, were synthesized. Also, while pD is a random copolymer, pV and pM have cations and anions arranged alternately. After polymer synthesis, physicochemical properties of solvents and solutes under freezing were observed using temperature-variable solid-state Magic-Angle-Spinning (MAS) NMR to correlate solution properties with cryoprotective effects and side chain structures. Correlating the polymer structure and cryoprotective effect in this way will deepen our understanding of the cryoprotection mechanism and lead to the optimal molecular design of cryoprotectants.

2.2 Materials & methods

2.2.1 Materials

AMPS, APTAC (74~76 % in water), 2-(dimethylamino)ethyl methacrylate, vinyl acetate monomer, maleic anhydride (MA), 2-(dimethyl amino)ethanol, potassium ethylxanthate and benzyl bromide, succinic anhydride(SA) were purchased from Tokyo Chemical Industry Co. (Tokyo, Japan); MAA was purchased from Fuji Film Wako Pure Chemical Co. (Osaka, Japan); 25 %(w/w) ε-poly-l-lysine was purchased from JNC Co. (Tokyo, Japan); Poly (MVE-alt-MA) (average Mw ~216000), 2-(dodecylthiocarbonothioylthio)-2-methylpropionic acid (DDMAT) and 4,4'-azobis(4-cyanovaleric acid) (V-501) were purchased from Sigma-Aldrich (St. Louis, MO, USA). All the reagents were used as received without further purification.

2.2.2 Characterization

^{1}H NMR for synthesized materials characterization was measured using a Bruker Avance III 400. The deuterated solvent used was purchased from Sigma-Aldrich. The NMR data were analysed using Topspin 3.5 software. The molecular weights and distributions (polydispersity index; PDI) of the polymers were determined by gel permeation chromatography (GPC; BioSep-s2000, Phenomenex, Inc., CA, USA) using a Waters Alliance HPLC system. A PBS was used as the mobile phase (flow rate, 0.75

mL/min) and pullulan as the standard.

2.2.3 Synthesis of pA

Scheme 1 shows the pA synthesis. AMPS (0.829 g, 4 mmol) was dissolved in 3 ml of water, and AMPS was neutralized by adding 780 μl of 5M NaOH (AMPS-Na). APTAC (1.102 g, 4 mmol), DDMAT (0.0729 g, 0.2 mmol), and V-501 (0.0112 g, 0.04 mmol) were dissolved in 12 ml of methanol and added to AMPS-Na. After N_2 bubbling for 1 hour, the reaction was carried out at 70 ° C for 1 hour. After the reaction was completed, a sample was taken out and the monomer conversion was determined by ^{1}H NMR. The polymer was obtained by dialysis against distilled water for 24 hours using a dialysis membrane (Mw 3500, Repligen Corp., Waltham, MA ,USA) and then freeze-drying. The structure of the compound was determined by ^{1}H-NMR and ^{13}C NMR using D_2O as a solvent.

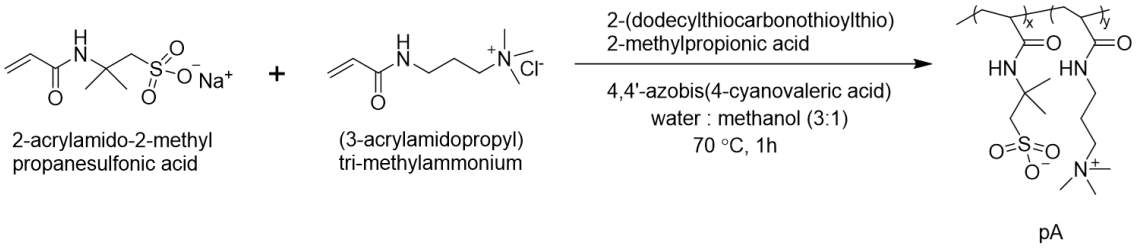

Scheme 2.1 Synthesis of pA.

2.2.4 Synthesis of pD

Scheme 2 shows the pD synthesis. MAA (0.344 g, 4 mmol) and DMAEMA (0.629 g, 4

mmol) were added to 20 ml of water and methanol mixed solvent (1:1 [v/v]). Then DDMAT (0.0729 g, 0.2 mmol) and V-501 (0.0112 g, 0.04 mmol) were added. After N_2 bubbling for 1 hour, the reaction was carried out at 70° C for 24 hours. After the reaction was completed, a sample was taken out and the monomer conversion was determined by ^{1}H NMR. The polymer was reprecipitated against 2-propanol, recovered by centrifugation, and dried in vacuum. The structure of the compound was determined by

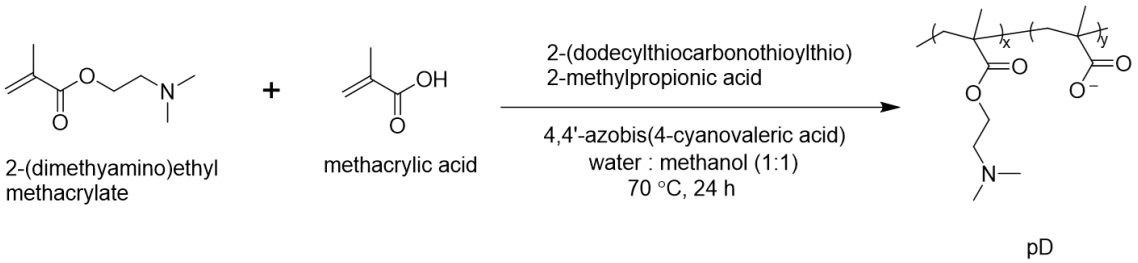

Scheme 2.2 Synthesis of pD.

^{1}H-NMR using D_2O as a solvent.

2.2.5 Synthesis of *S*-benzyl-*O*-ethyl dithiocarbonate

S-benzyl-*O*-ethyl dithiocarbonate was synthesized according to a previous report[6] (Scheme 2.3). Specifically, first, Potassium ethylxanthate (0.8 g, 5.0 mmol) was dissolved in 10 ml of ethanol at 50 ° C. Benzyl bromide (590 μl, 5.0 mmol) was added as is, and the reaction was allowed to proceed for 5 hours. After the reaction was completed, 30 ml of water was added, and the mixture was extracted three times with 25 ml of diethyl ether. It was dried over $MgSO_4$ and the solvent was removed on a rotary evaporator (0.75 g,

yield 70.6%). ^{1}H NMR ($CDCl_3$, 400 MHz): δ -7.55-7.20 (m, 5H, Ar-H), 4.68 (q, 2H,

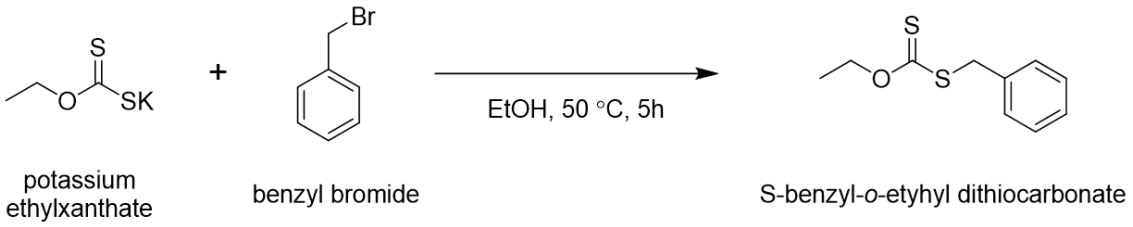

Scheme 2.3 Synthesis of poly(VA-*alt*-MA).

OCH2), 4.39 (s, 2H, SCH2), 1.44 (t, 3H, CH3).

2.2.6 Synthesis of poly(VA-*alt*-MA)

Scheme 4 shows the synthesis of poly(VA-alt-MA). VA (1.0 g, 11.6 mmol), MA (1.96 g, 20 mmol), S-benzyl-O-ethyl dithiocarbonate (80 mg, 0.337 mmol) and V-501 (15.1 mg, 0.054 mmol) were dissolved in 8 ml of dioxane. N_2 bubbling was performed for 1 hour, and the reaction was carried out at 80 ° C for 16 hours. After 16 hours, the reaction was terminated by immersing the flask in liquid nitrogen. After returning to room temperature, the product was reprecipitated in diethyl ether. The polymer was collected by centrifugation and dried under vacuum overnight. The structure of the compound was determined by ^{1}H-NMR and ^{13}C NMR using DMSO-d_6 as a solvent.

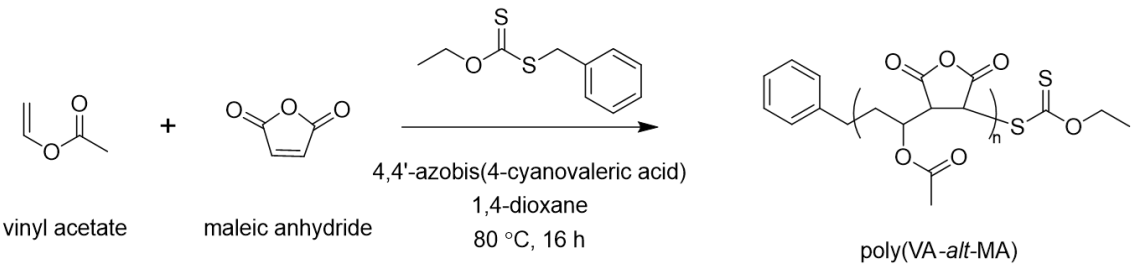

Scheme 2.4 Synthesis of poly(VA-*alt*-MA).

2.2.7 Modification of poly(VA-*alt*-MA) and poly(MVE-*alt*-MA) with 2-(dimethyl amino)ethanol

The synthesis of alternating array polyampholytes are shown in Scheme 2.5. 2 g of polymer was dissolved in 50 ml of THF and heated to 50° C. After dissolution, excess addition of 2-(dimethyl amino)ethanol (4 g, 44.9 mmol) produced a pink or purple solid, which was stirred for 30 minutes. 50 ml of water was added to dissolve the product and allowed to react overnight. After the reaction was completed, dialysis was performed against distilled water for 48 hours using a dialysis membrane (14 kDa, Sekisui Chemical Co., Ltd., Tokyo, Japan or 3500 Da, Repligen.), followed by freeze-drying to obtain a polymer. The structure of the compound was determined by ^{1}H-NMR using D_2O as a solvent.

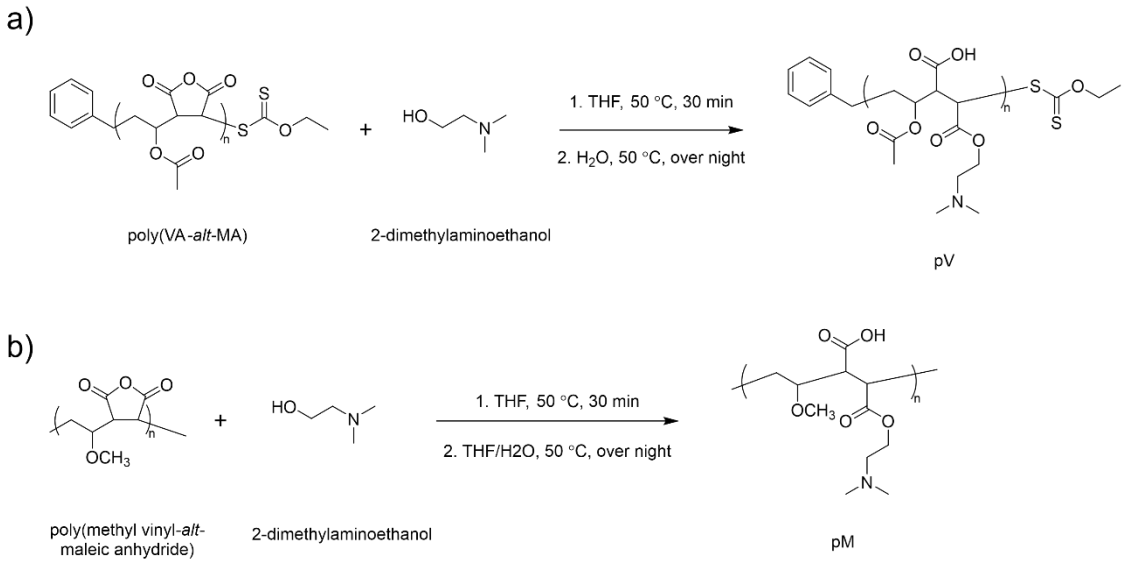

Scheme 2.5 Modification of poly(VA-alt-MA) and poly(MVE-alt-MA). a) pV, b) pM.

2.2.8 Modification of ε-poly-l-lysine with SA

PLL was synthesized according to a previous report (Scheme 2.5). PLL was obtained by dissolving SA (1.27 g, 12,67 mmol) in 25 w/w% ε-poly-l-lysine and reacting at 50 ° C for 1 hour. The introduction rate of carboxyl groups was confirmed by ^{1}H NMR using D_2O as a solvent.

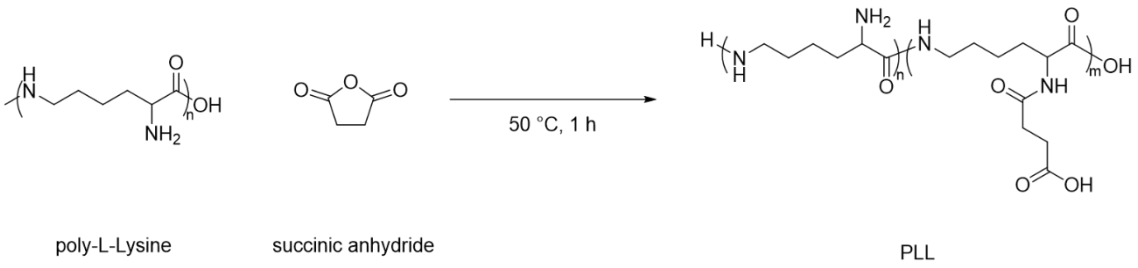

Scheme 2.6 Modification of PLL with SA.

2.2.9 Cell culture

Mouse fibroblasts (L929; American Type Culture Collection, Manassas, VA, USA) were prepared in Dulbecco's modified Eagle's medium (DMEM, Sigma-Aldrich, St. Louis, MO, USA) supplemented with 10 % foetal bovine serum (FBS). Cells were cultured in an incubator at 37 ° C with 5 % CO_2. Passaging was performed when the cells exceeded 80 % of the bottom of the dish. For passaging, the cells were detached by treatment with trypsin solution (0.25 % [w/v] trypsin containing 0.02 % [w/v] ethylenediaminetetraacetic acid in PBS).

2.2.10 Cryopreservation

The polymer was dissolved in 0.3 M NaCl solution to 15 w/w%. The solution was sterilized through a 0.22 μm filter to obtain a cryoprotective solution. L929 cells were adjusted to 1 × 10^6 cells, suspended in 1 ml of polymer solution, and stored at -80 ° C without controlling the cooling rate. After 24 hours, the samples were immersed in a 37° C water bath to thaw the cells. The cell suspension was then diluted 10 times with DMEM and centrifuged at 1000 rpm for 4 min. The recovery rate was determined by suspending the cell pellet in a small amount of DMEM and staining with trypan blue (Eq. 2.1).

$$\text{Recovery rate (\%)} = \frac{\text{Living cell}}{\text{Frozen cell}} \times 100 \qquad \text{(Eq. 2.1)}$$

2.2.11 Ice Recrystallization Inhibition (IRI) assay

The solution for IRI assay was prepared in the same manner as for cryopreservation. 2 μl of the prepared solution was sandwiched between two microcover glasses (diameter = 15 mm). The sample was then placed in the low temperature stage and the temperature was lowered to -40 ° C at 20 ° C/min and then increased to -6 ° C at 10 ° C/min. Thereafter, the material was annealed for 30 minutes in a nitrogen atmosphere at that temperature, and the ice crystals were photographed after 0 and 30 minutes. ImageJ was

used for image analysis, and the average of the long sides of 10 randomly selected ice crystals was taken as the maximum particle size.

2.2.11 Temperature variable solid state Magic-Angle-Spinning(MAS) NMR measurements

Temperature-variable solid-state NMR measurements were performed on a 700 MHz JEOL ECZ spectrometer (JEOL). The cryoprotectant-containing solution samples were sealed in a DSI internally sealed cell for the XC4 rotor, and the samples were rotated between 3.6 and 5.8 kHz and measurements were taken from room temperature to around -40 ° C. In the temperature change experiment, I first cooled the sample slowly to below -40℃, left it in that state for over an hour to stabilize it, and then started measurements. Next, the temperature was increased to around 2 to 3 degrees, and the following measurements were performed. The samples in the cell were allowed to stand for about 10 minutes until they reached each measurement temperature, and then measurements were taken. All data were processed using Delta Ver. 6.1 (JEOL).

2.3 Results & discussion

2.3.1 Polymer characterization

In order to polymerize poly(VA-alt-MA), a precursor of pV, by reversible addition-fragmentation chain transfer (RAFT) polymerization, I synthesized *S*-benzyl-*O*-ethyl dithiocarbonate, a chain transfer agent (Fig. 2.1).

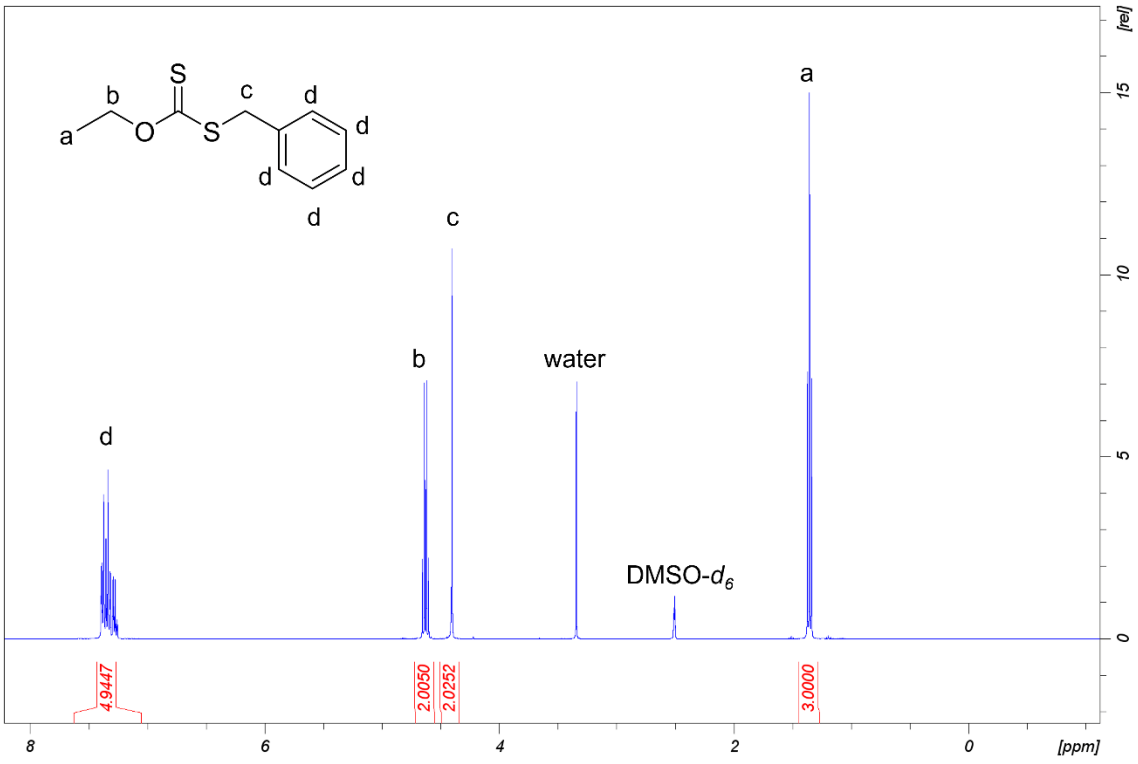

Figure 2.1 ^{1}H NMR spectrum of *S*-benzyl-*O*-ethyl dithiocarbonate.

pA, pD and poly(VA-alt-MA) were synthesized by RAFT polymerization. When the samples of pA and pD at the completion of the reaction were confirmed by ^{1}H NMR, loss of the vinyl proton of the monomer appearing at around 5.2 ppm to 6.2 ppm was observed, confirming that polymerization of the polymer had progressed. For poly(VA-*alt*-MA), an

excess amount of MA was added to VA to ensure the realization of an alternating array of poly(VA-*alt*-MA), and the reaction was terminated regardless of the conversion rate[7]. When the composition ratio of the polymers pA and pD was confirmed by ^{1}H NMR, it was shown that the composition of pD was approximately 49.1% DMAEMA, which was able to be polymerized at a composition ratio of approximately 1:1 (Figures 2.2 & 2.3).

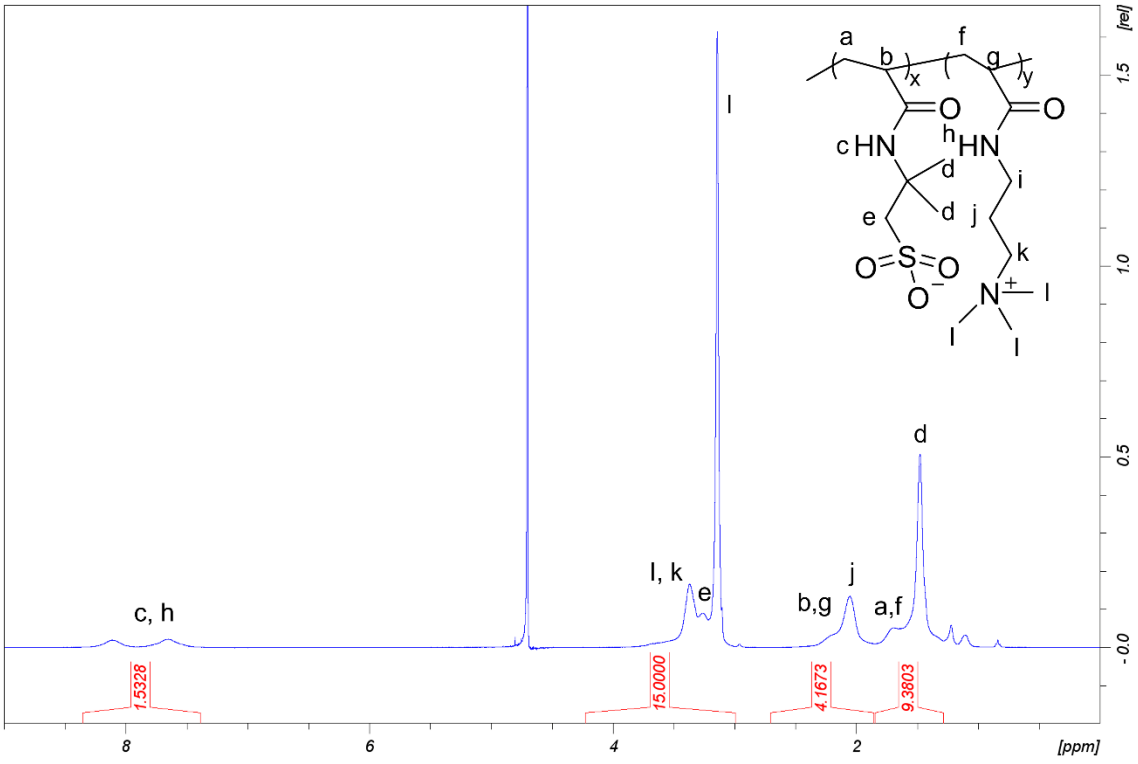

Figure 2.2 ^{1}H NMR spectrum of pA.

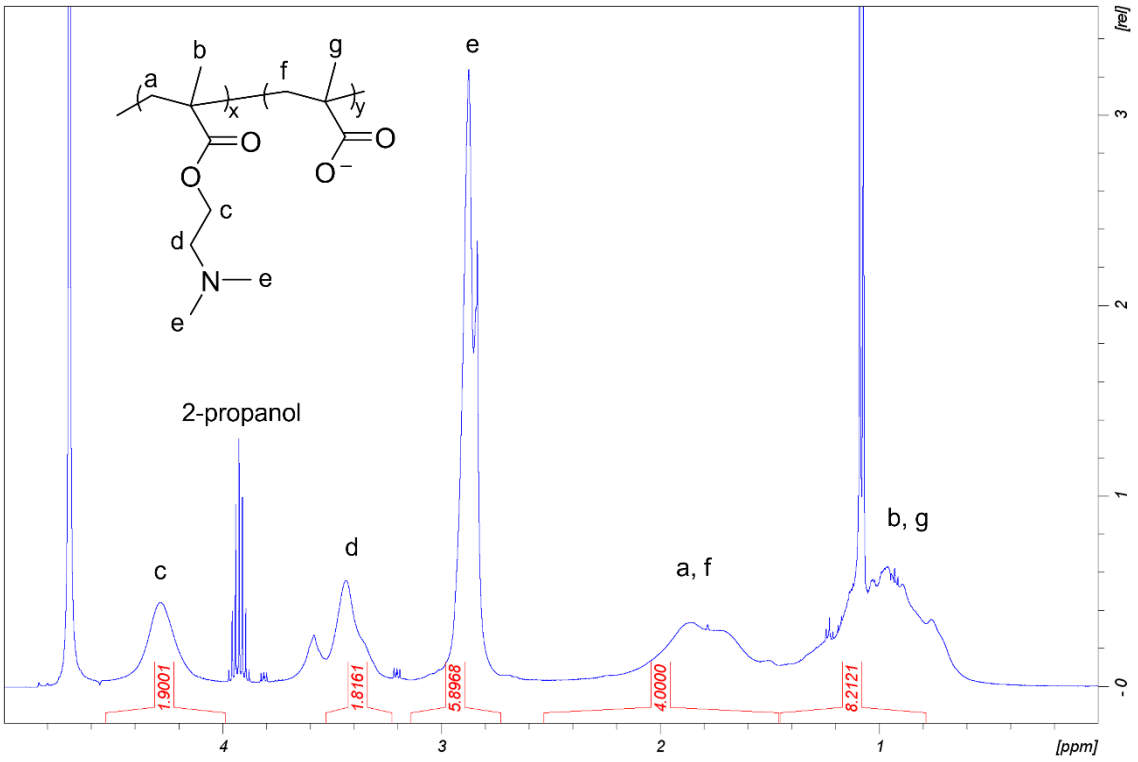

Figure 2.3 ^{1}H NMR spectrum of pD.

However, the composition ratio of pA could not be determined because the peaks of pendant methylene and pendant methyl protons of AMPS and APTAC overlapped in a complicated manner, and the peaks of methine and methylene protons in the main chain overlapped in a complicated manner. In addition, the pendant amide protons around 7.5 ppm to 8.3 ppm overlapped, so an accurate integral ratio could not be obtained. In a previous study, the composition was determined by measuring reverse gated decoupled ^{13}C-NMR, so a similar method was used in this study[8]. The ^{13}C-NMR results are shown in Figure 2.4.

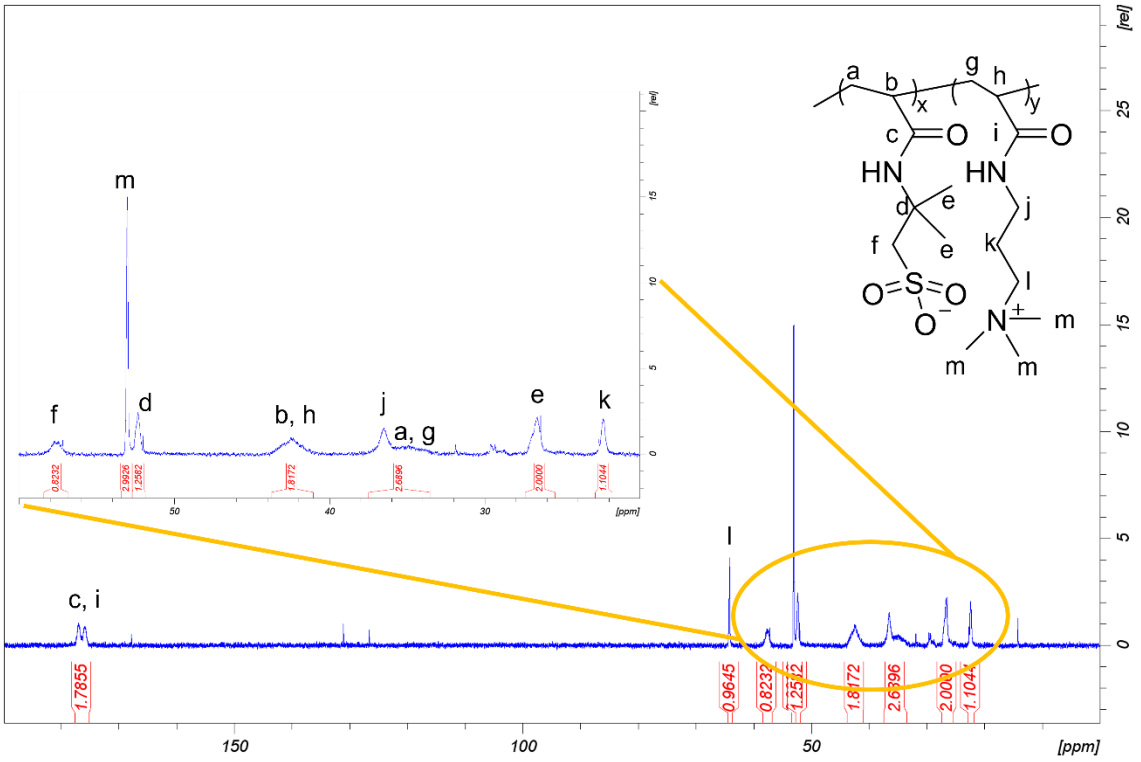

Figure 2.4 ^{13}C NMR spectrum of pA.

The composition ratio of AMPS and APTAC was determined from the integral ratio of methylene carbon around 57 ppm and 64 ppm. The results showed that the content of AMPS was approximately 49.9%, and it was possible to synthesize it at a composition ratio of 1:1, similar to pD. In addition, pA and pD showed narrow dispersity by size exclusion chromatography (Table 2.1).

The structure of poly(VA-*alt*-MA) was also measured using reverse gated decoupling ^{13}C-NMR in the same way as pA (Figure 2.5).

Table 2.1 Characteristics of polyampholytes prepared via RAFT polymerization.

		Conposition		Molar ratio[c)]	M_n[d)]	M_w/M_n[d)]
		Cation	Anion			
pA	in feed	50	50	100 : 1 : 0.2	7156	1.03
	in polymer[a)]	49.9	50.1			
pD	in feed	50	50	100 : 1 : 0.2	9719	1.42
	in polymer[b)]	49.1	50.9			
pV		50	50	93 : 1 : 0.16	7419	1.95

a) Determined by inverse gated decoupling ^{13}C NMR, b) Determind by ^{1}H NMR, c) [monomer]:[CTA]:[initiator], d) determined by GPC.

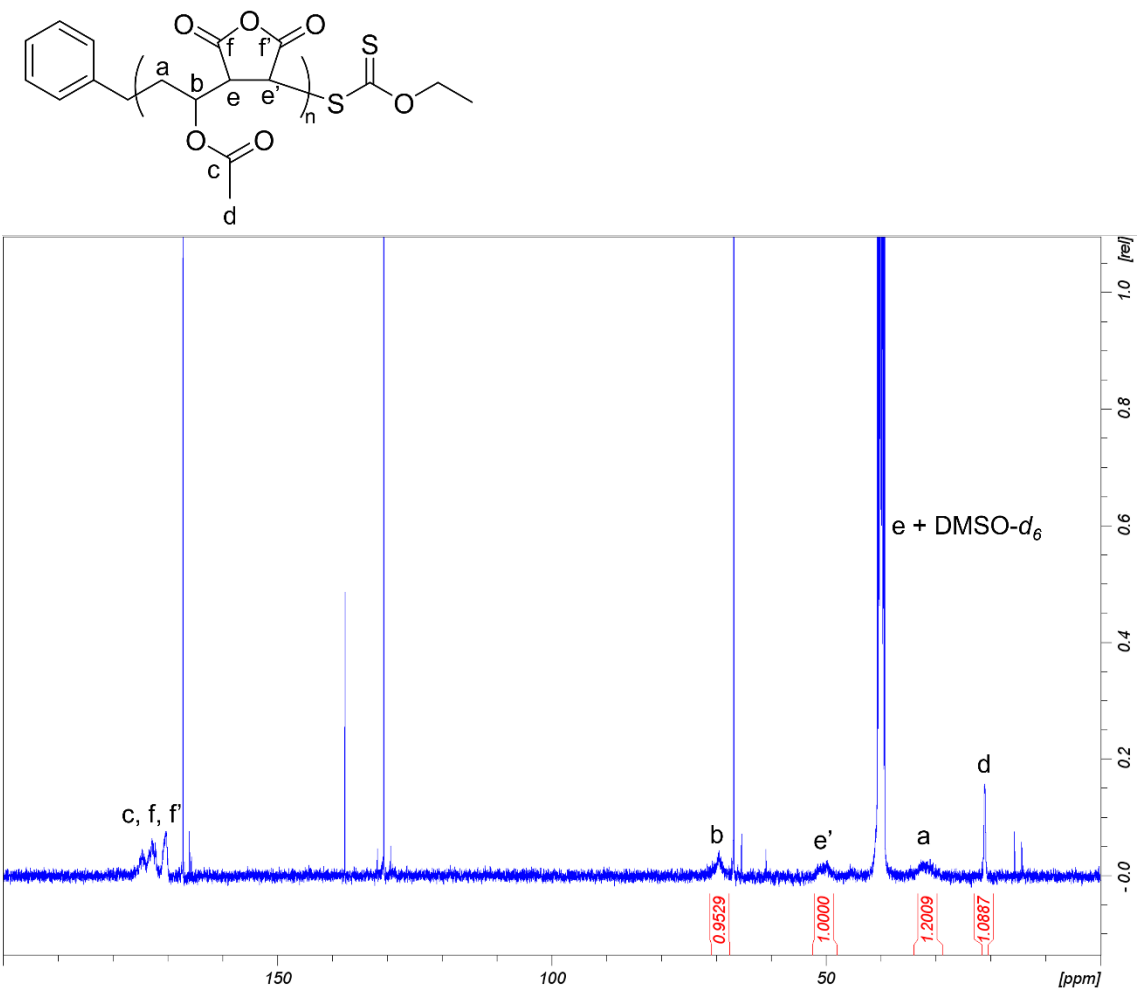

Figure 2.5 ^{13}C NMR of spectrum poly(VA-*alt*-MA).

Since the integral values of a, d, b derived from VA and the integral value of e' derived from MA are approximately 1:1, this polymer was shown to be an alternating array of VA and MA[7].To obtain ampholyte polymers, 2-(dimethyl amino)ethanol was used as a nucleophile to open the rings of (VA-*alt*-MA) and poly(MVE-*alt*-MA). By ^{1}H NMR, the methine peak around 3.8-4.2 ppm disappeared, confirming the success of ring opening (Figures 2.6 & 2.7).

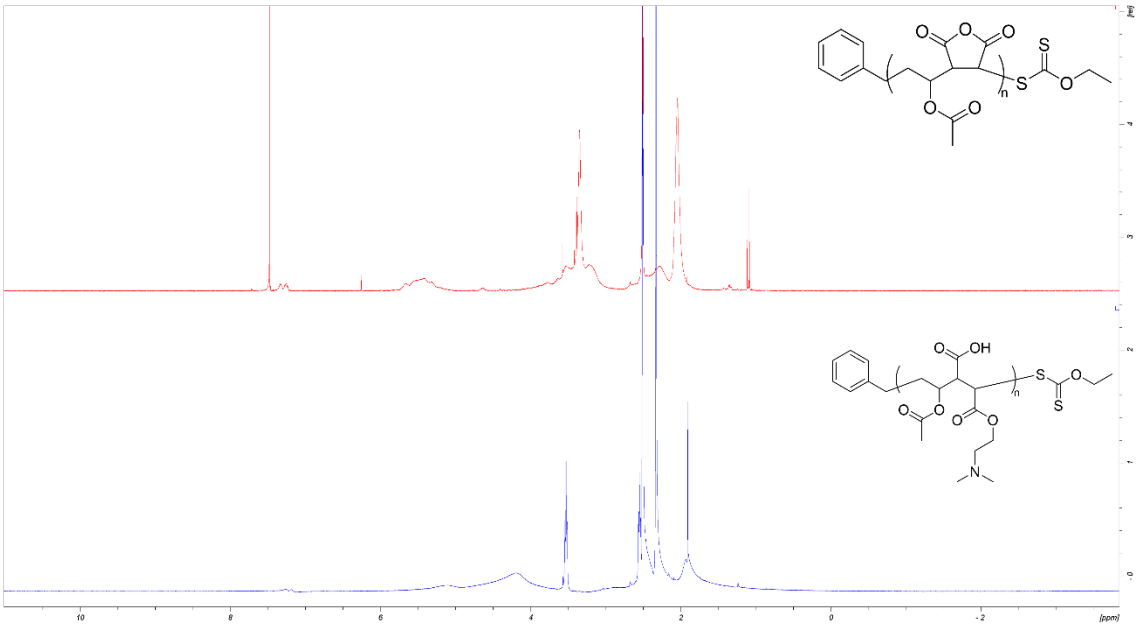

Figure 2.6 Confirmation of ring opening by ^{1}H NMR. Red; poly(VA-*alt*-MA), Blue; pV.

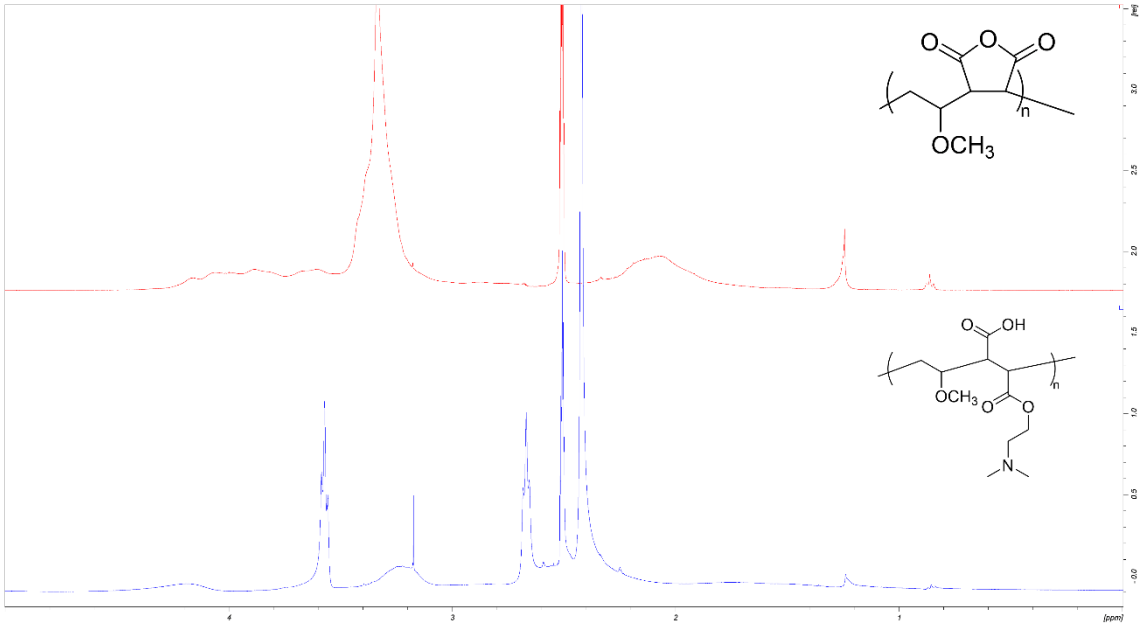

Figure 2.7 Confirmation of ring opening by ^{1}H NMR. Red; poly(MVE-*alt*-MA), Blue; pM.

Figure 2.8 shows the ^{1}H NMR peak of the prepared PLL. The SA introduction rate was approximately 67% based on the peak integral ratio of the methine proton adjacent to the amino group.

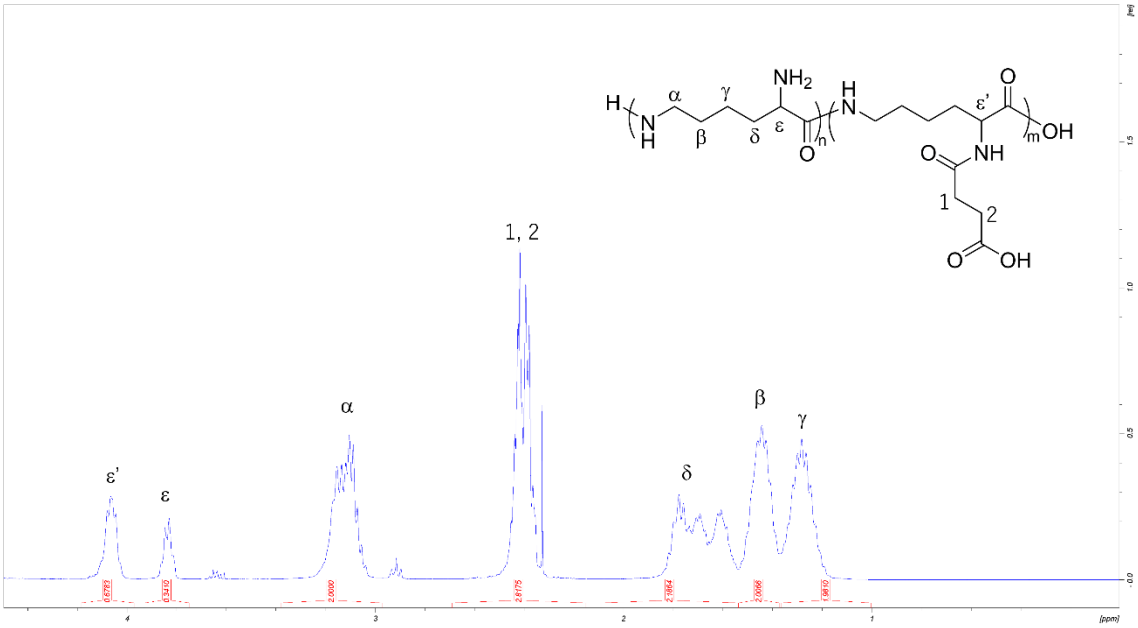

Figure 2.8. ^{1}H NMR signal assignments for PLL-SA.

2.3.2 Cryopreservation

To confirm the cryoprotective effect of the synthesized polymer, L929 cells were frozen at -80 ° C by dissolving the polymer at 15 w/w% in a 0.3 M NaCl aqueous solution (Figure 2.9). pV and PLL had a high cryoprotective effect and a cell recovery rate of about 85% was confirmed. In addition, the cell recovery rate for pD was approximately 47%, which was lower than previous reports, but in previous studies, the cell viability was calculated as the ratio of the number of viable cells after thawing to the number of cells recovered after thawing. In this study, the cell recovery rate was calculated from the number of viable cells after freezing and the total number of cells at the time of freezing[3, 9]. It is not possible to recover 100% of dead cells after cryopreservation, and cell survival rates tend to be low with this calculation method, so there is no problem with the results. High molecular weight (M_w 226000) pM and pA had poor cryoprotective effects, with cell recovery rates of 26.6% and 14.4%, respectively.

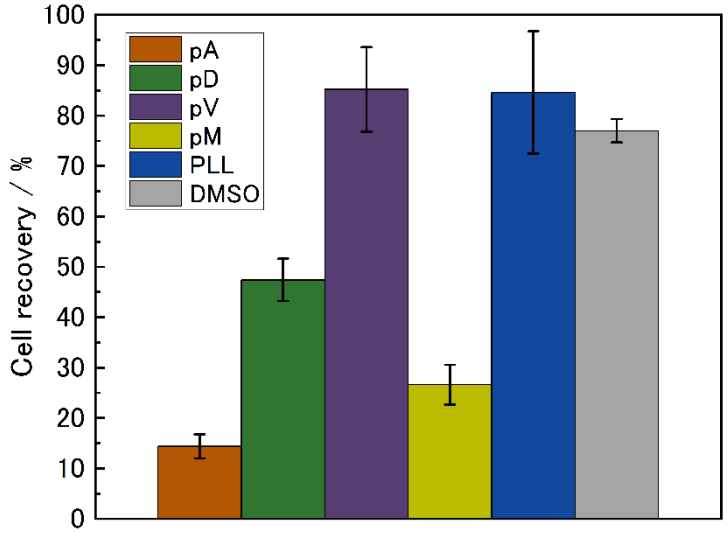

Figure 2.9 Cell Recovery and of the polymer against L929 cells.

2.3.3 IRI activity

It has been reported that adding a polymer with high IRI activity during cryopreservation suppresses ice crystal fusion and improves cell recovery. Therefore, IRI activity was measured to investigate the cause of the difference in cryoprotective effect of each polymer. Splat cooling assays are often used to examine IRI activity, but the boundaries become vague due to overlapping ice crystals. Therefore, this time I used a sandwich method in which a polymer solution was sandwiched between two cover glasses. Figure 2.10 a) is an image of ice crystals annealed with a polymer solution on a -6 ° C low temperature stage for 30 minutes. When the polymers were added, the ice crystal size was smaller compared to the 0.3 M NaCl aqueous solution, but the mean large grain size (MLGS) was not significantly different between each polymer (Figure 2.10 b)). In

addition, with poly vinyl alcohol whose IRI activity contributes to cryoprotection, ice crystals are smaller compared to the polymer synthesized this time even at a lower concentration of 1 mg/ml. It has also been reported that there is a difference in the cryoprotective effect of AFP with similar IRI activity, so it is thought that there is no significant correlation between the cryoprotective effect and IRI activity[10-13].

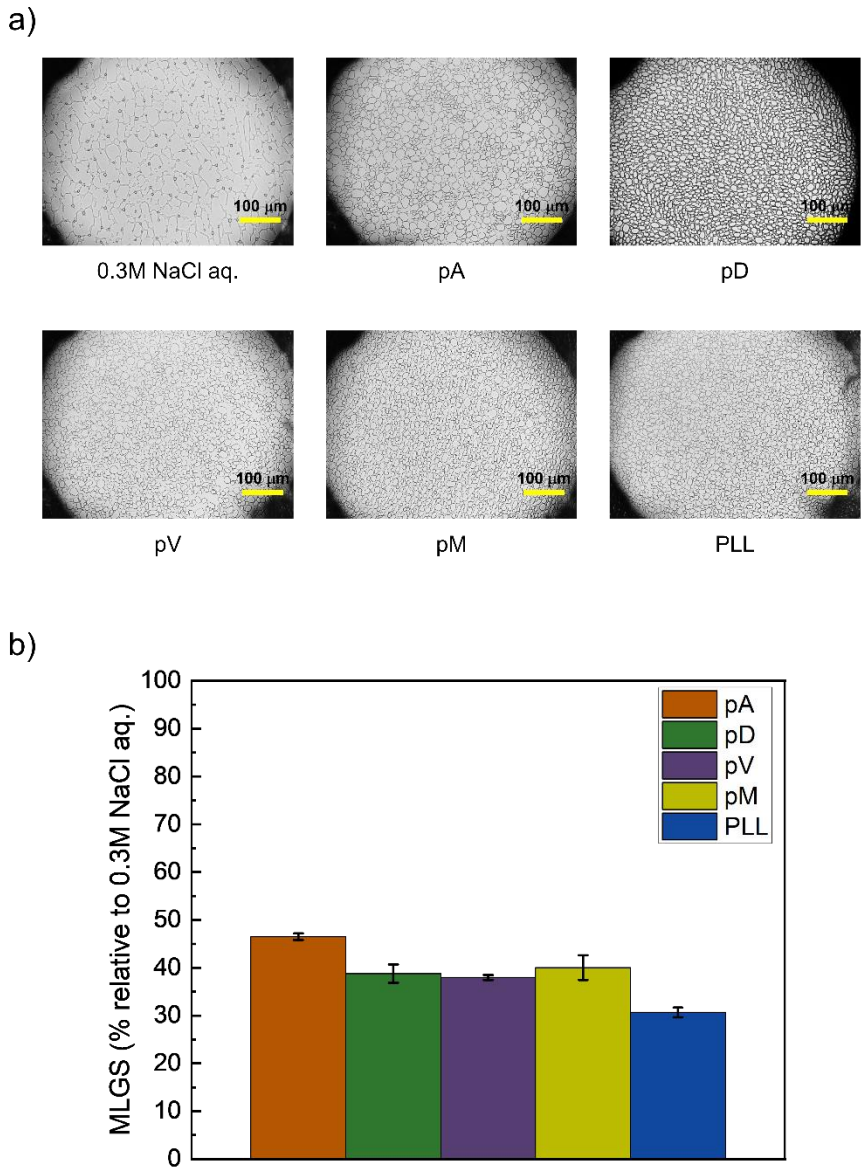

Figure 2.10 Polynucleated ice crystals after 30 minutes annealing -6 ° C. a) Microscope image, b) Mean large grain size (MLGS) with 0.3 M NaCl aq.

2.3.4 NMR measurements

NMR enables real-time observation of information on the structure, chemical environment, amount, and dynamics of functional groups from information such as resonance positions (chemical shifts), intensities, and line widths obtained from spectra. Furthermore, since the motion of molecules is related to the relaxation process, it is possible to detect changes in molecular motion by observing this. During freezing, residual water provides space to the cells, which may protect them from mechanical damage. Furthermore, the increase in osmotic pressure caused by freeze concentration causes serious damage to cells. In NMR spectra, it is possible to compare the broad peaks of solid components with the narrower peaks of solution-based molecules[14]. Therefore, I discussed the freezing mechanism by investigating the physicochemical properties of a polymer solution during freezing using temperature-variable solid-state Magic Angle Spinning (MAS)- NMR. A typical ^{1}H NMR signal is shown in Figure 2.11. Figure 2.12 shows the amount of residual water during freezing. Using a semi-logarithmic plot representation, we found that the residual water decreases with different time constants at the high and low temperature sides (Figure 2.12 g)). This phenomenon can be interpreted as the freezing of free water on the high temperature side and the freezing of coordination water on the low temperature side. In the pA solution, which has the lowest

freezing protection effect, the freezing speed of the free water was clearly faster than that of the other polymer solutions. Comparing the amount of water remaining at -10° C, 80% of the water in the pA solution froze, leaving only 20% as residual water, whereas the other polymers left approximately 30% of water as residual water. pA is an amphoteric electrolyte polymer that has quaternary ammonium as a cation and sulfonic acid as an anion. Sulfobetaine polymers (polySPB) with similar ion pairs have close charge densities of cations and anions, making it easy to form intramolecular salts[15]. In addition, poly(SPB) has salt response and blocks the electrostatic interactions that form internal salts with NaCl, allowing it to be used as a polymer brush hydrated in salt solutions[16, 17]. However, it has been reported that hydration water within poly(SPB) brushes forms a network structure similar to hydrogen bonds in the bulk state[18]. In other words, it is thought that this rapid decrease in the amount of residual water occurred in pA because the network structure of hydrated water is similar to that of bulk water.

Since the line width of the peak mainly reflects the mobility of molecules, the line width (full width at half maximum; FWHM) of water protons in the polymer solution was measured while changing the temperature (Figure 2.13). The line width begins to widen in the temperature range where freezing of bulk water ends and freezing of water coordinated to the polymer begins. The temperatures were pA; -17 ° C, pD; -19 ° C,

pV; -21 ° C, pM; -27 ° C, PLL; -18 ° C, respectively. The temperature at which the bulk water freezes and the coordinated water freezes is around -20 ° C, except at very high molecular weight pM. In addition, as in previous reports, the line width of PLL broadened significantly, eventually increasing to around 3440 Hz (Figure 2.13 e))[2]. The linewidths of pV and pM also broadened to some extent, increasing to 2000 and 1500 Hz, respectively (Figure 2.13 c) & d)). Furthermore, I investigated the temperature dependence of the spin-lattice relaxation time (T1) by conducting water relaxation experiments (Figure 2.14). ^{1}H relaxation experiments can give an indication of the rotational diffusion rate of residual water. It was confirmed that for all polymers, T1 has a minimum value at the switching temperature from bulk water to residual water freezing, and T1 rises again as the temperature decreases. Furthermore, when T1 rose again, a sharp increase in the line width of the residual water signal was simultaneously observed, indicating a decrease in mobility and an increase in viscosity[19, 20]. The degree of broadening of residual water was particularly remarkable in PLL, followed by pV and pM. (Figure 2.14 c), d), f)).

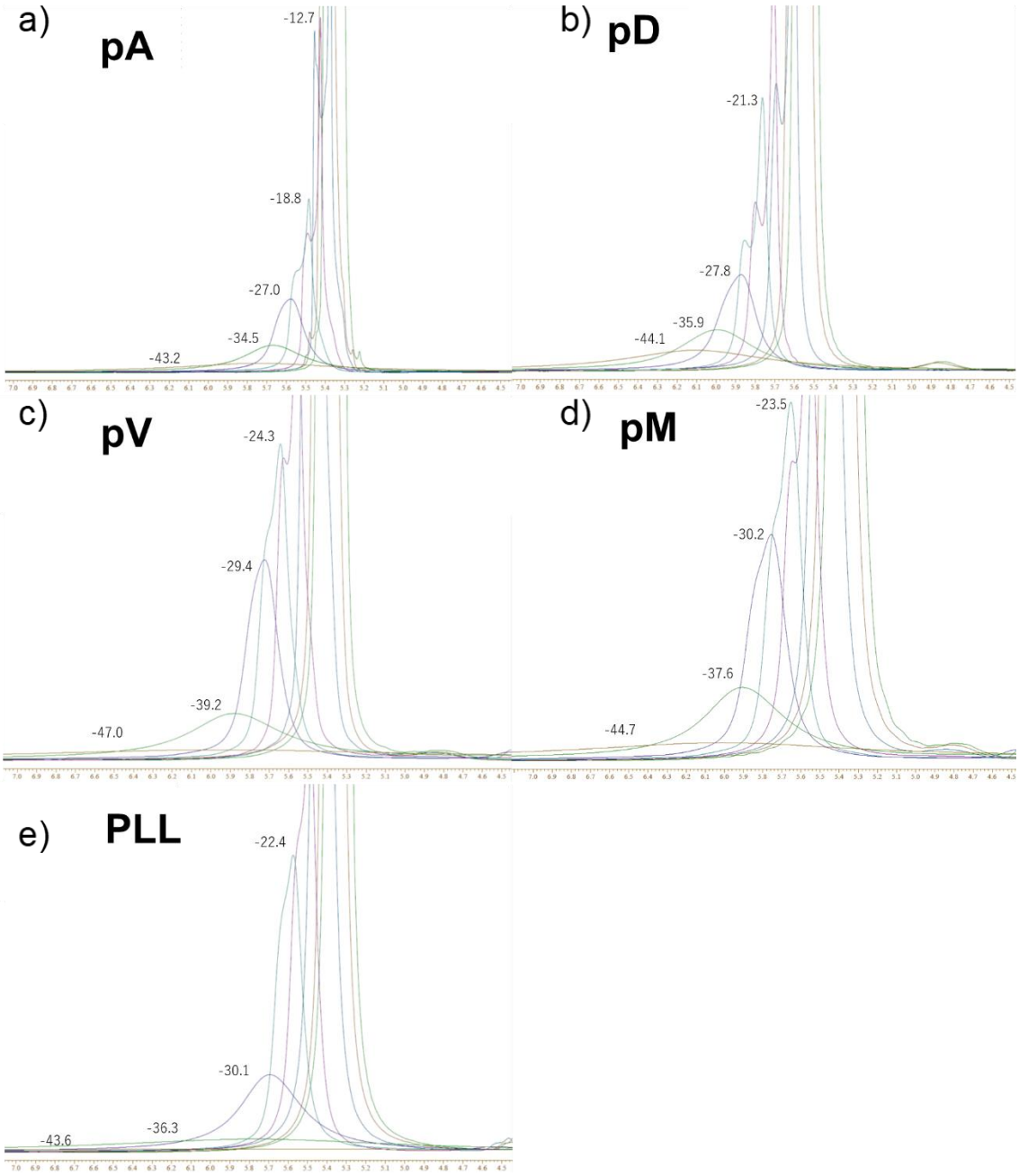

Figure 2.11 ^{1}H NMR signal of water. a) pA, b) pD, c) pV, d) pM, e) PLL, f) Comparison between each polymer.

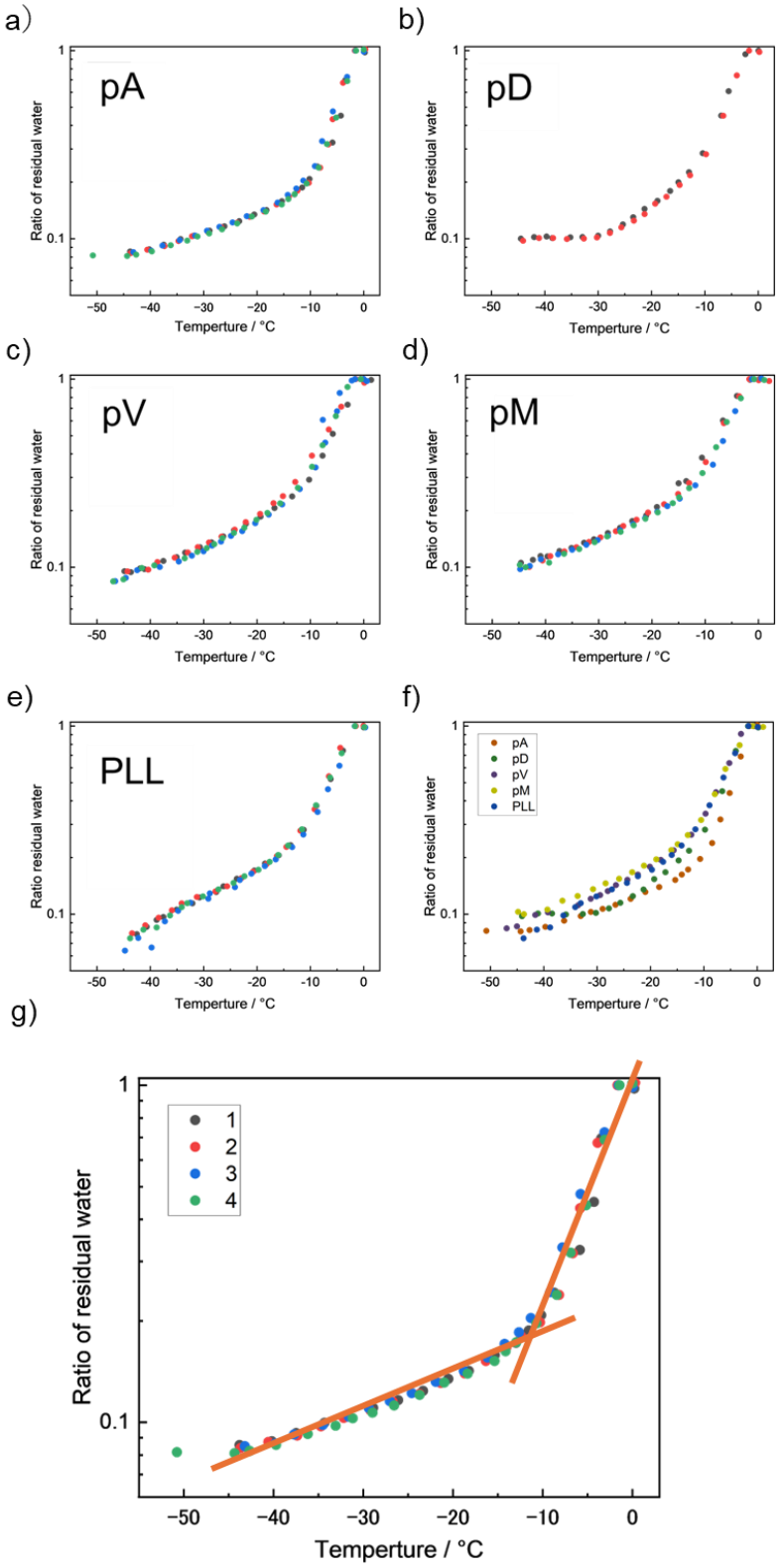

Figure 2.12 Temperature dependent residual water ratio. a) pA, b) pD, c) pV, d) pM, e) PLL, f) Comparison between each polymer.

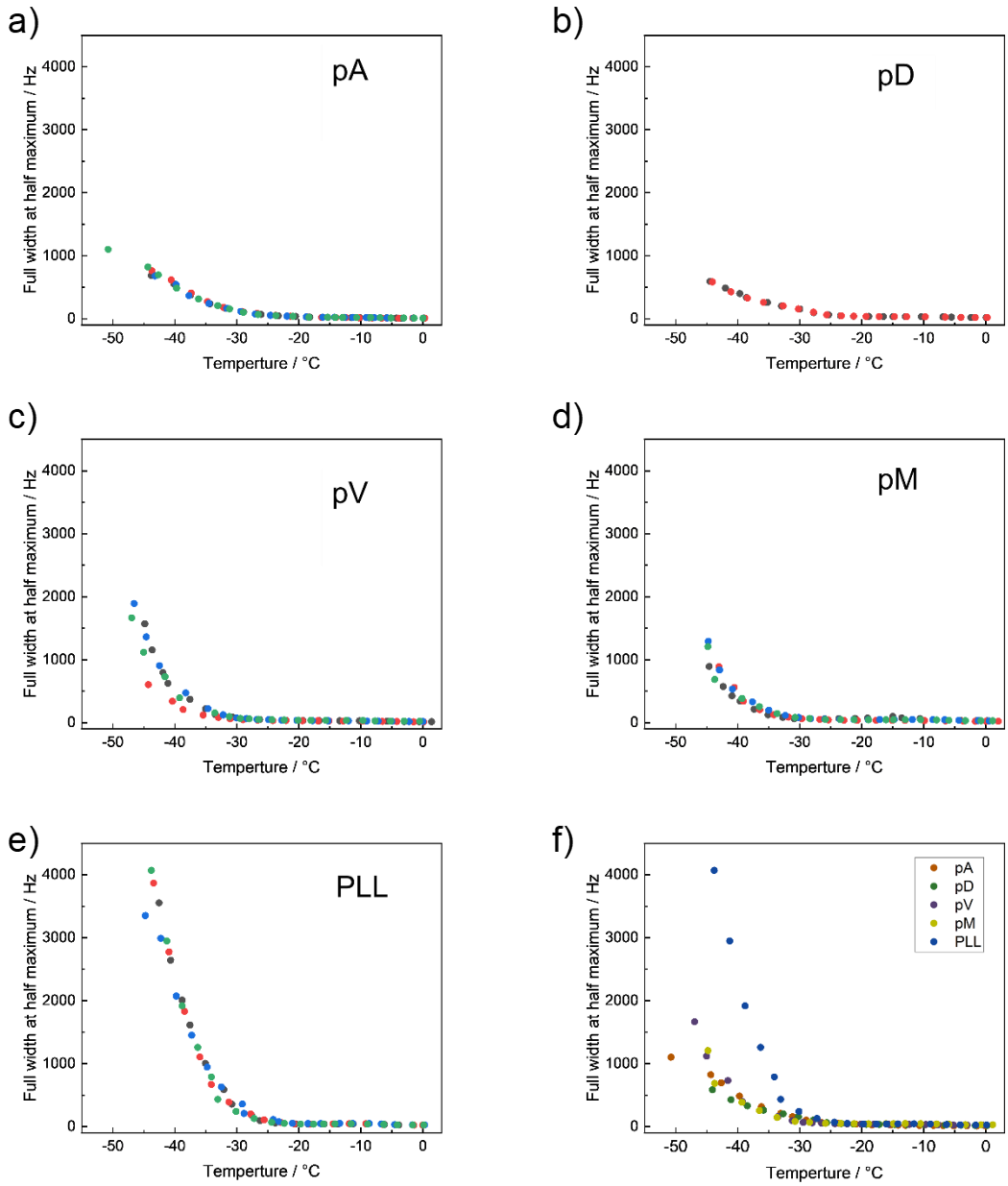

Figure 2.13 Temperature dependent full-widths-at-half-maximum of the proton signals. a) pA, b) pD, c) pV, d) pM, e) PLL, f) Comparison between each polymer.

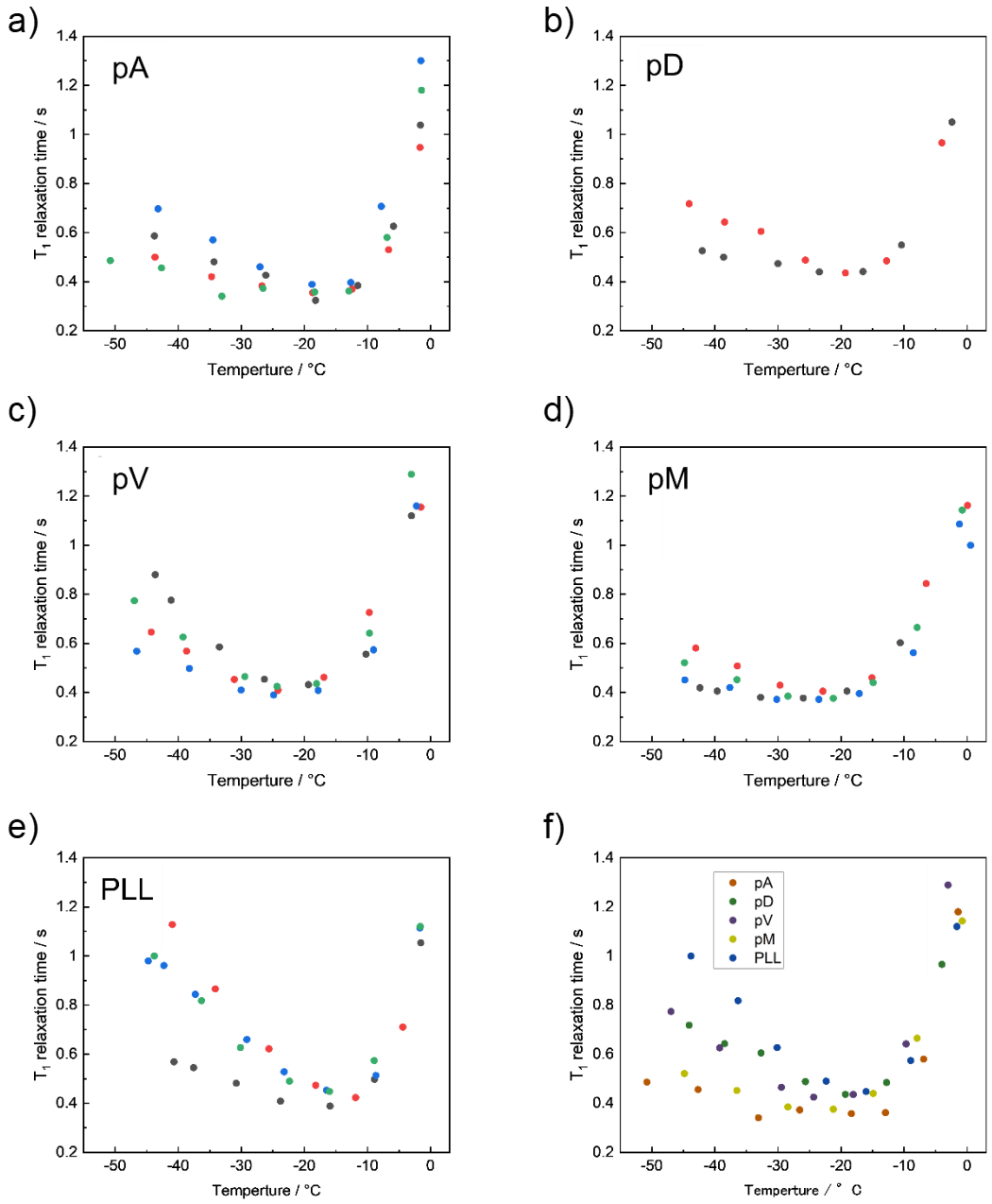

Figure 2.14 Water proton T_1 relaxation times as functions of temperature. a) pA, b) pD, c) pV, d) pM, e) PLL, f) Comparison between each polymer.

^{23}Na NMR was used to investigate the behavior of Na ions in polymer solutions during freezing (Figure 2.15). Figure 2.16 shows that the chemical shift value of the Na ion peak changes with temperature. It was revealed that all polymers have a maximum chemical shift value at approximately the same temperature as the freezing of bulk water. For PLL and pV, minimum values exist in even lower temperature ranges (Figure 2.16 c & e)). A report on the vitrification ability of Trehalose-agarose gel observed by Fourier transform infrared spectroscopy (FT-IR) positioned three transitions of glycosidic bond peaks during melting as glass melting of frozen concentrate, rapid growth of ice crystals due to recrystallization, and melting of ice crystals, respectively[21]. In this study, the melting process of the polymer solution was observed by NMR. The increase in the mobility of the glassy water increases the amount of coordinating water, and thus the peaks that had shifted to the high-field side are shifted to the low-field side due to reorientation to ions, which are considered to be the PLL and pV minima.

Previous studies have shown that the Na peak in polymer solutions is divided into two types, central transition and satellite transition, as freezing progresses[2, 22, 23] (Figure 2.14 f)). Na ion in aqueous solution has a single peak due to the presence of a surrounding hydration shell, but the freezing of bulk water reduces the number of water molecules around the Na ion, causing the polymer chain to penetrate into the second hydration shell,

resulting in an asymmetric transition and two separate peaks, one broad and one sharp. Broad peaks are satellite transitions, and this time I will only discuss sharp peaks (center transition) without making them the subject of discussion. Figure 2.17 shows the temperature dependence of the intensity of the sharp component of the Na ion peak. The first large drop in the intensity of each peak corresponds to the broadening and separation of the satellite peaks from the main peak due to the breaking of the electric field symmetry around the Na ion, indicating that the polymer approaches around the Na ion in this temperature range and affects the orientation of the coordination water. The temperatures were pA; -7 ° C, pD; -10 ° C, pV; -7 ° C, PLL; -11 ° C, respectively for each polymer. Since the temperature for all polymers is roughly the same as that at which bulk water freezes, it was suggested that the decrease in bulk water around Na causes the polymer chains and Na ions to approach each other, causing a break in the electric field symmetry of the Na ions. Interestingly, at pM, the intensity of the Na ion peak is low at 0 ° C. Since water is hardly frozen at around 0 ° C, it is thought that the polymer is more likely to coordinate with Na at pM (Figure 2.17 d)). In addition, the decrease in peak intensity starting around -35 ° C is the temperature at which Na ions of the polymer chain penetrate into the first hydration shell, that is, coordinate to the polymer chain. For pV and pM with cations and anions introduced regioregularly and PLL the peak intensity

decreases significantly after -35° C, so it is thought that more Na ion coordination occurs than for pA and pD (Figure 2.17 c-e)).

Figure 2.18 compares the half-widths of the sharp peaks (central transitions). Chemical exchange between the two states of Na ions, namely asymmetric and symmetric states of the electric field around the Na ion broadens the peaks, and when the chemical shift difference between the central and satellite transitions and the exchange rate between the two states are comparable, a local increase in line width (of the peak) is observed. There were no major differences in local maximum values among the polymers, but local minimum values appeared for PLL, pV, and pM (Figure 2.18 c-e)). Similar to the discussion on chemical shift positions earlier, this is thought to be because in these polymers, the mobility of Na ions increases first due to glass melting, and then water rearranges. T1 of Na ions also gives an indication of the rotational diffusion rate of Na ions, as in the water relaxation experiment. At low temperatures, there is no significant difference among the polymers, but there is a difference in the relaxation time at 0 ° C, suggesting that pV and pM have a higher ability to trap Na ions than the other polymers because the motion of Na ions is more inhibited than the other polymers (Figure 2.19).

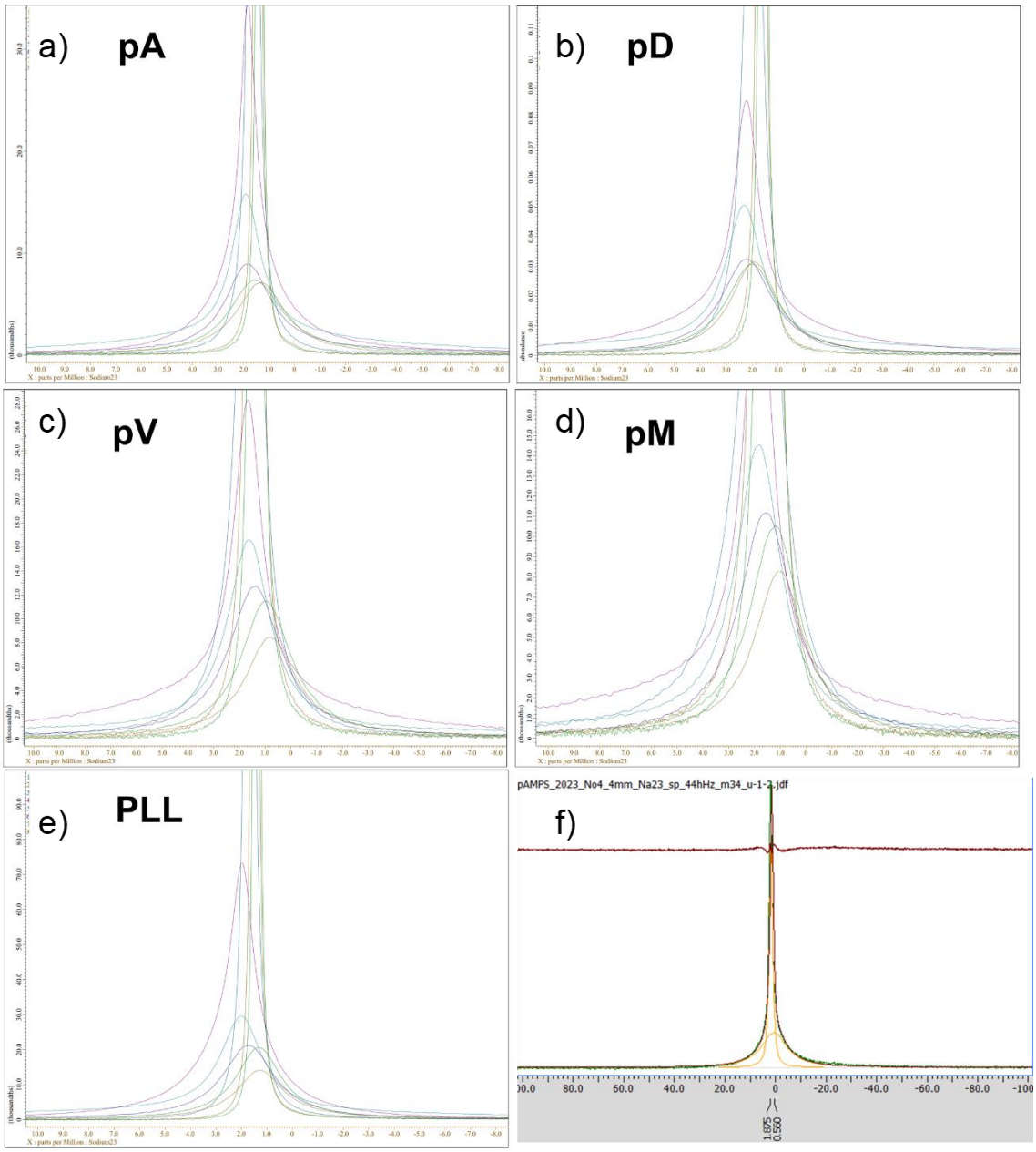

Figure 2.15 ^{23}Na NMR signal. a) pA, b) pD, c) pV, d) pM, e) PLL, f) Center transition and satellite transition

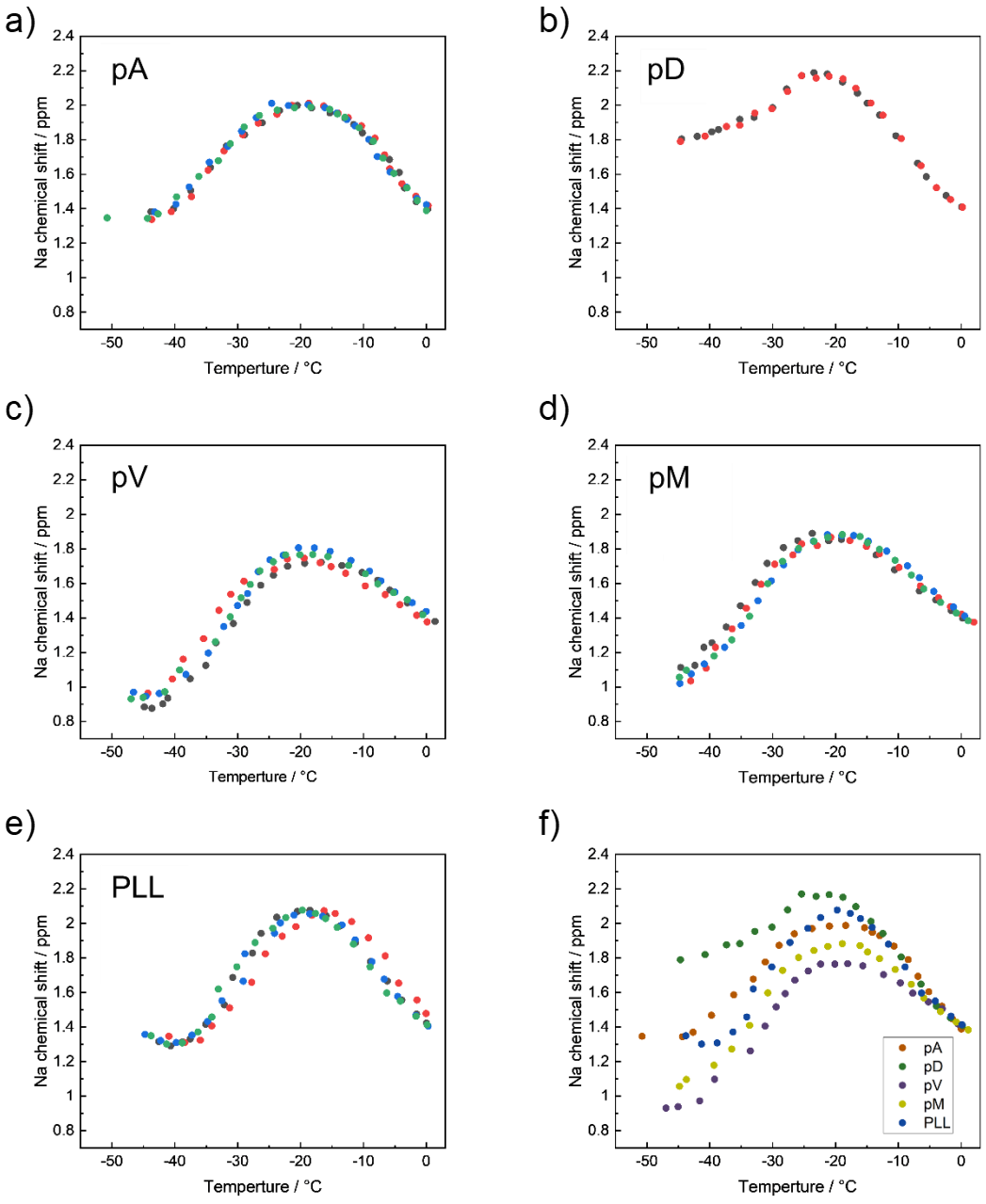

Figure 2.16Temperature dependence of Na ion peak shift position. a) pA, b) pD, c) pV, d) pM, e) PLL, f) Comparison between each polymer.

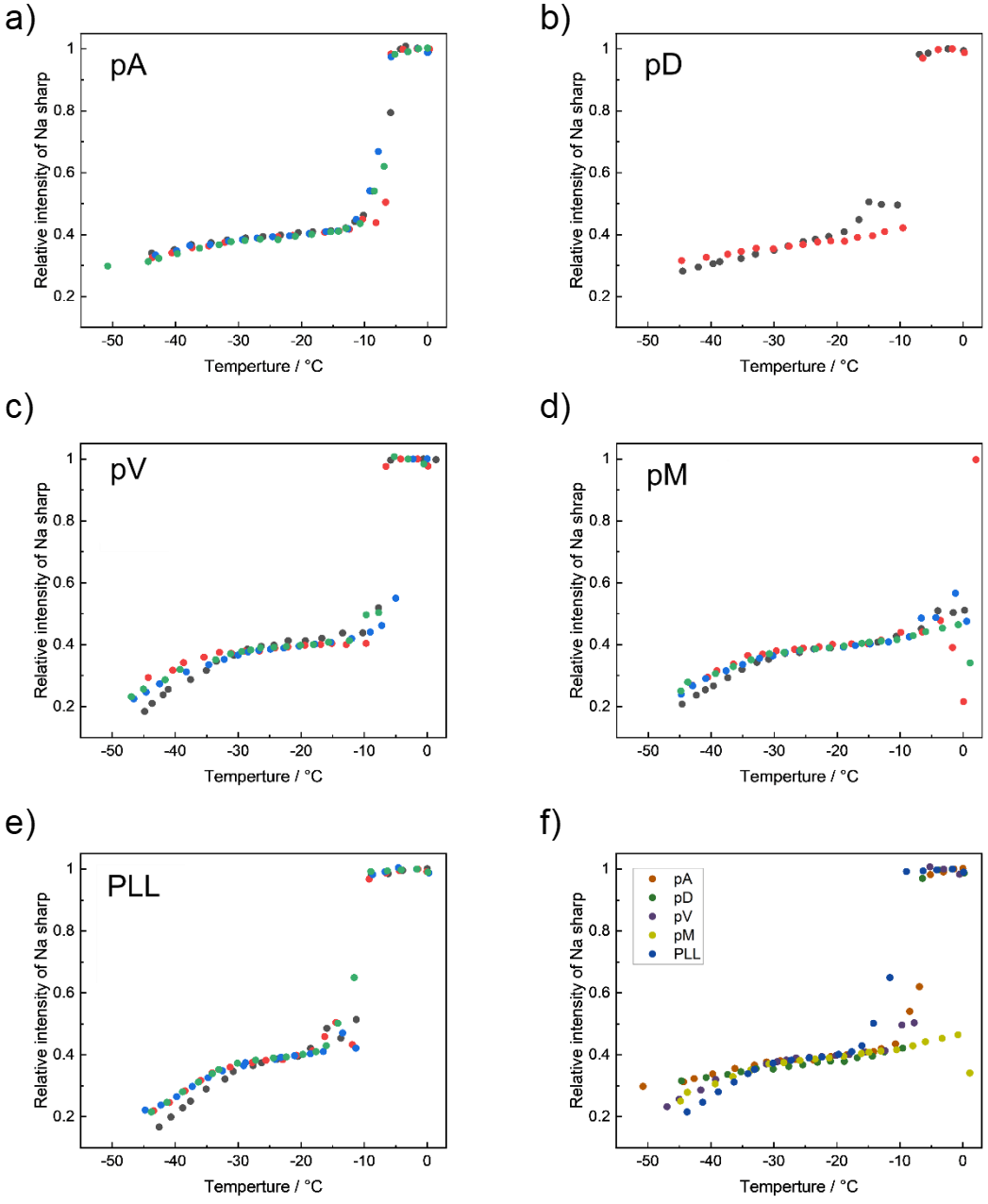

Figure 2.17 Temperature dependence of Na ion sharp peak shift intensity. a) pA, b) pD, c) pV, d) pM, e) PLL, f) Comparison between each polymer.

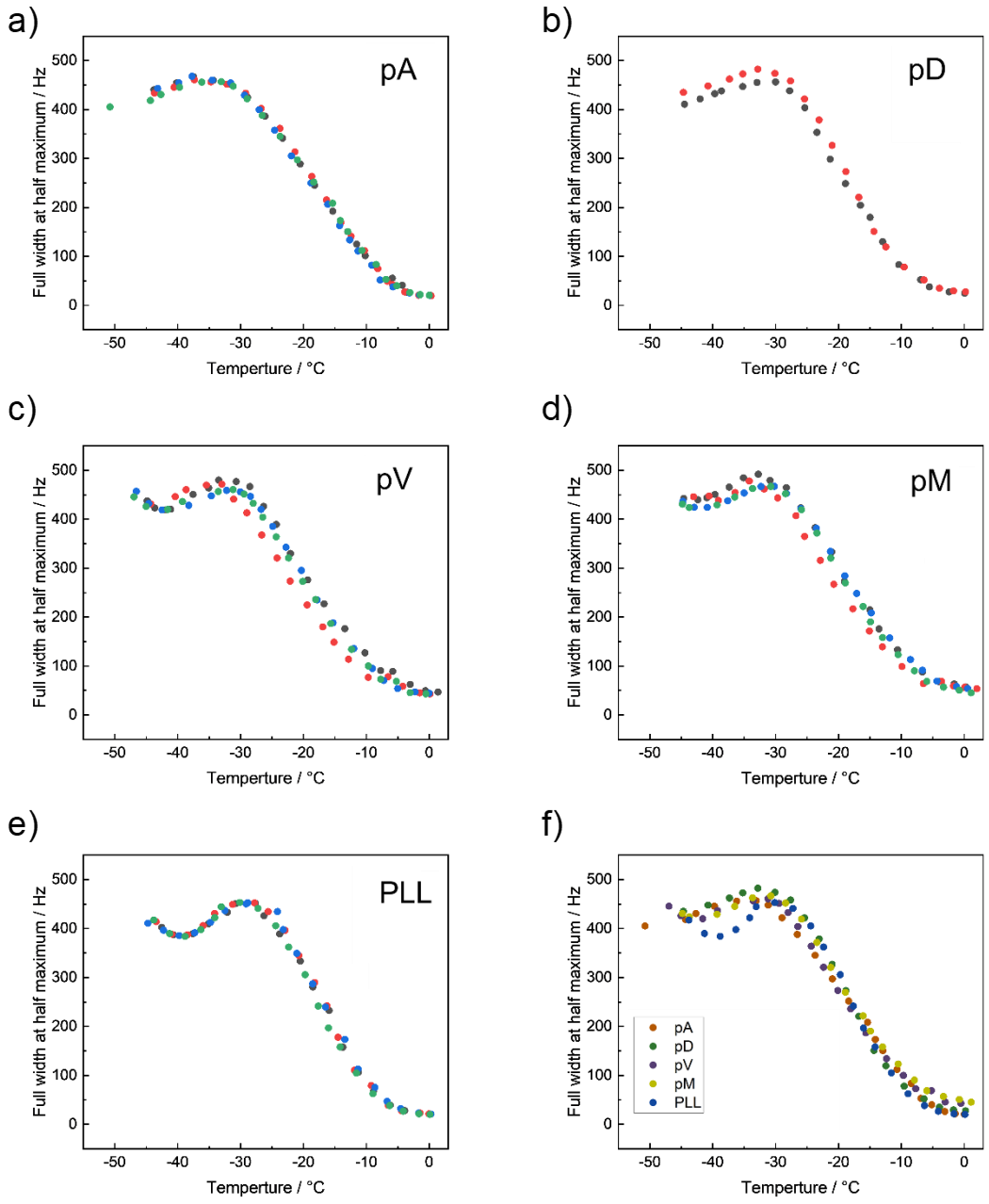

Figure 2.18 Temperature dependent full-widths-at-half-maximum of the Na ion signal. a) pA, b) pD, c) pV, d) pM, e) PLL, f) Comparison between each polymer.

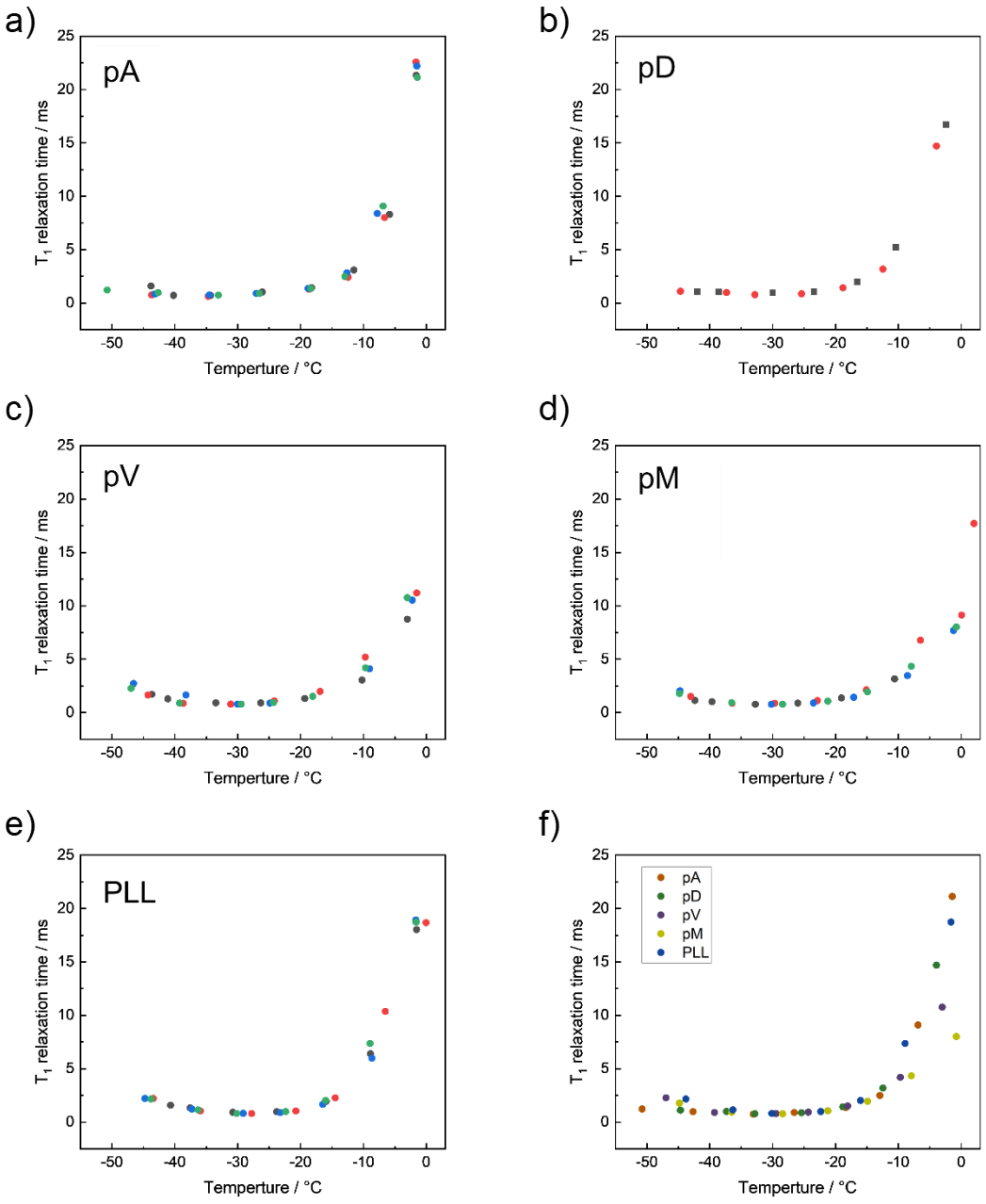

Figure 2.19 Na ion T_1 relaxation times as functions of temperature. a) pA, b) pD, c) pV, d) pM, e) PLL, f) Comparison between each polymer.

The physical meanings of the important parameters correlated between the behavior of water and the Na ions of each polymer are outlined in Table 2.2. In the case of pA, the water hydrated in the polymer has a hydrogen bond close to that of bulk water, so the amount of residual water decreases rapidly, and the amount of residual water at -10 ° C is 20.2%, about 10% lower than that of other polymers. In addition, the temperature at which Na ions coordinate with the polymer chain is around -31 ° C, which is the same as other polymers. This is thought to cause a sudden increase in osmotic pressure, leading to excessive cell dehydration and a decrease in the cryoprotective effect [24, 25]. Furthermore, since the Na ion intensity at -45 ° C is similar to that of pD, which has a moderate cryoprotective effect, it is thought that rapid dehydration immediately after freezing leads to the low cryoprotective effect of pA. For pV and PLL, the minima in the chemical shift position of Na around -40 ° C and the increase in the line width of water suggest that a rapid increase in viscosity (vitrification) is occurring, and water is expected to become amorphous during freezing (Figures 2.14 c), d) & 2.16 c), d)). Furthermore, since the Na ion intensity of these polymers at around -45 ° C is lower than that of pA and pD, it is thought that the polymer chains coordinate more Na ions. In other words, polymers with a high cryoprotective effect are thought to have an ability not only to vitrify the solution but also to prevent an excessive rise in osmotic pressure during freezing. PD, which has

a similar structure to pV, has a bulkier methyl group in its main chain, which reduces the degree of freedom in rotation and orientation of the polymer structure, making it more likely to generate ice nuclei[25, 26]. Therefore, it is thought that it does not have the vitrification ability that was seen with pV. The higher Na trapping capacity of pV is also expected to be due to the 1:1 and alternating sequence of anions and cations in pV, whereas in pD the anions and cations are completely random. pD has a specific temperature dependence of residual water and Na ion signals compared to other polymers, and both hardly decrease from around -30 ° C. In addition, since the peak of polymer chain of pD is broad in the higher temperature region, it is thought that a cryoprotective effect can be obtained by forming a polymer matrix and isolating water and Na ions (Figure 2.20). From the T1 measurement results for Na, it can be seen that pV and pM have the same degree of motility (in a low state) at 10.3 ms and 8.3 ms, respectively, at near 0 ° C (Fig. 2.17 c), d)). In fact, satellite transitions appear from around 0 ° C in pM, suggesting that polymer-Na interactions occur at higher temperatures in pM. Furthermore, since the decrease in residual water is about the same as that in pV and PLL, it is thought that trapping of Na ions occurs at higher temperatures, resulting in insufficient cell dehydration and a decrease in the cryoprotective effect[27, 28]. This is consistent with the fact that the switching temperature from freezing bulk water to

freezing coordination water is significantly lower at -27° C at pM than for other polymers. Also, in pM, the line width of the water proton peak appears to broaden as in pV and PLL. However, since the increase in T1 does not occur in parallel, means no increase in the viscosity, it can be seen that the broadening is not caused by vitrification. Since pM has a weight average molecular weight of 216,000, which is extremely large compared to other polymers, it is thought that the decrease in residual water may have increased chain entanglement, making the gaps in the matrix coarser. Although this study only measured temperatures down to around -50 ° C, general cryopreservation uses -80 ° C or lower temperature, so polyampholytes with no or lower vitrification capacity are likely to cause cryoinjury because salt and water are difficult to isolate from the cells. Therefore, in order for a polyampholytes to exhibit a cryoprotective effect, it is thought that salt concentration adjustment during freezing by trapping salt or water and vitrification ability are necessary.

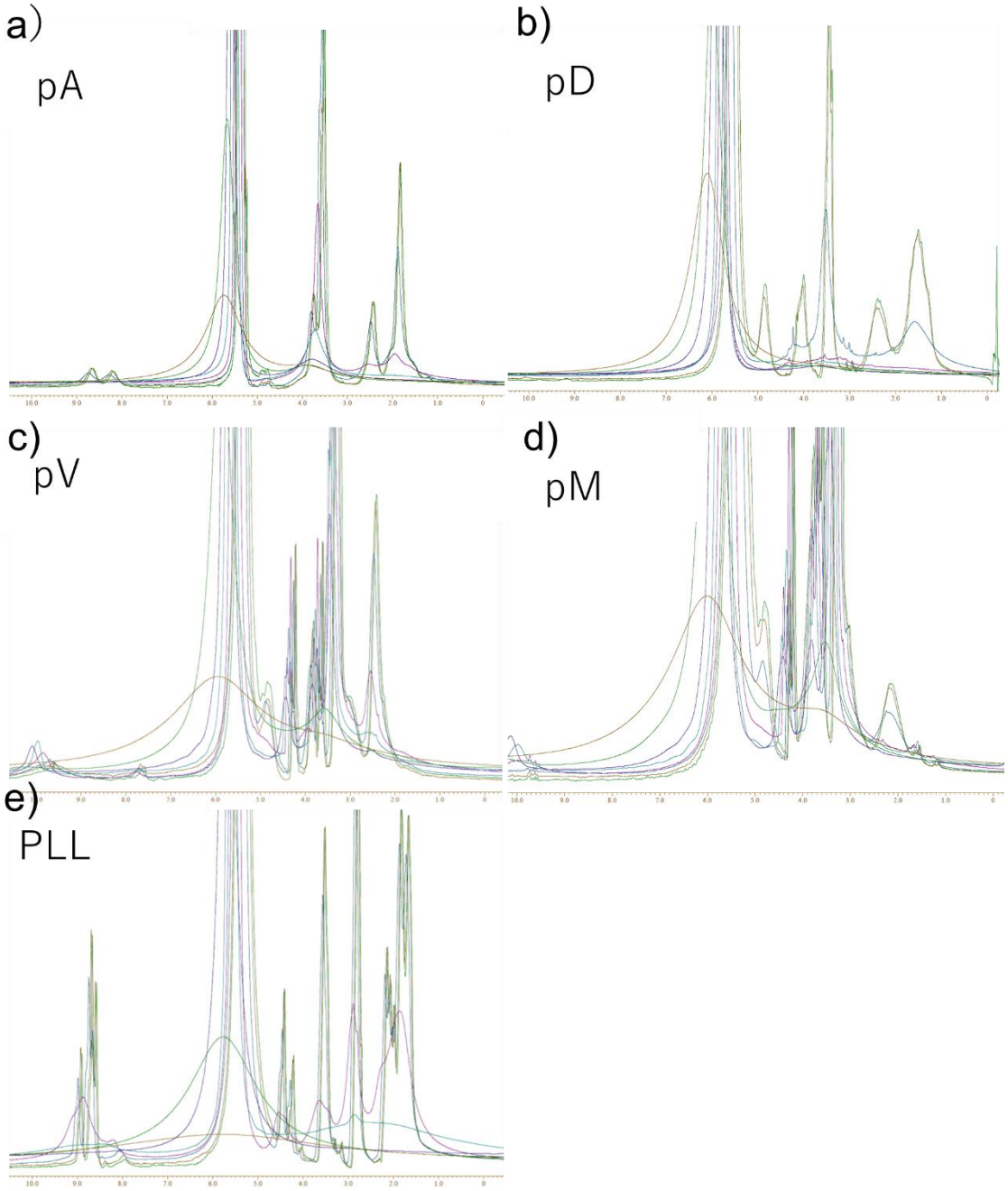

Figure 2.20 Change in peak intensity of polymer due to temperature change. a) pA, b)pD, c) pV, d) pM, e) PLL.

Table 2.2 Various data for each polymer obtained by temperature-variable solid-state NMR.

	Water proton peak intensity		Water proton line width		T_1 of water proton	Chemical shift change of Na		Na signal strength		Na signal line width		T_1 of Na signal
	Around -10°C residual water / %	Around -45°C residual water / %	Temperature at which widening starts / °C	Line width at around -45 °C / Hz	Longitudinal relaxation time around -45 °C / s	First inflection point / °C	Second inflection point / °C	Satellite peak appearance temperature / °C	Na signal intensity around -45°C	Maximum line width temperature / °C	Second widening of line width / °C	Longitudinal relaxation time around 0 °C / ms
pA	20.2	8.4	-17	740	0.56	-18	No	-7	0.33	-31	No	22
pD	28.3	9.9	-19	590	0.58	-21	No	-10	0.3	-31	No	16
pV	34.1	9.9	-21	1430	0.72	-19	-44	-7	0.23	-32	-42	10.3
pM	33.4	10.2	-27	1070	0.49	-21	No	≧ 0	0.24	-32	-42	8.3
PLL	29.7	7.4	-18	3440	0.92	-18	-40	-11	0.21	-28	-39	14.3

2.4 Conclusion

In Chapter 2, I synthesized polyampholytes with different side chain structures and correlated their cryoprotective effects and structures. pA with stronger anions and cations and pM with higher molecular weight and polydispersity had poor cryoprotective effects. The IRI assay revealed that there was no significant difference in the ability of each polymer to inhibit ice crystals, and that there was no clear correlation between the cryoprotective function and IRI activity of these polymers. Temperature-variable solid-state MAS-NMR confirmed a rapid decrease in the amount of residual water immediately after freezing in pA. This is thought to be due to the fact that the hydrogen bonds of the hydration water in pA are relatively close to the bulk water. For polymers with high cryoprotective effect such as pV and PLL, vitrification and coordination of Na ions to the polymer chain were observed at higher temperatures, suggesting that, as in previous studies, vitrification is an important factor for cryoprotective effect. In the future, it is believed that a deeper understanding of polymer structure and vitrification ability will enable the molecular design of more effective cryoprotectants.

2.4Reference

1) K. Matsumura, F. Hayashi, T. Nagashima and S. -H. Hyon, *J. Biomater. Sci. Polym. Ed.,* 2013, **24**(12), 1484-1297.

2) K. Matsumura, F. Hayashi, T. Nagashima, R. Rajan and S. -H. Hyon, *Commun. Mater.*, 2021, **2**, 15.

3) R. Rajan, M. Jain and K. Matsumura, *J. Biomater. Sci., Polym. Ed.*, 2013, **24**(15), 1767-1780.

4) R. Rajan, F. Hayashi, T. Nagashima and K. Matsumura, *Biomacromolecules*, 2016, **17**(5), 1882-1893.

5) J. Zhao, M. A. Johnson, R. Fisher, N. A. D. Burke, and H. D. H. Stöver, *Langmuir*, 2019, **35**(5), 1807-1817

6) C. Ladavière, N. Dörr and J. Claverie, *Macromolecules*, 2001, **34**(16), 5370-5372.

7) C. Stubbs, J. Lipecki and M. I. Gibson, *Biomacromolecules*, 2017, **18**(1), 295-302.

8) R. Nakahata and S. Yusa, *Langmuir,* 2019, **35**(5), 1690-1698.

9) K. A. Murray and M. I. Gibson, *Biomacromolecules*, 2020, **21**(7), 2864-2873.

10) R. C. Deller, M. Vatish, D. A. Mitchell and M. I. Gibson, *Nat. Commun.*, 2014, **5**, 3244.

11) B. Graham, A. E. R. Fayter, J. E. Houston, R. C. Evans and M. I. Gibson, *J. Am. Chem.*

Soc., 2018, **140**(17), 5682-5685.

12) B. Graham, T. L. Bailey, J. R. J. Healey, M. Marcellini, S. Deville and M. I. Gibson, *Angew. Chem. Int. Ed.*, 2017, **56**, 15941-15944.

13) Y. Sun, D. Maltseva, J. Liu, T. Hooker II, V. Mailänder, H. Ramløv, A. L. DeVries, M. Bonn and K. Meister, *Biomacromolecules*, 2022, **23**(3), 1214-1220.

14) D. W. Aksnes and L. Gjerdåker, *J. Mol. Struct.*, 1999, **475**(1), 27-34.

15) Q. Shao, L. Mi, Z. Han, T. Bai, S. Liu, Y. Li and S. Jiang, *J. Phys. Chem. B*, 2014, **118**(24), 6956-6962.

16) T. Wang, X. Wang, Y. Long, G. Liu and G. Zhang, *Langmuir*, 2013, **29**(22), 6588-6596.

17) Y. Chang, S. Chem, Z. Zhang, and S. Jiang, *Langmuir*, 2006, **22**(5), 2222-2226.

18) Y. Higaki, Y. Inutsuka, T. Sakamaki, Y. Terayama, A. Takenaka, K. Higaki, N. L. Yamada, T. Moriwaki, Y. Ikemoto and A. Takahara, *Langmuir,* 2017, **33**(34), 8404-8412.

19) N. Bloembergen, E. M. Purcell and R. V. Pound, *Phys. Rev*, 1948, **73**, 679-712.

20) I. Solomon, *Phys. Rev*, 1955, **99**, 559-565.

21) M. Wang, A. Mahajan, A. Mahajan, J. S. Miller, D. H. McKenna and A. Aksan, *ACS Appl. Bio Mater*, 2023, **6**(6), 2226-2236.

22) D. J. Morales and S. Greenbaum, *Int. J. Mol. Sci.*, 2020, **21**(9), 3402.

23) C. Naumann and P. W. Kuchel, *Polym, Chem.*, 2010, **1**, 1109-1116.

24) N. E. Hoffmann and J. C. Bischof, *Urology*, 2002, **60**(2), 40-49.

25) J. H. Crowe, J. F. Carpenter, L. M. Crowe and T. J. Anchordoguy, *Cryobiology*, 1990, **27**(3), 219-231.

26) M. Mousazadehkasin and J. G. Tsavalas, *Biomacromolecules*, 2020, **21**(11), 4626-4637.

27) P. Mazur, *J. Gen. Physol.* 1963, **47**(2), 347-369.

28) P. Mazur, S. P. Leibo and E. H. Y. Chu, *Exp. Cell. Res.*, 1972, **71**(2), 345-355.

Chapter 3

Enhancement of cryopreservation with intracellularly permeable zwitterionic polymers

3.1 Introduction

Polymeric cryoprotectants are often studied as alternatives because they are usually large and cannot easily pass through the cell membrane. Polymers that inhibit ice crystallization, such as polyvinyl alcohol, antifreeze glycoproteins, glycopeptides, and polyampholytes (that are composed of carboxylated polylysine or N-dimethylamine and carboxylic acids), have been extensively studied as alternative polymeric cryoprotectants.[1–5] Studies have also been conducted on small-molecule cryoprotectant structures in polymer side chains. Burkey et al. reported that polymers with a polyol structure in the main chain and a DMSO-like methyl sulfinyl structure in the side chain provide higher cryoprotection than DMSO[6]. Similarly, a methacrylate polymer with a methyl sulfoxide structure has been reported, but its cryoprotective properties are inferior to those of methacrylate polymers[7]. A notable difference between the two polymers is that the methacrylate form does not penetrate intracellularly, whereas the polyol form is taken up by the cell via endocytosis.

Another promising membrane-impermeable cryoprotectant that enhances cryoprotection upon intracellular permeation is trehalose[8, 9]. Outside the cell, trehalose

inhibits ice formation via hydration, while inside the cell, trehalose interacts with membrane lipids and contributes to membrane stabilisation. Furthermore, it has been reported that the low-molecular-weight polyethylene glycol (PEG) can permeate cells and improve cryoprotection by suppressing the increase of osmotic pressure during freezing, stabilising cell membranes, and inhibiting ice formation, suggesting that the intracellular introduction of membrane-impermeable cryoprotectants is crucial for improving cryoprotective efficacy[10]. Zwitterionic polymers are polymers that contain both cations and anions in their molecules. Zwitterionic polymers have been the subject of much research in applications such as drug delivery systems, antifouling coatings, and hydrogels[11-15]. Zwitterionic polymers, such as sulfobetaine polymers and poly(MPC/BuMA), a copolymer of 2-methacryloyloxyethyl phosphorylcholine (MPC) and butyl methacrylate (BuMA), have been shown to permeate the entire cytoplasm without requiring endocytosis[16–18]. Because sulfobetaine polymers have also been reported to have a cryoprotective effect, the development of a cell-permeable copolymer with a sulfobetaine polymer and a DMSO structure is expected to improve the cryoprotective effect[19].

In chapter 3, copolymers of 3-((3-acrylamidopropyl)dimethylammonio)propane-1-sulfonate (SPB) and 2-(methyl sulfinyl)ethyl methacrylate (MSEMA), which has the

same methyl sulfinyl structure as DMSO, were synthesised, and their cryoprotective effect was confirmed. After investigating the penetration and reverse diffusion of the fluorescent-modified polymers into cells, the effectiveness of the zwitterionic polymers as the carriers of membrane-impermeable cryoprotectants was confirmed by performing cryopreservation with the polymers penetrating the cells. Poly(SPB) enhanced cryoprotection via intracellular penetration, indicating that it could be used as a novel cryoprotectant carrier. Expanding upon established cryoprotective properties of SPB, our innovative approach integrates DMSO-mimicking monomers through strategic copolymerization, highlighting the potential to exploit SPB's intrinsic intracellular permeability for superior cryoprotection of 3D tissue constructs. To the best of our knowledge, this work represents the first incorporation of methylsulfinyl motifs into the zwitterionic polymer structure, generating a material with significantly enhanced properties and indicating a substantial advancement in the cryoprotection field.

3.2 Materials & methods

3.2.1 Materials

Methacryloyl chloride, 2-(methylthio)ethanol, *n*-butyl amine, and 2,2'-azobis(isobutyronitrile) (AIBN) were purchased from Tokyo Chemical Industry Co. (Tokyo, Japan); fluorescein *o*-acrylate, triethyl amine (TEA) and 2-(dodecylthiocarbonothioylthio)-2-methylpropionic acid (DDMAT) were purchased from Sigma-Aldrich (St. Louis, MO, USA); tris(2-carboxyethyl)phosphine hydrochloride and 3-(4,5-dimethylthial-2-yl)-2,5-diphenyltetrazalium bromide (MTT) were purchased from FUJIFILM Wako Pure Chemical Corporation (Osaka, Japan); dichloromethane (DCM), dimethyl sulfoxide (DMSO), methanol and hydrogen peroxide (30%) was purchased from Nacalai Tesque, Inc. (Kyoto, Japan); and 3-((3-acrylamidopropyl)dimethylammonio)propane-1-sulfonate was supplied by Osaka Organic Chemical Industry, Ltd (Osaka, Japan). All the reagents were used as received without further purification.

3.2.2 Characterization

^{1}H NMR was measured using a Bruker Avance III 400. The deuterated solvent used was purchased from Sigma-Aldrich. The NMR data were analysed using Topspin 3.5 software. FT-IR was measured using JASCO FT/IR-6X in attenuated total internal reflection mode.

Measurements were performed with 16 scans per spectrum and a resolution of 4 cm^{-1}. The molecular weights and distributions (polydispersity index; PDI) of the polymers were determined by gel permeation chromatography (GPC; BioSep-s2000, Phenomenex, Inc., CA, USA) using a Waters Alliance HPLC system. A 0.1 M sodium bromide aqueous solution was used as the mobile phase (flow rate, 1 mL/min) and pullulan as the standard.

3.2.3 Synthesis of 2-(methylthio)ethyl methacrylate (MTEMA)

The synthesis of MTEMA is shown in scheme 3.1. TEA (4.46 g, 44.1 mmol) and 2-(methylthio)ethanol (3.64 g, 39.5 mmol) were added to 50 mL of DCM and kept at 0 ° C. Then, methacryloyl chloride (4.60 g, 44.0 mmol) was added dropwise and the mixture was allowed to react for 10 h. After completion of the reaction, the precipitates were filtered and washed thrice with a saturated aqueous sodium hydrogen carbonate solution. They were then washed with saturated saline and dehydrated using magnesium sulphate. The solvent was removed using an evaporator and dried under a vacuum (5.71 g, yield 52.0 %). ^{1}H NMR ($CDCl_3$, 400 MHz): δ –6.13 (s, 1H, H_{cis}), 5.59 (s,1H, H_{trans}), 4.33 (t, 2H, –O–CH_2), 2.77 (t, 2H, –CH_2–S–), 2.17 (s, 3H, –S–CH_3), 1.95 (s, 3H, –CH_3).

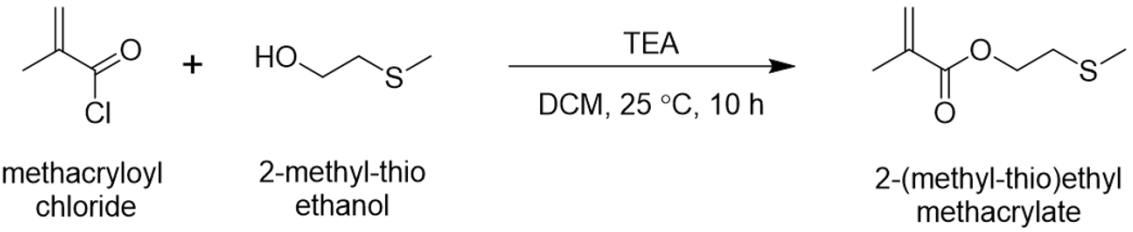

Scheme 3.1 Synthesis of MTEMA.

3.2.4 Synthesis of MSEMA

The synthesis of MSEMA is shown in scheme 3.2. MTEMA (4.0 g, 25 mmol) was cooled to 0 ° C in an ice bath, and N_2 was bubbled through for 30 min. Then, hydrogen peroxide water (3.12 g, 27.5 mmol) was added to the mixture dropwise to raise its temperature back to 25 ° C for reaction to proceed for 24 h, following which 50 mL distilled water was added to terminate the reaction. The product was then extracted with DCM thrice, and the collected organic layers were removed by evaporation and dried under vacuum (3.44 g, yield 78.3 %). ^{1}H NMR ($CDCl_3$, 400 MHz): δ –6.15 (s, 1H, H_{cis}), 5.64 (s, 1H, H_{trans}), 4.59 (m 2H, –O–CH_2), 3.07 (m, 2H, –CH_2–SO–), 2.67 (s, 3H, –S–CH_3), 1.96 (s, 3H, –CH_3).

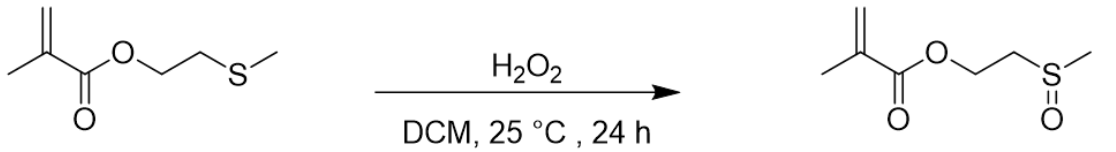

2-(methyl-thio)ethyl methacrylate

2-(methylsulfonyl)ethyl methacrylate

Scheme 3.2 Synthesis of MSEMA.

3.2.5 Synthesis of zwitterionic polymer

The synthesis of zwitterionic polymer is shown in scheme 3.3. Poly(SPB) was prepared by dissolving SPB (5.57 g, 20 mmol) in DDMAT (72.9 mg, 0.2 mmol), and AIBN (6.57 mg, 0.04 mmol) in 40 mL of a 1:3 water/methanol solution. When synthesizing

copolymers with MSEMA, MSEMA was added to the reaction mixture at 10, 20, and 30 % of the total polymer content. For example, when the introduction rate was 10 %, SPB (5.01 g, 18.0 mmol), MSEMA (0.352 g, 2.0 mmol), DDMAT (72.9 mg, 0.2 mmol), and AIBN (6.57 mg, 0.04 mmol) were dissolved in 40 mL of 1:3 water/methanol solution. N_2 bubbling was performed for 1 h, and the mixture was reacted at 70 ° C for 6 h. Samples were subsequently taken for ^{1}H NMR analysis. Monomer conversion was determined using vinyl protons near 5.8 ppm and 6.2 ppm based on the methylene peak of the polymer near 2.9 ppm. After completion of the reaction, the sample was dialysed against methanol and water for 24 h (MWCO of 3.5 kDa, Spectra/Por® 3 Dialysis Membrane, Spectrum Labs, Inc., Rancho Dominguez, CA, USA) and freeze-dried. The chemical structure of the compound was confirmed by ^{1}H NMR spectroscopy, using D_2O as the solvent.

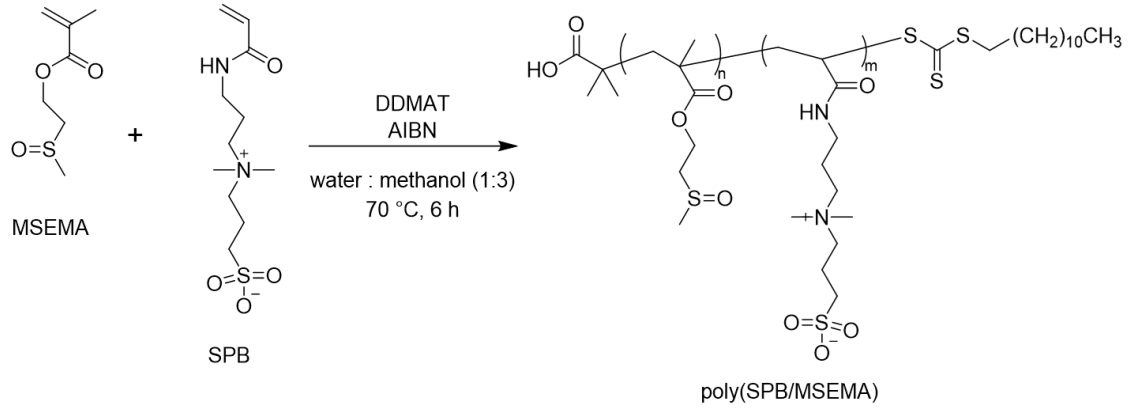

Scheme 3.3 Synthesis of zwitterionic polymer.

3.2.6 Synthesis of fluorescence-modified polymers

The synthesis of fluorescence-modifies polymer is shown in scheme 3.4. Each polymer (0.76 μmol) was dissolved in 1 M NaCl aqueous solution, and tris(2-carboxyethyl)phosphine hydrochloride (17.4 μmol) was added. *N*-butyl amine (0.76 mmol) was added, reacted at room temperature for 2 h, dialysed for 7 d (MWCO of 3.5 kDa), and freeze-dried. The obtained polymer (6.08 μmol) was dissolved in PBS containing a small amount of tris(2-carboxyethyl)phosphine hydrochloride. Fluorescein *o*-acrylate (18.2 μmol) was dissolved in DMSO, mixed with the polymer solution, and allowed to react at room temperature for 10 h in the dark. Following the completion of the reaction, the solution was dialysed for 7 days (MWCO of 3.5 kDa) and then freeze-dried.

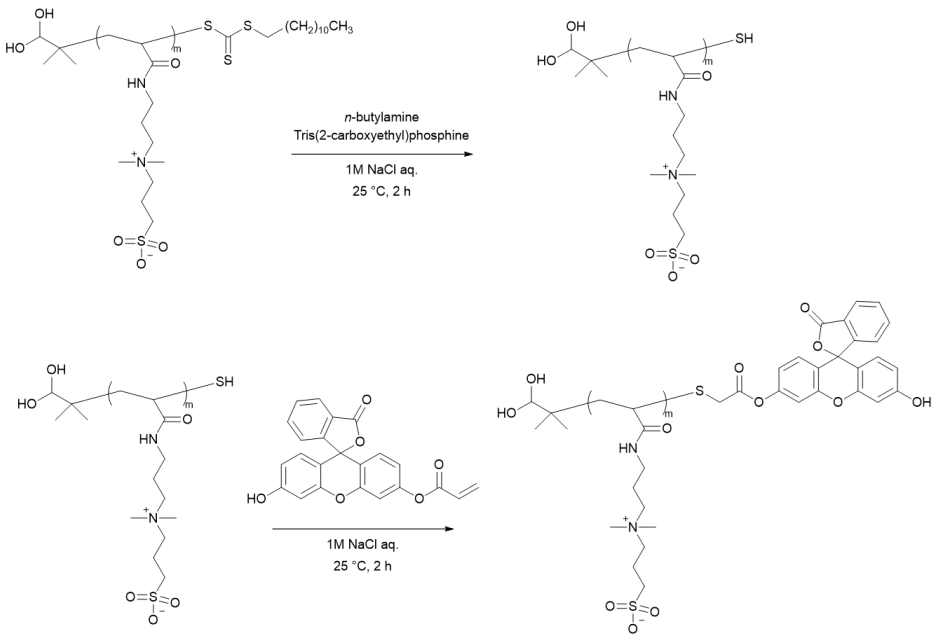

Scheme 3.4 Synthesis of fluorescence-modified polymers.

3.2.7 Cell culture

Mouse fibroblasts (L929; American Type Culture Collection, Manassas, VA, USA) were prepared in Dulbecco's modified Eagle's medium (DMEM, Sigma-Aldrich, St. Louis, MO, USA) supplemented with 10 % foetal bovine serum (FBS). Cells were cultured in an incubator at 37 ° C with 5 % CO_2. Passaging was performed when the cells exceeded 80 % of the bottom of the dish. For passaging, the cells were detached by treatment with trypsin solution (0.25 % [w/v] trypsin containing 0.02 % [w/v] ethylenediaminetetraacetic acid in PBS).

3.2.8 Cryopreservation

The polymer solution was dissolved in an aqueous 0.3 M NaCl aqueous solution to 10 w/w%. The solution was filter-sterilised through a 0.22 μm filter. Then, 1×10^6 L929 cells were suspended in 1 mL of the polymer solution and stored at –80 ° C; cooling was conducted without a controlled cooling rate. After permeation of the cells with the polymer, 1×10^6 permeated-L929 cells were seeded in a 35 mm dish and cultured for 24 h. Then, the medium was removed and 1 mL of polymer solution was added to the culture, which was incubated at 4 ° C for 10 min. After washing thrice with PBS, the cells were treated with trypsin and collected by centrifugation (1000 rpm). They were then suspended in 1 mL of the polymer solution and stored at -80 ° C in the same manner.

After 24 h, the cells were thawed by immersing the samples in a water bath at 37 ° C. The cell suspension was then diluted 10-fold with DMEM and centrifuged at 1000 rpm for 4 min. The cells were then suspended in a small amount of DMEM and viability was determined by staining them with trypan blue. Cell viability and recovery were determined using the following formula (Eq. 3.1).

$$\text{Recovery rate (\%)} = \frac{\text{Living cell}}{\text{Frozen cell}} \times 100 \quad \text{(Eq. 3.1)}$$

3.2.9 Mitochondrial membrane potential

Mitochondrial membrane potential was measured using the Tetramethylrhodamine Methyl Ester Perchlorate (TMRM, TCI). Before the experiment, 2.5 mg of TMRM was dissolved in 500 μL of DMSO to create a 10 mM DMSO stock solution. First, cells were incubated in 35 mm glass bottom dishes for 24 hours after freeze-thawing. Once the medium was removed, 1 ml of DMEM without FBS was added. Thereafter, 1 mL of TMRM staining solution diluted to 250 nM was added and left standing in a CO2 incubator for 30 minutes. After staining, cells were washed with DMEM without FBS and observed under a confocal microscope. For control, carbonyl cyanide 4-(Trifluoromethoxy)phenylhydrazone (FCCP), an uncoupler for electron transport and oxidative phosphorylation, was added to a final concentration of 20 mM before staining

with TMRM, and the cells were incubated for 10 minutes. Depolarization was performed.

3.2.10 Cytotoxicity test

L929 cells were dispensed into 96-well plates at 1×10^3 cells/100 μL and cultured in an incubator for 3 days. Samples were prepared by dissolving in DMEM so that the concentrations of the polymer and DMSO ranged between 0 and 20 %, followed by filter sterilisation. After culturing, 100 μL of each prepared sample was dispensed and further incubated again in an incubator for 2 days. MTT was dissolved to 0.3 mg/mL in DMEM without FBS, and 100 μL of the solution was dispensed and incubated for 3 h. Subsequently, all solutions were removed from the plate, 100 μL of DMSO was dispensed, and the absorbance was measured at $\lambda = 540$ nm using a microplate reader (Infinite 200 PRO M Nano, Tecan).

3.2.11 Confocal Microscopy

For fluorescence observation, 1×10^6 L929 cells were seeded in a 35-mm glass-bottom dish and cultured for 24 h. Then, the medium was removed, 1 w/w% fluorescence-modified polymer solution was added dropwise, and the mixture was incubated at 4 ° C for 10 min. After removing the polymer solution and washing with PBS thrice, the cells were treated with PBS again and observed under a confocal laser microscope (FV1000D, Olympus).

3.2.12 Observation of counter diffusion

To observe the counter diffusion, 1 × 10^6 L929 cells were seeded in a 35 mm dish and cultured for 24 h. Subsequently, the medium was removed, 1　w/w% of the fluorescence-modified polymer solution was added dropwise, and the mixture was incubated at 4 ° C for 10 min. After washing thrice with PBS, the cells were trypsinised and collected by centrifugation. The harvested cells were suspended in 10 mL of medium, and 1 mL of the suspension was plated on a 35-mm glass-bottom dish and incubated at 37 ° C. Fluorescence observations were performed every 10 min using BZ-X800 (Keyence, Osaka, Japan).

3.2.13 Differential scanning calorimetry

Differential scanning calorimetry (DSC) was performed using the EXTAR SII-6200 (Seiko Instruments, Japan). After cooling from 5 ° C to –50 ° C at a cooling rate of 1 ° C/min under a nitrogen flow of 50 mL/min, the temperature was maintained for 5 min and then heated to 20 ° C at 1 ° C/min.

3.3 Results & Discussion

3.3.1 Polymer characterization

MSEMA was synthesised in two steps. First, 2-(methylthio)ethanol was reacted with methacryloyl chloride to prepare MTEMA (Figure 3.1). Then, MTEMA was oxidised with 1.1 equiv. of hydrogen peroxide to obtain MSEMA; ^{1}H NMR results confirmed the complete oxidation of the MTEMA[20, ,21] (Figure 3.2). In addition, in the Fourier-transform infrared spectrum, the peak near 1300 cm^{-1} showed no significant change and the S=O stretching vibration of sulfone could not be observed, suggesting that excessive oxidation did not occur (Figure 3.3).

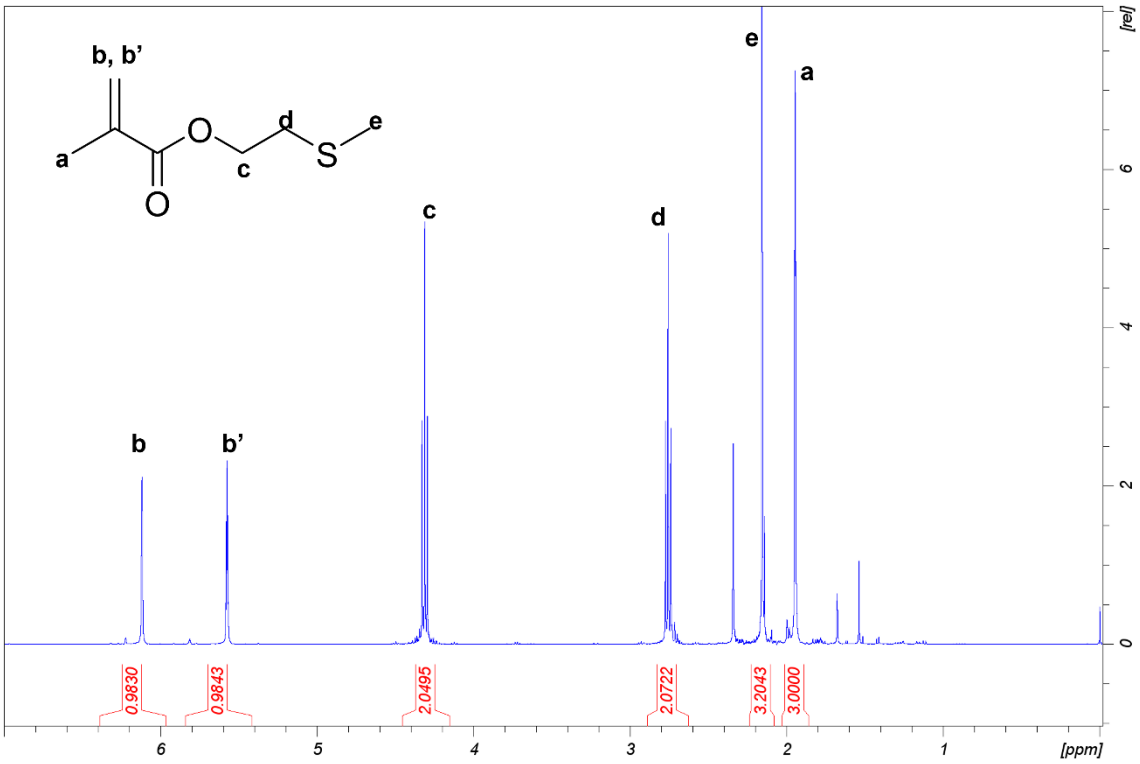

Figure 3.1 ^{1}H NMR spectrum of MTEMA.

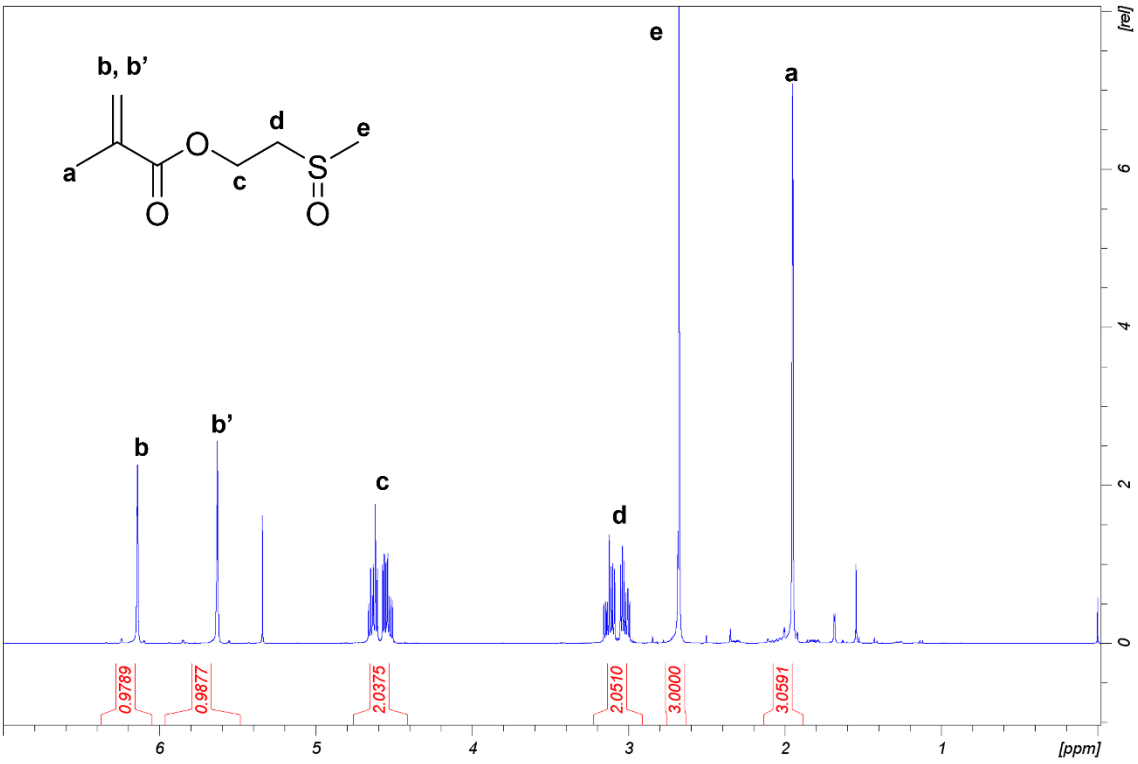

Figure 3.2 ^{1}H NMR spectrum of MTEMA.

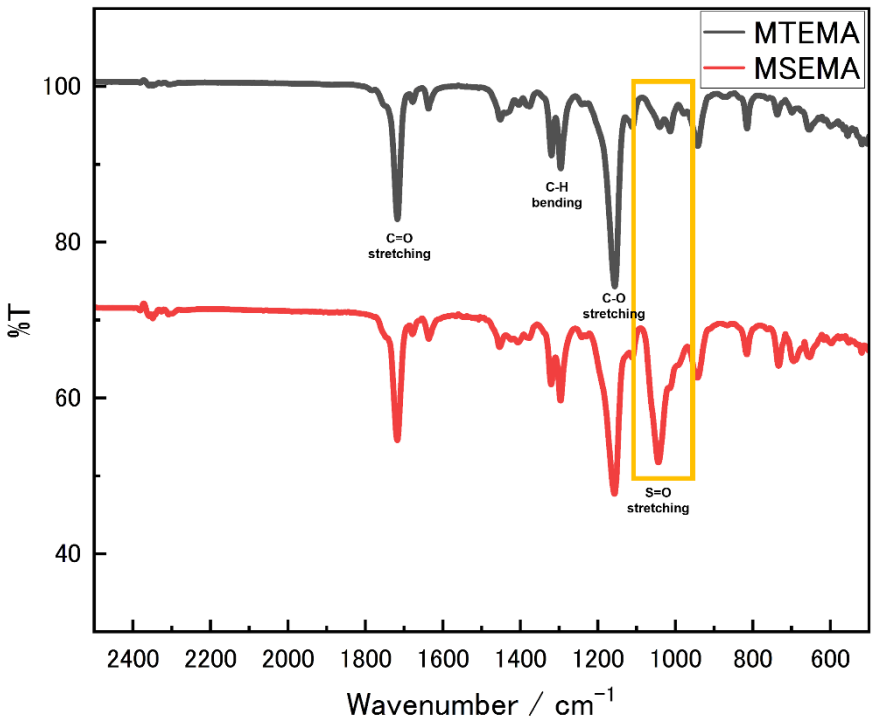

Figure 3.3 FT-IR spectra of MTEMA and MSEMA.

Poly(SPB) and poly(SPB/MSEMA) were synthesised via reversible addition–fragmentation chain-transfer polymerisation, using DDMAT and AIBN as the chain transfer agent (CTA) and initiator (In), respectively. Polymerisation was performed with an initial feed ratio of [monomer]:[CTA]:[In] = 100:1:0.2, aiming at a degree of polymerisation of 100. In addition, for poly(SPB/MSEMA10), poly(SPB/MSEMA10), and poly(SPB/MSEMA10), the ratios of MSEMA were set to 10, 20, and 30 of the total monomers, respectively. The peak in the NMR spectrum corresponding to the sulfinyl methyl protons at approximately 2.4 ppm increased with increasing MSEMA feed ratio (Figure 3.4-7). The synthesized polymers exhibited very high monomer conversions of over 90 % and exhibited narrow size disparities, as demonstrated by size exclusion chromatography (Figure 3.8, Table 3.1). The incorporation rate of MSEMA was calculated from the peak of 2.6 - 2.8 ppm (3H of MSEMA) compared to the peak of 2.8 - 3.7 ppm (12H of SPB).

Table 3.1 Characterization of zwitterionic polymer.

	Composition (in feed)		Composition (NMR)[a)]		Molar ratio[b)]	Conversion / %[c)]	M_n $\times 10^{4}$ [d)]	M_w/M_n[d)]
	SPB	MSEMA	SPB	MSEMA				
poly(SPB)	100	0	100	0	100 : 1 : 0.2	96.7	1.47	1.25
poly(SPB/MSEMA10)	90	10	89.9	10.1	100 : 1 : 0.2	98.6	1.48	1.29
poly(SPB/MSEMA20)	80	20	81.8	18.2	100 : 1 : 0.2	98.5	1.25	1.24
poly(SPB/MSEMA30)	70	30	75.7	24.3	100 : 1 : 0.2	97.5	1.29	1.27

a) Using the integral value of the NMR peak in Figure 3.4-7, the amount of MSEMEA was calculated by Eq.3.2. b) [monomer]:[CTA]:[initiator]. c) Determined using vinyl protons near 5.8 ppm and 6.2 ppm based on the methylene peak of the polymer near 2.9 ppm by ^{1}H NMR. d) Determined by GPC (Figure 3.8).

$$\text{MSEMA (\%)} = \frac{\frac{I\,(2.8\ \text{ppm})}{3}}{\frac{I\,(3.0 - 3.6\ \text{ppm})}{12} + \frac{I\,(2.8\ \text{ppm})}{3}} \times 100 \qquad \text{(Eq. 3.2)}$$

where *I* refers to the area under the peak corresponding to the chemical shift

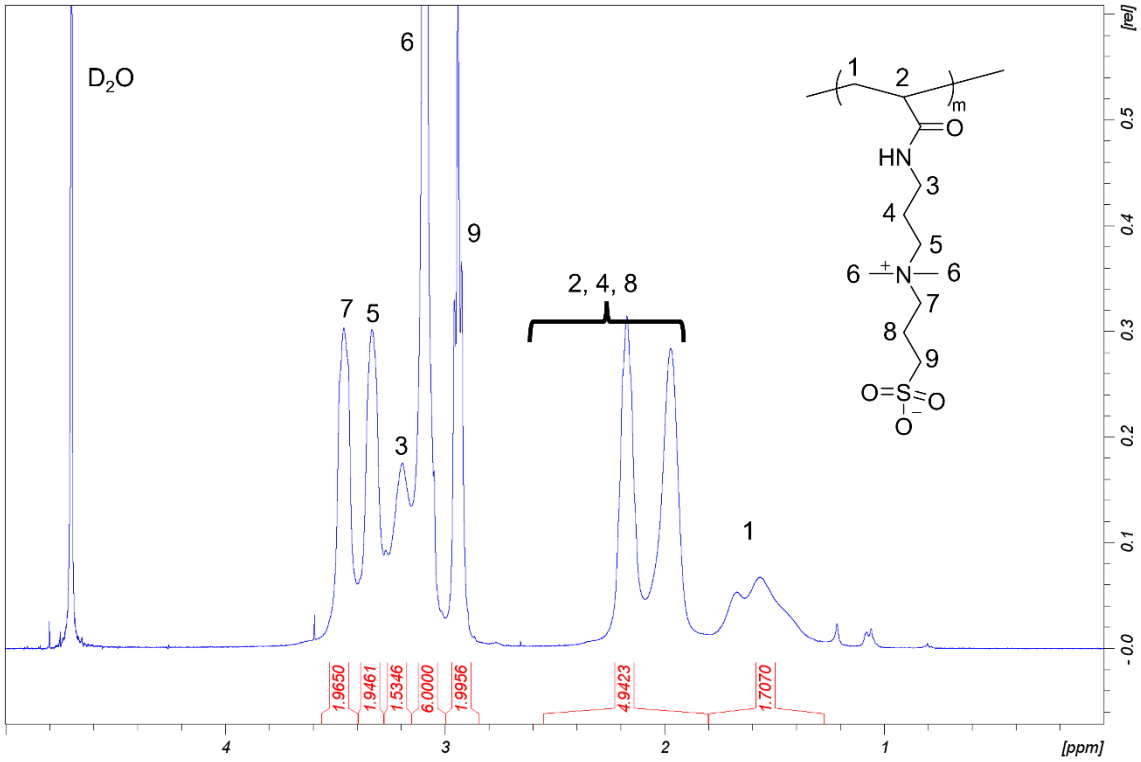

Figure 3.4 ^{1}H NMR spectrum of poly(SPB).

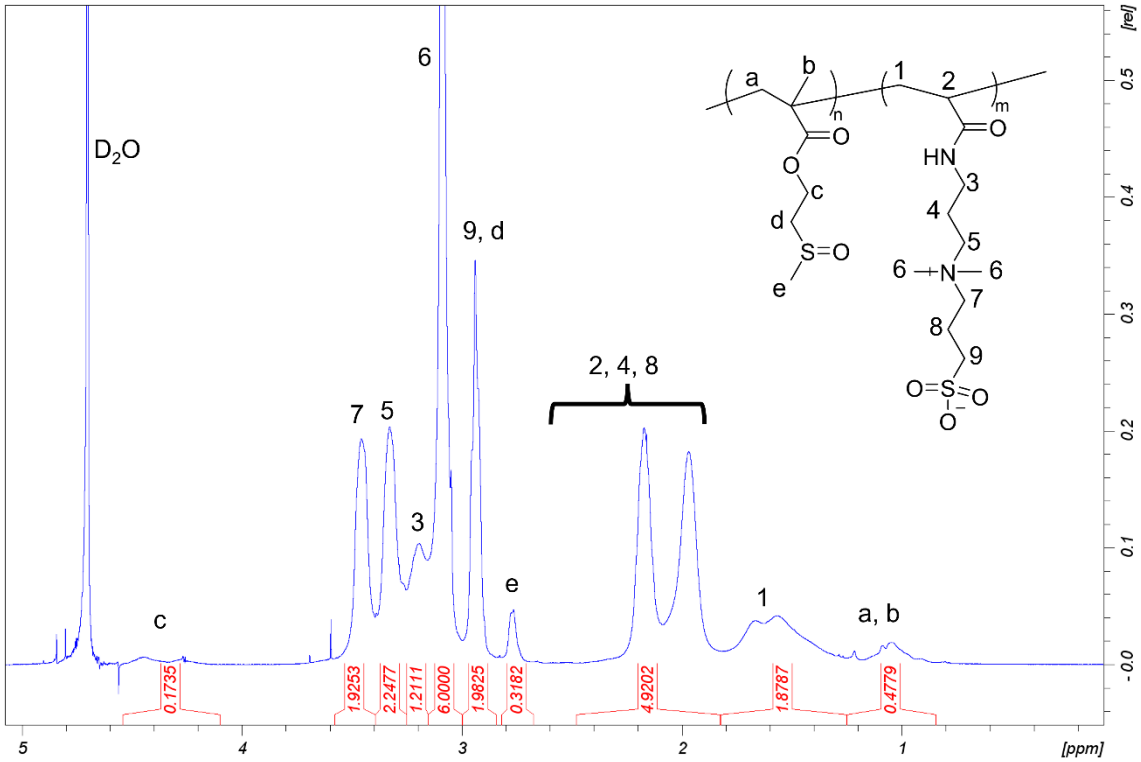

Figure 3.5 ^{1}H NMR spectrum of poly(SPB/MSEMA10).

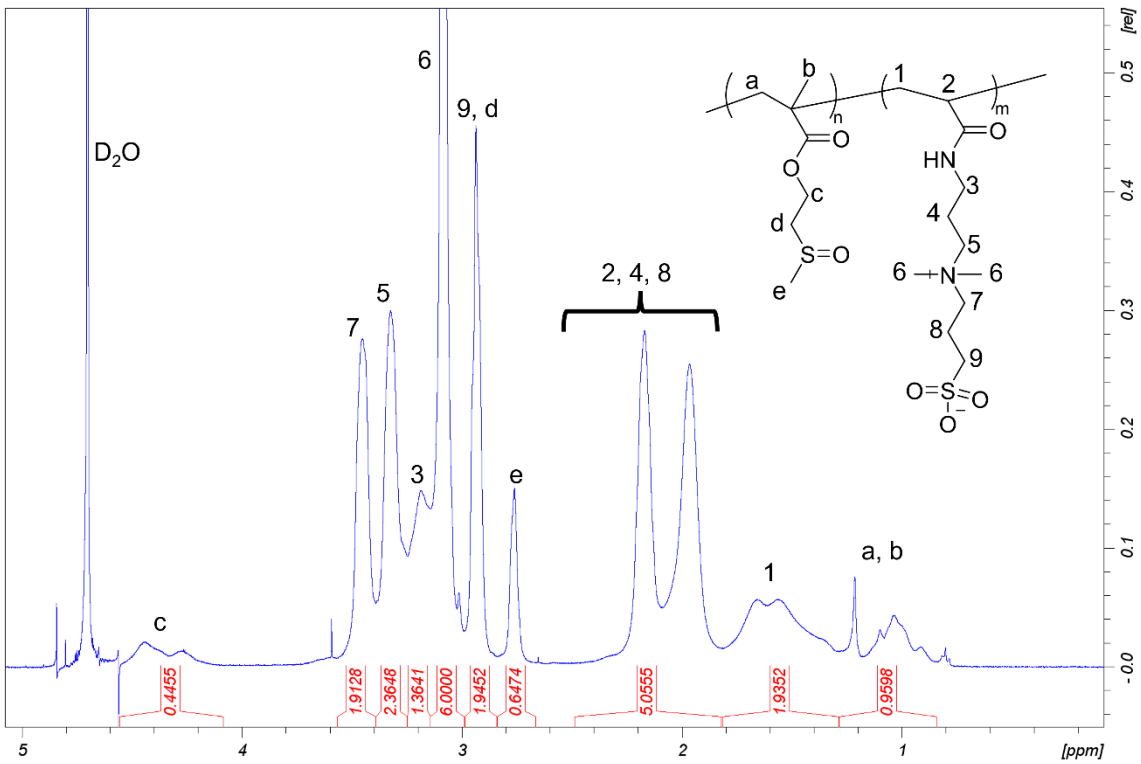

Figure 3.6 ^{1}H NMR spectrum of poly(SPB/MSEMA20).

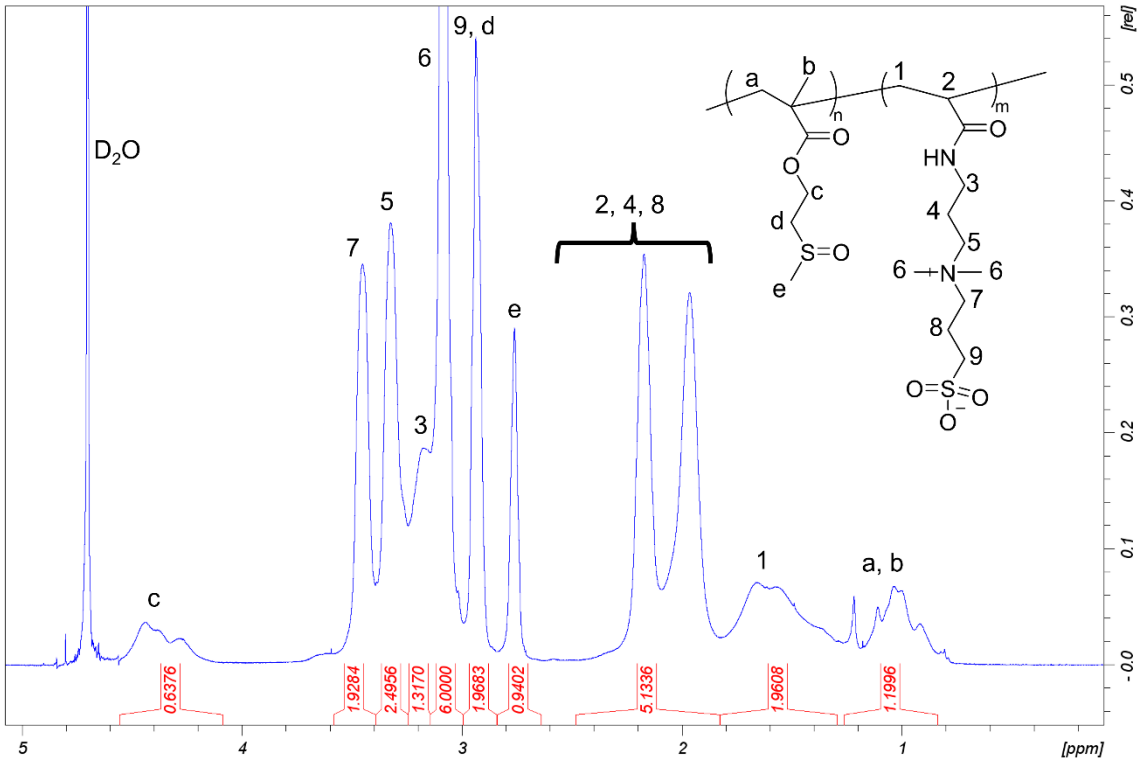

Figure 3.7 ^{1}H NMR spectrum of poly(SPB/MSEMA30).

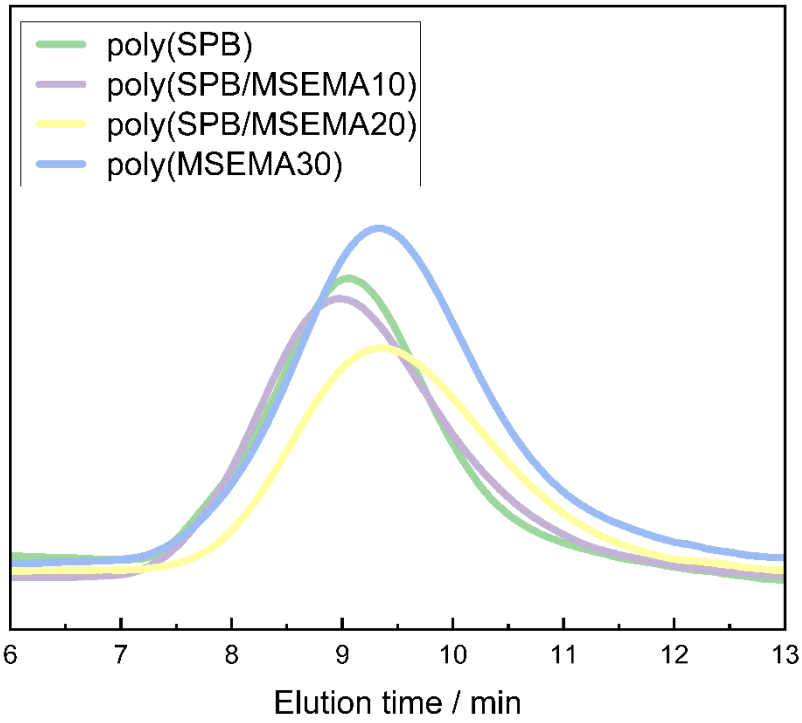

Figure 3.8 GPC curve of polymers.

3.3.2 Cytotoxicity

The cytotoxicity of each polymer is shown in Figure 3.9. During the freeze–thaw cycle, the cells are exposed to the polymer for a short duration. Because the maximum intracellular permeation time of the polymer was approximately 1 h, a cytotoxicity test was conducted by exposing L929 cells to a 10 w/w% polymer solution for 1 h. The results showed that after 1 h of exposure, the cell recovery rate was comparable to that observed without the polymer solution, indicating that there was no adverse effect on the cell recovery rate attributed to polymer toxicity during cryopreservation by intracellular permeabilisation.

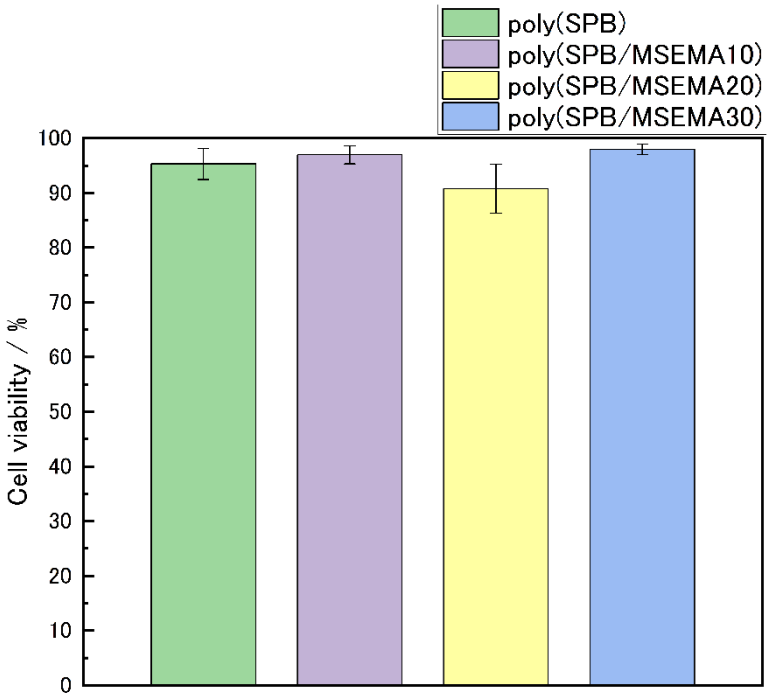

Figure 3.9 Cytotoxicity of each polymer against L929 cells 1 hour after exposure.

3.3.3 Intracellular permeability

To confirm permeation of the polymer into the cells, the RAFT ends of the polymer were treated with butylamine and then modified with fluorescein-*o*-acrylate via a thiol–ene reaction. Confocal microscopy was then used to confirm that the fluorescein-modified polymers had permeated the cells. Because intracellular permeation of sulfobetaine polymers is reported to be enhanced at 4 ° C, polymer permeation was performed at 4 ° C for 10 min[17, 18] (Figure 3.10 a)). The fluorescence-modified polymer was also found to diffuse throughout the cell, including the nucleus (Figure 3.10 c)). Poly(MPC/BuMA) has been reported to diffuse out of cells depending on the incubation time after intracellular permeation[22]. As counter diffusion may occur for poly(SPB) as well, after permeation of the fluorescein-labelled polymer, it was incubated at 37 ° C and the fluorescence of the cells was checked every 10 min using a fluorescence microscope. Figure 3.10 b) shows fluorescence microscopy images of the cells incubated at 37 ° C after polymer penetration. Following a 30-min incubation period, the fluorescence of the cells decreased compared to the initial levels observed immediately after polymer penetration, confirming that the polymers were counter-diffusing, as reported previously. This indicated that these polymers did not require complex manipulations to be removed from the cells after the freeze–thaw cycle.

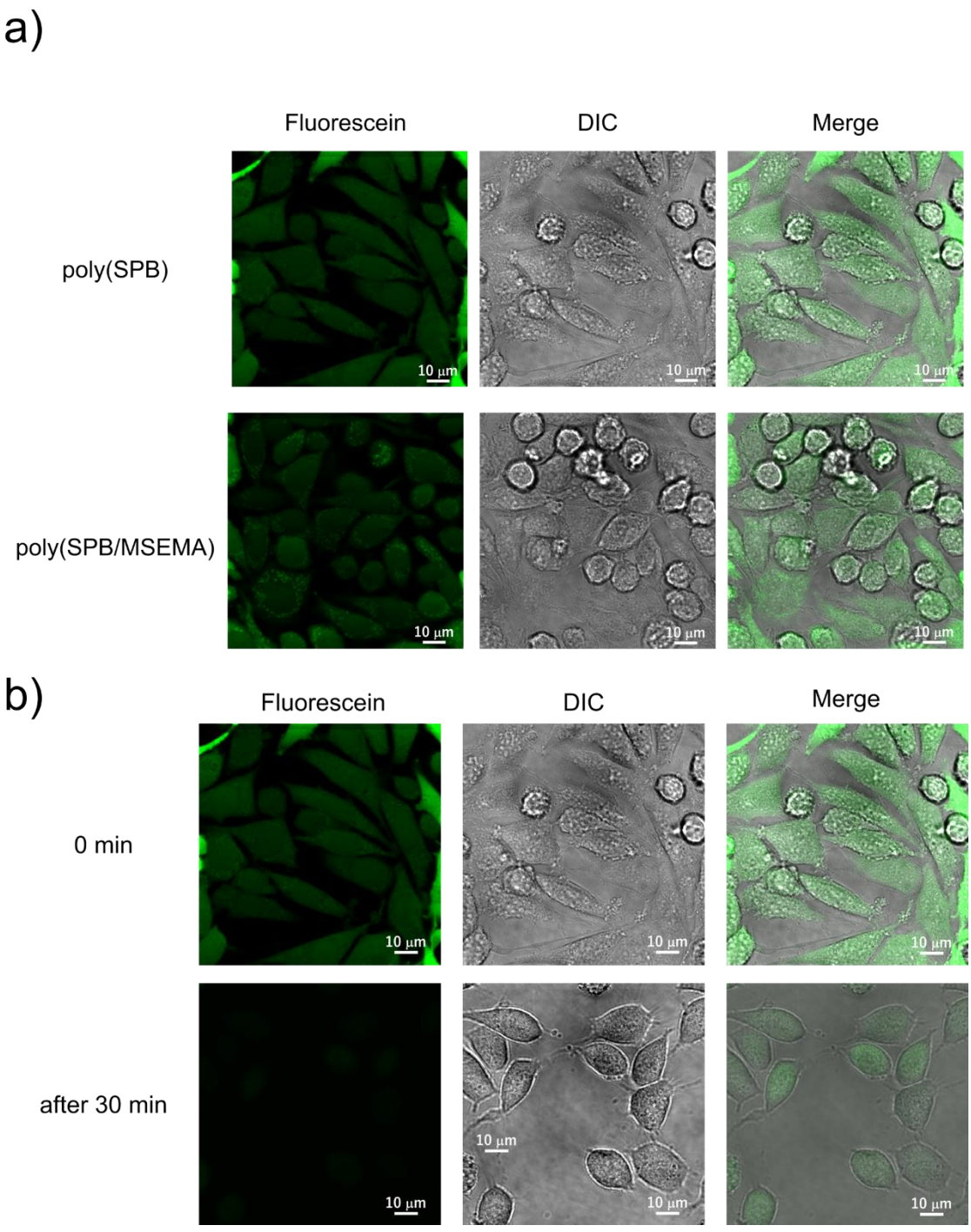

Figure 3.10 Fluorescence images of L929 cells. a) Confocal microscope images of fluorescein-labelled poly(SPB) and poly(SPB/MSEMA10) in L929 cells. b) Fluorescence images of L929 cells at 10-minute intervals after incubating at 37 ° C after permeation of fluorescein-labelled poly(SPB). Scale bars: 10 μm.

3.3.4 Cryoprotective effects

To confirm the cryoprotective effect of the synthesised polymers, L929 cells were cryopreserved at –80 ° C in 0.3 M NaCl aqueous solution with 10 w/w% polymers. In addition, to investigate the cryoprotection effect by the intracellular permeation of the polymer, 1.0×10^6 L929 cells were pre-seeded and incubated with 10 w/w% polymer solution at 4 ° C for 10 min before freezing. Figure 3.11 a) shows that the cell recovery rate decreased as the percentage of MSEMA increased. By contrast, when the polymer was allowed to permeate the cells, the cell recovery rate increased for poly(SPB) and poly(SPB/MSEMA10); In particular, for poly(SPB/MSEMA10) with a methyl sulfinyl structure, an increase of more than 20 % was observed. To confirm that the introduction of the polymer improved the cryoprotective effect, I also checked the cryoprotective effect of counter diffusion at 37 ° C for 1 h after polymer infiltration and found that the cell recovery rates were significantly lower for both polymers compared to those at the infiltration conditions, indicating that the cryoprotective effect was improved by polymer permeation (Figure 3.11 b)).

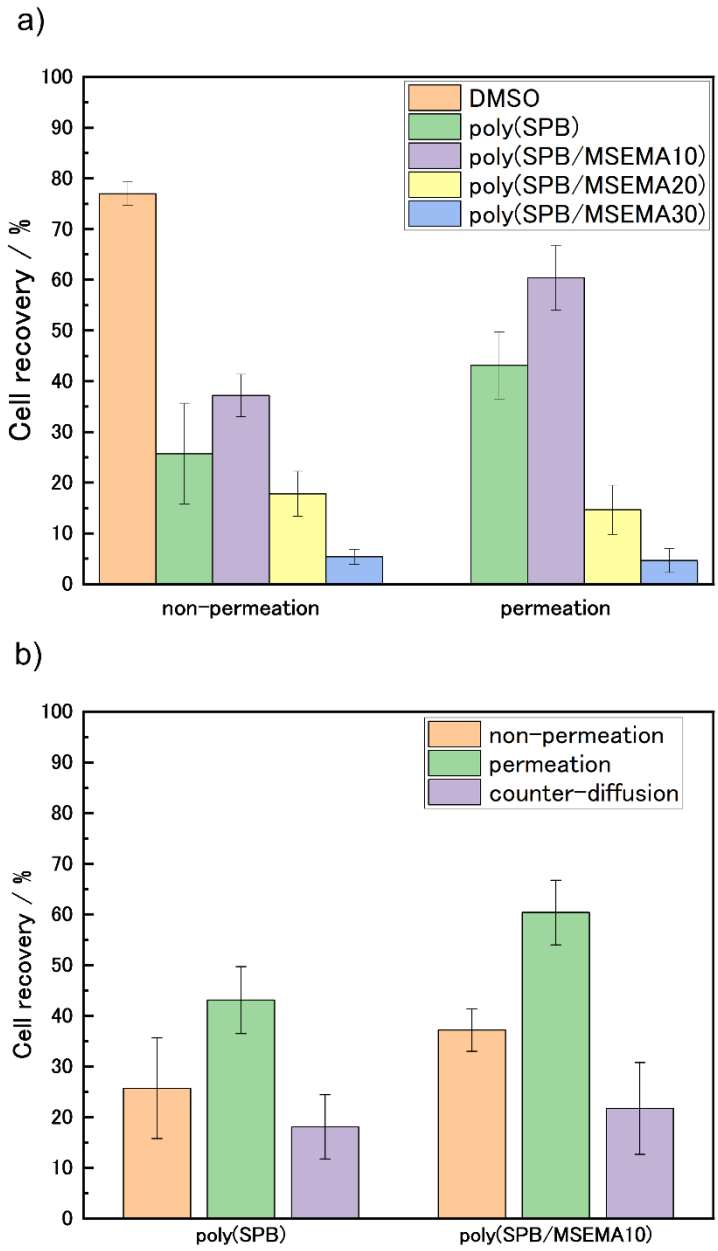

Figure 3.11 Cryoprotective properties of poly(SPB) and poly(SPB/MSEMAn). a) Comparison of cryoprotective effects with and without polymer permeation. b) Cell recovery after permeation and counter-diffusion of poly(SPB) and poly(SPB/MSEMA10).

When the percentage of MSEMA was increased to 20 % or 30 %, no improvement in cell recovery was observed even after intracellular permeabilisation. Cell proliferation after thawing showed that the number of cells after 7 days was 60–70 %, although the

proliferation rate was lower than that of fresh cells or DMSO, indicating that the growth rate of cells was not affected by intracellular infiltration of the polymer (Figure 3.12).

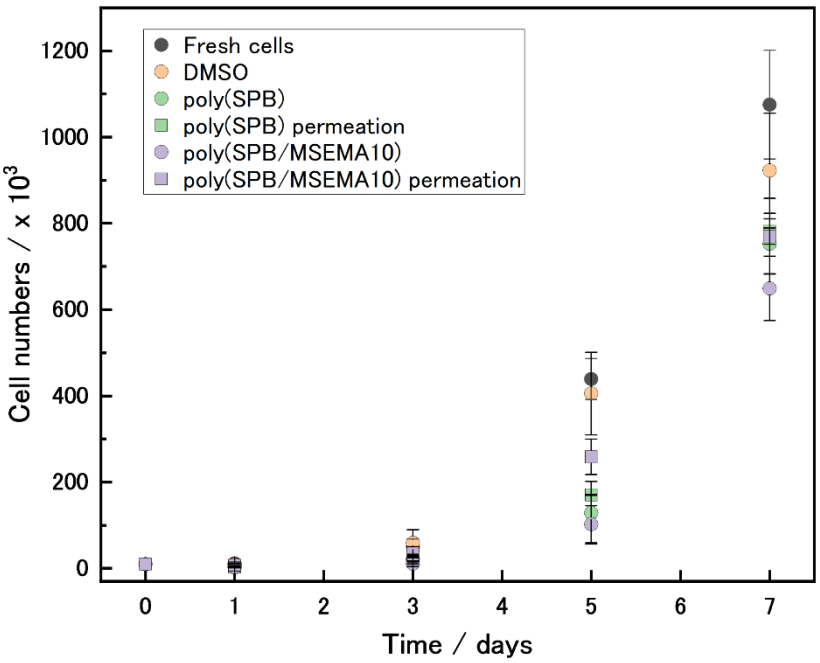

Figure 3.12 Cell growth curve after freeze–thaw cycle.

3.3.5 Thermal behavior of polymers

As membrane-permeable cryoprotectants such as DMSO and glycerol are known to displace intracellular water molecules during freezing, which causes freezing-point depression and vitrification, I used differential scanning calorimetry (DSC) to measure the freezing point and amount of ice formed during the freezing of a 0.3 M NaCl aqueous solution containing 10 w/w% polymers[23,24]. All the polymers showed less ice

formation than the 0.3 M NaCl aqueous solution. Notably, there were no significant differences between the solidification and melting enthalpies of the polymers, and the total amounts of ice formed were similar (Fig. 3.13, Table 3.2). This suggests that the amount of antifreeze water did not directly affect the cryoprotective effect. The freezing point of poly(SPB/MSEMA10) was slightly higher than those of the other polymers, suggesting that the salt ions in the solution were captured faster, possibly alleviating osmotic shock.

Table 3.2 Thermal properties of zwitterionic polymers as measured by DSC.

	T_f[a] (°C)	ΔH_f[b] (J/g)	ΔH_m[c] (J/g)
0.3 M NaCl aq.	−19.7 ± 6.52	−259.5 ± 12.20	225.5± 4.06
poly(SPB)	−19.4 ± 0.55	−227.5 ± 5.53	200.0 ± 4.50
poly(SPB/MSEMA10)	−16.40 ± 2.07	−240.6 ± 3.88	208.3 ± 4.91
poly(SPB/MSEMA20)	−19.9 ± 1.26	−233.7 ± 5.20	203.2 ± 3.45
poly(SPB/MSEMA30)	−17.9 ± 3.36	−235.00 ± 1.59	204.1 ± 6.09

a) T_f: Ice nucleation temperature of cryoprotectant solution, b) ΔH_f: solidification enthalpy, c) ΔH_m: Melting enthalpy.

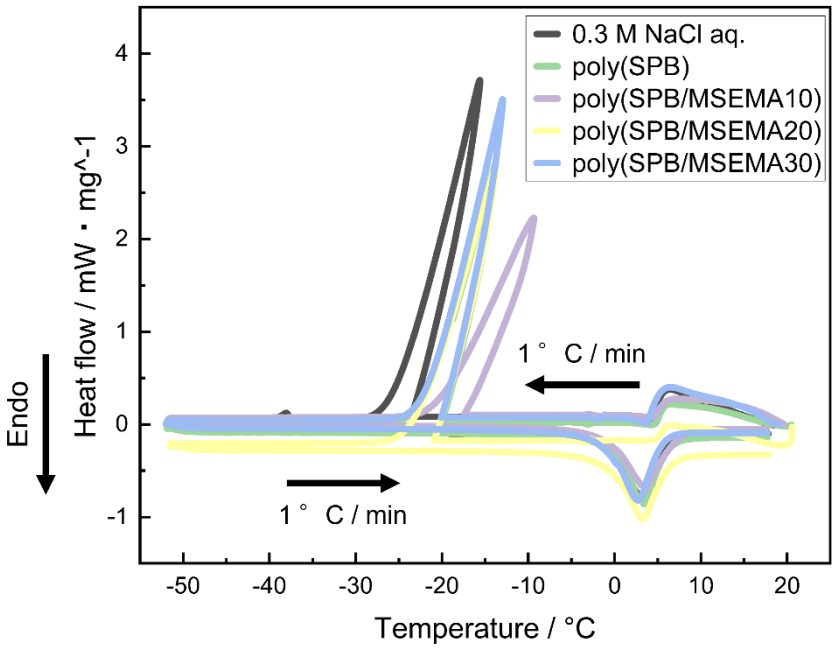

Figure 3.13 DSC trace of polymers.

Based on the two-factor hypothesis proposed by Mazur et al.,[24] lethal cell damage during freezing can be divided into two major categories: osmotic damage due to dehydration and damage due to intracellular ice crystal formation. Matsumura et al. have previously reported the mechanism of cryoprotection by polyampholytes using solid-state NMR[25]. The dynamics of the water, salt, and macromolecules during freezing were also evaluated. The effects of the inhibition of ice crystal growth by improving the viscosity of water during freezing, and the control of dehydration by the dynamics of the salt and polymer chains in solution that inhibit salt concentration increase during freezing, are important. The mechanism is that the ions in the polyampholytes interact strongly with the salt ions in the residual water during freezing,

thereby suppressing the rapid increase in osmotic pressure due to the freezing concentration and dehydration under sufficiently high and mild conditions, thus suppressing intracellular ice crystal formation and dehydration damage. The degree of ion trapping is affected by the charge density of the amphoteric electrolyte. The amphoteric portion that can trap salt ions was reduced in poly(SPB/MSEMA20) and poly(SPB/MSEMA30), which might have resulted in osmotic shock and, consequently, lower cell recovery rates.

3.3.6 Freezing and thawing of cell pellets.

To confirm that cryoprotection can be achieved with intracellular polymers alone, I removed the extracellular solution after polymer permeation and cryopreserved the cell pellets (Fig. 3.14).

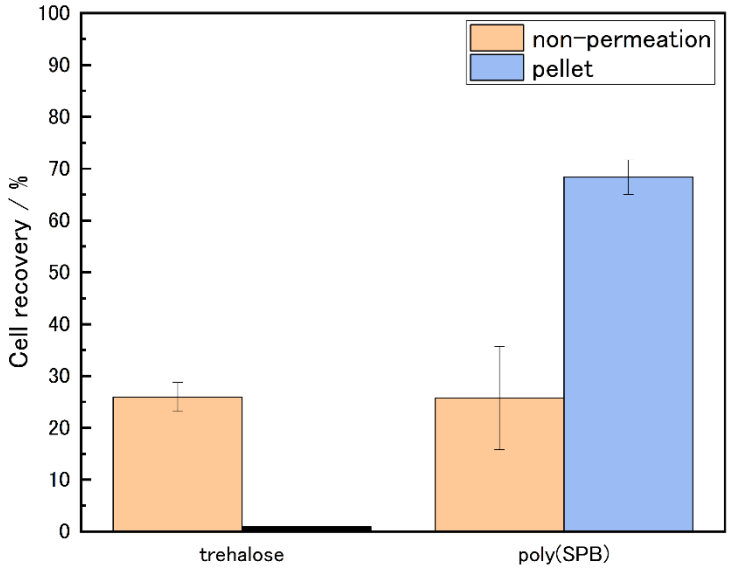

Figure 3.14 Cryoprotective capacity of trehalose- and poly(SPB)-permeabilized cell pellets.

For comparison, trehalose, a protective agent that does not penetrate into cells, was used. After suspension in trehalose solution, the cells were pelleted by centrifugation, the supernatant was removed and frozen. Poly(SPB) improved the cell recovery rate, which was approximately 45% compared with the case without permeation into the cells. The above recovery rate is comparable to that of DMSO. Furthermore, after permeating the cells with 1% fluorescently modified polymer, the cell pellets were cryopreserved (Figure 3.15). As a result, polymer fluorescence was observed only in living cell groups that were not stained with trypan blue. In addition, by incubating the cells at 37° C and 5% CO_2 for 30 minutes after thawing, intracellular fluorescence was greatly reduced, similar to the observation of counter-diffusion. This experiment reconfirmed the enhanced cryoprotective effect of the polymer through intracellular penetration and its reverse diffusion after thawing.

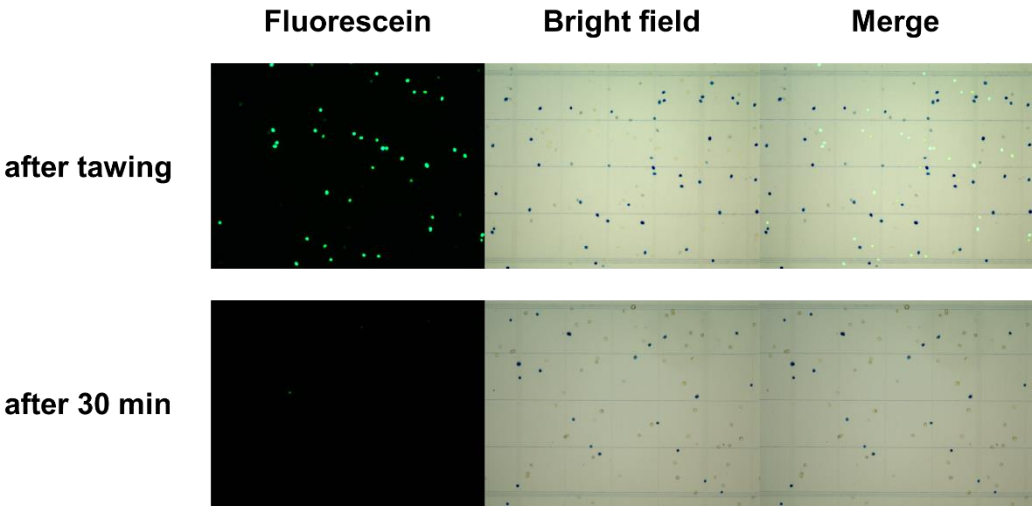

Figure 3.15 Cryoprotective capacity of fluorescence-modified poly(SPB)-permeabilized cell pellets.

Furthermore, the membrane potential of mitochondria was observed by TMRM fluorescent dye 24 h after thawing of the cell (Figure 3.16).

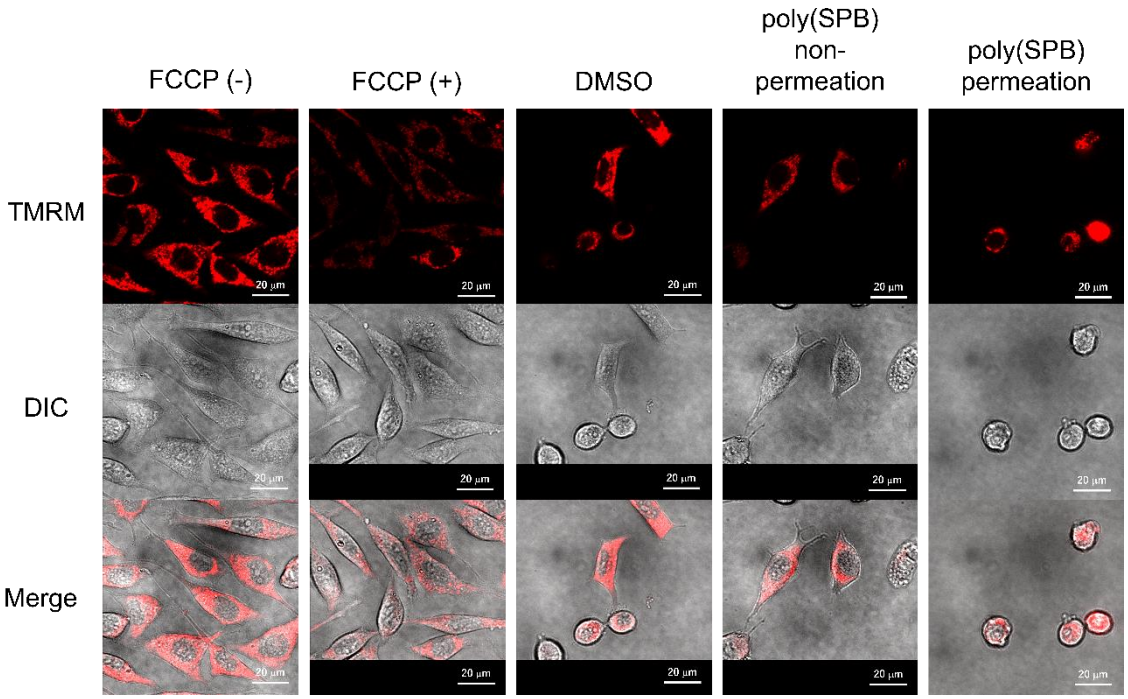

Figure 3.16 Mitochondrial membrane potential before and after freeze-thaw. Scale bars: 100 μm.

Mitochondria play a role in intracellular ATP production and apoptosis, allowing observation of cell activity after thawing. TMRM is a fluorescent dye has a rhodamine backbone and is the most commonly used non-cytotoxic cell-permeable fluorescent dye to assess mitochondrial function. TMRM accumulates in mitochondria in response to mitochondrial membrane potential. However, when the mitochondrial membrane potential is reduced, as in the case of FCCP(+), which depolarizes mitochondria, TMRM is either not taken up by mitochondria or is released from mitochondria.

Therefore, staining cells with TMRM allows one to examine the ATP activity of cells after thawing. Regardless of the permeation or non-permeation of poly(SPB), red fluorescence due to high mitochondrial activity was observed in both non-frozen and frozen cells. Therefore, the amount of ATP production after thawing is considered to be equivalent to that of non-frozen cells. However, when the cells were permeabilized with poly(SPB), their morphology was round; as shown in Figure 3.10, the cells maintained their spindle shape at the time of poly(SPB) permeabilization, suggesting that poly(SPB) in the cells after thawing trapped the magnesium ions necessary for cell adhesion In order to use poly(SPB) intracellular permeation for actual clinical application, it is necessary to evaluate cell adhesion and DNA damage in the future.

In contrast, poly(methylglycidyl sulfoxide) (PMGS) demonstrated a higher cell recovery rate than DMSO. However, it has been reported that while poly(SPB) quickly diffuses out of cells, PMGS is taken up by cells during freezing and remains within the cells even after 24 hours post-thawing[2]. Since low molecular weight PEG has been reported to stabilize cell membranes and improve cryoprotection after permeation into cells, PEG backbone of the main chain is believed to enhance the cryoprotective effect[10]. Similarly, poly(SPB) has been reported to exert cryoprotection by interacting with the cell membrane[19], suggesting that this occurs through membrane protection

similar to the PEG structure. The fact that poly(SPB) can cryoprotect cells and that the cryoprotective effect decreases with increasing MSEMA incorporation ratios potentially corroborate previous reports emphasizing the significance of PEG in the main chain[7]. Additionally, in the case of trehalose, the cells could not be recovered by cryoprotection using only pellets. Here, the cryoprotective effect was not observed because it is believed that trehalose was not present outside the cells. Intracellular trehalose usually enhances the cryoprotective effect. Methods for introducing trehalose, a membrane-impermeable cryoprotectant, into cells include the use of nanoparticles and the expression of trehalose transporter 1 (TRET 1). However, the use of nanoparticles requires long incubation times and involves the risk of endosomal escape, while the expression of TRET 1 requires the genetic modification of cells[26-28]. Poly(SPB) is therefore an excellent cryoprotectant because it can permeate membranes and can be easily introduced into cells.

3.4 Conclusion

In conclusion, I used poly(SPB) and poly(SPB/MSEMA) as intracellular permeable cryoprotectants because of their ability to permeate membranes, and confirmed that they enhanced the cryoprotective effect through intracellular permeation. In contrast, the cryoprotective effect of only poly(SPB) was observed to be comparable to that of DMSO. Fluorescence observations showed that, unlike common membrane-permeable cryoprotectants such as DMSO and glycerol, the developed polymers were easily removable from cells by counter diffusion and did not affect cell growth after freeze–thaw cycling. In addition, unlike nanoparticles, which are established carriers of membrane-impermeable cryoprotective agents, the polymer itself has a cryoprotective effect and a membrane-permeating ability that does not involve endocytosis, making introduction facile. Through this study, I have thus shown that polymers with optimized molecular configurations can achieve unparalleled cryoprotective efficacy. The proposed approach elucidates that DMSO integration plays a pivotal role in modulating cellular interactions. The synergistic interplay between DMSO and SPB underscores the influence of chemical structures on bio-interactions, and this is capable of surpassing conventional cryoprotectants and nanoparticles in both efficacy and potential. By integrating multifaceted cryoprotectants such as ethylene glycol analogues, trehalose,

and especially PEG structures, poly(SPB) may strongly enhance membrane elasticity and cryopreserve three-dimensional structures such as spheroids. The incorporation of these cryoprotectant structures will lead to improved safety and efficacy and is expected to open new avenues for the development of engineered polymers.

3.5 References

1) K. A. Murray and M. I. Gibson, *Nat. Rev. Chem.*, 2023, **6**, 579.

2) R. Peltier, M. A. Brimble, J. M. Wojnar, D. E. Williams, C. W. Evans and A. L. DeVries, *Chem. Sci.*, 2010, **1**, 538-551.

3) K. Matsumura and S. -H. Hyon, *Biomaterials*, 2009, **30**, 4842-4849.

4) K. Matsumura, S. Ahmed and R. Rajan, *Polym. J.*, 2023, **55**, 105.

5) J. Zhao, M. A. Johnson, R. Fisher, N. A. D. Burke, and H. D. H. Stöver, *Langmuir*, 2019, **35(5)**, 1807-1817.

6) A. A. Burkey, A. Hillsley, D. T. Harris, J. R. Baltzegar, D. Y. Zhang, W. W. Sprague, A. M. Rosales and N. A. Lynd, *Biomacromolecules*, 2020, **21(8)**, 3047-3055.

7) T. Ishibe, N. -G. Martinez, P. G. Georgiou, K. A. Murray and M. I. Gibson, *ACS Polym. Au*, 2022, **2(6)**, 449-457.

8) D. S. Moore and S. C. Hand, *Cryobiology*, 2016, **73(2)**, 240-247.

9) A. Eroglu, M. J. Russo, R. Bieganski, A. Fowler, S. Cheley, H. Bavyley and M. Toner, *Nat. Biotechnol.*, 2000, **18**, 163-167.

10) M. Patel, J. K. Park and B. Jeong, *Biomater. Res.*, 2023, **27**, 17.

11) L. D. Blackman, P. A. Gunatillake, P. Cass and K. E. S. Locock, *Chem. Soc. Rev.*, 2019, **48**, 757-770.

12) A. Erfani, J. Seaberg, C. P. Aichele, J. D. Ramsey, *Biomacromolecules*, 2020, **21**, 2557-2573.

13) M. Harijan, M. Singh, *J. Mol. Recognit.*, 2022, **35**, e2944.

14) J. Baggerman, M. M. J. Smulders and H. Zuilhof, *Langmuir*, 2019, **35**, 1072-1084.

15) N. Erathodiyil, H. -M. Chan, H, Wu, J. Y. Ying, *Mater. Today*, 2020, **38**, 84-98.

16) T. Goda, Y, Imaizumi, H. Hatano, A. Matsumoto, K. Ishihara and Yuji Miyahara, *Langmuir*, 2019, **35(24)**, 8167-8173.

17) N. Morimoto, M. Wakamura, K. Muramatsu, S. Toita, M. Nakayama, W. Shoji, M. Suzuki and F. M. Winnik, *Biomacromolecules*, 2016, **17(4)**, 1523-1535.

18) T. Goda, H. Hatano, M. Yamamoto, Y. Miyahara and N. Morimoto, *Langmuir*, 2020, **36(33)**, 9977-9984.

19) R. Rajan, F. Hayashi, T. Nagashima and K. Matsumura, *Biomacromolecules*, 2016, **17(5)**, 1882-1893.

20) S. Li, S. Chung, A. Simakova, Z. Wang, S. Park, L. Fu, D. C. -Karni, S. Averick, and K. Matyjaszewski, *Biomacromolecules*, 2017, **18(2)**, 475-482.

21) Doğuş Işık, Elisa Quaas and Daniel Klinger, *Polym. Chem.*, 2020, **11**, 7662.

22) Y. Yoshizaki and T. Konno, *Molecules*, 2023, **28(11)**, 4479.

23) N. Ghosh, S. Roy, M, Ahmed and J. A. Mondal, *J. Mol. Liq.*, 2018, **266(15)**, 118-121.

24) P. Mazur, S.P. Leibo and E.H.Y. Chu, *Exp. Cell. Res.*, 1972, **71**, 345

25) K. Matsumura, F. Hayashi, T. Nagashima, R. Rajan and S. -H. Hyon, *Commun. Mater.*, 2021, **2**, 15.

26) S. Stewart and X. He, *Langmuir*, 2019, **35(23)**, 7414-7422.

27) T. Chang and G. Zhao, *Adv. Sci.*, 2021, **8**, 2002425.

28) Y. Zhang, H. Wang, S. Stewart, B. Jing, W. Ou, G. Zhang and X. He, *Nano Lett.*, 2019, **19(12)**, 9051-9061.

Chapter 4

General Conclusion

4.1 Conclusion

This thesis focused on elucidating the cryoprotective mechanism of polyamoholytes and their application to cryopreservation using intracellular permeation. Because polyampholytes are less toxic than commonly used cryoprotectants such as dimethyl sulfoxide (DMSO), understanding the cryoprotective mechanism and the transport of cryoprotectants using polyampholytes are very important for regenerative medicine and other applications. The results obtained in this study are summarized below. In Chapter 2, four types of polyampholyte with different side chain structures were synthesized, and the correlation between their cryoprotective effects and polymer structures was investigated using temperature variable magic angle spinning (MAS) solid-state NMR. The cryoprotective effect of poly(vinyl acetate/acrylic acid (AA)/2-(dimethyl amino)ethyl acrylate (DMAEA) (pV), which has an alternating arrangement of cations and anions, showed a cell recovery rate of about 85 %, indicating that it is as effective as carboxylated ε-poly-l-lysine (PLL) in cryoprotection. Below, cryoprotective effect decreased in the order of poly(2-(dimethyl amino)ethyl methacrylate/methacrylic acid) (pD), a random copolymer with the same degree of dissociation, poly(methyl vinyl

ether/AA/DMAEA) (pM), which has the highest molecular weight with a similar structure to pV, Highly dissociated poly(2-acrylamido-2-methyl propanesulfonic acid/(3-acrylamidopropyl)trimethyl ammonium chloride)(pA). The results of growing ice crystals at -6 ° C suggested that the ice recrystallization inhibition (IRI) activity of these polymers was relatively low and did not affect their cryoprotective effects. We discussed the behavior of water molecules and Na ions during freezing of polymer solutions using temperature-variable solid-state MAS NMR. In pA, which has a low cryoprotective effect, the hydrogen bonds of hydrated water are relatively close to bulk water, and the amount of antifreeze water at -10 ° C is about 10% less than that of other polymers. Therefore, it was suggested that the cryoprotective effect would be poor due to exposure to osmotic shock at higher temperatures. In PLL and pV, vitrification and coordination of Na ions to polymer chains were observed at higher temperatures, suggesting that vitrification is an important factor in the cryoprotective effect, similar to previous studies. In the future, it is believed that a deeper understanding of polymer structure and vitrification ability will enable the molecular design of more effective cryoprotectants.

In Chapter 3, we attempted to enhance the cryoprotective effect by utilizing the penetration of the zwitterionic polymer poly(sulfobetaine (SPB)) into cells. I also synthesized a copolymer of 2-(methyl sulfinyl)ethyl methacrylate (MSEMA), which has

the same methyl sulfinyl group as DMSO, a cell-permeable cryoprotectant, and confirmed its cryoprotective effect. Cytotoxicity tests revealed that exposure time to the polymer solution during freezing resulted in little cytotoxicity. Intracellular permeation was confirmed using the fluorescently modified polymer, and it was found that counter diffusion was easily achieved by incubating at 37 ° C for about 30 minutes after permeation. Cells were suspended in each polymer solution (10 w/w%) and subjected to freeze/thaw cycles. As a result, poly(SPB) and poly(SPB/MSEMA10) improved cell recovery by approximately 20 or 30% due to intracellular permeation. The cell recovery rate after counter diffusion of polymer at 37 ° C is comparable to that before polymer infiltration, and it is possible to cryopreserve only the cell pellets after polymer permeation, suggesting that poly(SPB) can improve cryoprotection by intracellular infiltration. Furthermore, there was no significant difference in cell proliferation after thawing before and after permeation, suggesting that poly(SPB) is very promising as an intracellular permeable cryoprotectant. Poly(SPB) is a methacrylate polymer, so cryoprotectants such as polyethylene glycol and sugars that do not penetrate cell membranes can be easily incorporated into the polymer, and it is expected to be used for cryopreservation of three-dimensional cell structures such as spheroids in the future.

This study revealed that vitrification and interaction with salt and water are important

for cryoprotection of polyampholytes. This understanding of the cryoprotection mechanism will provide important guidelines for the molecular design of cryoprotectants in the future. Furthermore, the ability of zwitterionic polymers to reversibly permeate into cells and enhance their cryoprotective effects offers the potential for cryopreservation of more complex three-dimensional cellular structures such as spheroids, and the ability of artificial polymers to It is expected that this will open up new avenues for development.

Achievement

Publication

1. **Ryota Yamasaki**, Robin Rajan, Kazuaki Matsumura, Enhancement of cryopreservation with intracellularly permeable zwitterionic polymers, *Chem. Commun.*, 2023, **59**, 14001-14004, https://doi.org/10.1039/D3CC04092E.

Misc

1. **山﨑椋太**, Robin Rajan, 林文晶, 長嶋敏雄, 松村和明, 側鎖構造の異なる両性電解質高分子による細胞凍結保護効果, *低温生物工学会誌,* 2021, **67**(2), 125-128.

Conference

1. **山﨑椋太**, Robin Rajan, 林文晶, 長嶋敏雄, 松村和明, 凍結過程におけるポリマーと塩の相互作用, 第 66 回低温生物工学会大会、2021, 5. オンライン
2. **山﨑 椋太**, 林 文晶, 長嶋 敏雄, Rajan Robin, 松村 和明, 温度可変固体 NMR を用いた側鎖構造と凍結保護効果の相関, 第 71 回高分子討論会, 2022, 9. 北海道
3. **山﨑 椋太**, Rajan Robin, 松村 和明, 両性電解質高分子の構造と凍結保護効果の関係, 第 11 回北信越ブロック若手研究発表会, 2022, 12. オンライン
4. **Ryota Yamasaki**, Kazuaki Matsumura, Cryopreservation by intracellular permeation of zwitterionic polymers, 33rd Annual Conference of the European Society for Biomaterials, 2023, 9. Swiss Confederation

5. **Ryota Yamasaki**, Robin Rajan, Kazuaki Matsumura, Relationship Between Structure and Cryoprotective Effect of Synthesized Polyampholytes Using Variable-Temperature Solid-State NMR, 33rd Annual Conference of the European Society for Biomaterials, 2023, 9. Swiss Confederation

6. **Ryota Yamasaki**, Robin Rajan, Kazuaki Matsumura, Application of zwitterionic polymers to cryoprotection through intracellular permeation, 2023, 12. Online

ACKNOWLEDGEMENT

I would like to express my deep gratitude to my main supervisor, Professor Kazuaki Matsumura, for his enthusiastic guidance and encouragement in a wide range of areas, from conducting experiments to writing papers, in carrying out this research.

I would also like to thank Assistant Professor Robin Rajan, who gave me much advice in carrying out my research, including polymer synthesis.

I would like to express my deep gratitude to Professor Noriyoshi Matsumi, Professor Motoichi Kurisawa, Associate Professor Eijiro Miyako of the Japan Advanced Institute of Science and Technology, and Associate Professor Shinichi Yusa of the University of Hyogo, who served as my doctoral thesis review committee.

I would also like to express our deep gratitude to Keiko Kawamoto for providing guidance regarding cell culture experiments and basic experimental operations.

I would also like to express my deep gratitude to KEF Corporation's Representative Director Yoshitake Iyoku and Senior Managing Director Hiroyuki Shinbo for their guidance and support during my internship.

In addition, I would like to express my deep gratitude to Dr. Fumiaki Hayashi and Dr. Toshio Nagashima of the Advanced NMR Application and Platform Team, NMR

Research and Collaboration Group, NMR Science and Development Division, RIKEN for providing us with much advice and equipment, including variable temperature NMR measurements.

Finally, I would like to thank all my friends and family for supporting me during my student life.

March 2024

Ryota Yamasaki